DEVELOPMENT AND VALIDATION OF A SLINKY^{TM} GROUND HEAT EXCHANGER MODEL

By

ZEYU XIONG

Bachelor of Science in Mechanical Engineering

Southwest Jiaotong University

Chengdu, Sichuan

2010

Submitted to the Faculty of the
Graduate College of the
Oklahoma State University
in partial fulfillment of
the requirements for
the Degree of
MASTER OF SCIENCE
May, 2014

DEVELOPMENT AND VALIDATION OF A

SLINKY^{TM} GROUND HEAT EXCHANGER MODEL

Thesis Approved:

D. E. Fisher

Thesis Adviser

J. D. Spitler

L. Cremaschi

ACKNOWLEDGEMENTS

I would like to take this opportunity to express my gratitude to many people who have supported and helped me during my my master study.

First and foremost, I would like to thank my thesis advisor, Dr. Daniel Fisher. His enthusiasm, optimism and friendliness keep encouraging me in every stage of my master study. His guidance and efforts are crucial to the completion of this work.

My sincere appreciation goes to Dr. Jeffrey Spitler. He gave me valuable instructions on doing research as well as writing a paper. Besides gaining knowledge in thermal science, I received important academic training from his lessons.

I would like express my thanks to Dr. Lorenzo Cremaschi, who guided me in the first year of my graduate study.

I really appreciate all the help and support from my friends and colleagues.

At last, my deepest gratitude goes to my parents.

Name: ZEYU XIONG

Date of Degree: May, 2014

Title of Study: DEVELOPMENT AND VALIDATION OF A SLINKY^{TM} GROUND HEAT EXCHANGER MODEL

Major Field: MECHANICAL AND AEROSPACE ENGINEERING

Abstract: Ground source heat pump systems are an energy efficient heating and cooling technology for residential and commercial buildings. The main barrier to adoption is the higher investment cost compared to conventional systems. Where available land area permits, horizontal ground heat exchangers are generally less expensive than vertical borehole-type ground heat exchangers (GHXs). A further cost reduction can be made by using Slinky^{TM} ground heat exchangers, which require less trench space and hence reduce the installation cost, in many cases. It is desirable to formulate an accurate model for simulation purposes; such simulations can be used in both design tools and in energy analysis programs.

The model formulated in this paper relies on analytical ring source solutions to compute temperature response functions for both horizontal and vertical Slinky^{TM} heat exchangers. The algorithm used to calculate the response factors have several features that significantly increase computation speed. The thermal effect of the detailed ground heat balance on the GHXs is considered by superimposing the undisturbed ground temperature calculated using a numerical model. For use in whole-building simulations where the GHX may be connected to other components, the model is formulated to calculate both heat transfer rate and exiting fluid temperature, given entering fluid temperature. The model has been validated against the previously published experimental data; and is implemented in a whole-building energy simulation program EnergyPlus.

TABLE OF CONTENTS

Chapter Page

1. INTRODUCTION 1

2. LITERATURE REVIEW 6

2.1 Analytical GHX Models 7
2.1.1 Theoretical Background 7
2.1.2 Line Source Models 10
2.1.3 Ring or Spiral Source Models 14
2.2 Numerical GHX Models 25
2.2.1 Numerical Models for GHXs with Straight Tubes 25
2.2.2 Numerical Models for GHXs with Coiled Tubes 34
2.3 Numerical Simulations and Experimental Studies of Slinky™ GHXs 35
2.3 Applicability of Previous Work 37

3. DEVELOPMENT OF A SLINKY™ GHX MODEL 41

3.1 Ring Source Model and Its Analytical Solutions 41
3.1.1 Description of the Model 42
3.1.2 Solutions for Horizontal Slinky™ GHXs 43
3.1.3 Solutions for Vertical Slinky™ GHXs 49
3.2 Calculation of Temperature Response Factors 51
3.3 Calculation of Fluid Temperature 57
3.3.1 Calculation of Mean Tube Wall Temperature 57
3.3.2 Simple Tube Model 59

4. VALIDATION, VERIFICATION AND APPLICATION 63

4.1 Verification of Ring Source Solution 63
4.2 Validation against Experimental Data 66
4.2.1 Short-term Thermal Response Tests 67
4.2.2 Long-term System Test 73
4.3 Verification of Fast Algorithm 76
4.4 Application to Vertical Slinky™ GHXs 8

Chapter Page

5. IMPLEMENTATION IN ENERGYPLUS....85

5.1 Ground Heat Transfer Model....85
5.2 Implementation in EnergyPlus....90
5.3 Preliminary Evaluation....96
5.3.1 Input Description....96
5.3.2 Simulation Results....98

6. CONCLUSIONS AND RECOMMENDATIONS....102

6.1 Conclusions....102
6.2 Recommendations....103

REFERENCES....105

LIST OF TABLES

Table Page

4.1: Constant Parameters in the Tests 69
4.2: Variable Parameters in the Tests 69

5.1: Input Parameters for Temperature Response Factors Calculation Program 91
5.2: Input Parameters for the EnergyPlus Module 95

LIST OF FIGURES

Figure Page

1.1: Schematic of a Typical Slinky™ Tube....2
1.2: Schematics of Horizontal and Vertical Slinky™ Ground Heat Exchangers....2

2.1: Schematic of the Superposition Principle....8
2.2: Schematic of the Method of Images....10
2.3: A Typical Set of Temperature Response Factors....14
2.4: (a) Ring Tube Wall Temperature Response to This Ring Tube (b) Ring Tube Wall Temperature Response to Adjacent Ring Source....22
2.5: A Cross-section Represents the Whole Ring Tube in Calculating Mean Tube Wall Temperature Response of This Ring....23
2.6: A Centerline Represents the Ring Tube in Calculating the Temperature Influence of Adjacent Ring Source....24
2.7: Schematic of Mei's (1986) First Model Considering Soil Freezing....26
2.8: Schematic of Mei's (1986) Second Model Considering Seasonal Ground Temperature Variation....29
2.9: Schematic of Mei's (1986) Third Model Considering Thermal Interference....30
2.10: Schematic of the Discretization of the Soil Region in Two Coordinates....32
2.11: Schematic of the Simplification of the Three-dimensional VDSC Heat Conduction Problem....34

3.1: Simplification of a Slinky™ Tube....41
3.2: Schematic of the Slinky™ GHX model....42
3.3: Distance between Fictitious Point P_i and Point P_j on Ring Source j....44
3.4: Three-dimensional View of Fictitious Ring Source of Ring j....46

Figure Page

3.5: Two-dimensional View of the Calculation of the Thermal Interaction between Two Rings for Vertical Slinky™ GHXs.....51
3.6: Schematic of the First Improvement to the Algorithm: Use of Symmetry.....52
3.7: Temperature Perturbation versus Distance from the Point Source.....53
3.8: Schematic of the Second Improvement to the Algorithm: Dividing Surrounding Rings into Three Categories.....54
3.9: Comparisons of the Computation Speed of the Original Program and the New Program with the Fast Algorithm 57
3.10: Decomposition of the Heat Inputs into Piecewise Constant Step Heat Inputs 58
3.11: Superposition of Step Heat Inputs 58
3.12: Schematic of Simple Tube Model 60

4.1: Comparisons of the Calculated Mean Tube Wall Temperature Response by Using Our Solution and Li et al.'s (2012) Solution, at D=0.6 m (24 in.) 64
4.2: Comparisons of the Calculated Mean Tube Wall Temperature Response by Using Our Solution and Li et al.'s (2012) Solution with Different Pitches.....65
4.3: Comparisons of the Calculated Mean Tube Wall Temperature Response by Using Our Solution and Li et al.'s (2012) Solution, at p=0.25 m (10 in.).....66
4.4: Simplification of the Slinky™ GHXs Used in the Field Tests.....67
4.5: Schematic of the Experimental Facilities in TRTs 68
4.6: Calculated Sets of Temperature Response Factors.....70
4.7: Comparison of Hourly Outlet Fluid Temperature of the Slinky™ GHX in TRT1 71
4.8: Comparison of Hourly Outlet Fluid Temperature of the Slinky™ GHX in TRT2.....72
4.9: Comparison of Hourly Outlet Fluid Temperature of the Slinky™ GHX in TRT3.....72
4.10: Schematic of the Experimental Facilities in the System Test (A/C Test) 73

Figure Page

4.11: Comparison of Every Ten Minutes Outlet Fluid Temperature of the Slinky™ GHX in Long-term System (A/C) Test....75
4.12: Annual Hourly Building Load Profile for the Example Building in East Lansing, MI....77
4.13: Annual Hourly Building Load Profile for the Example Building in Tempe, AZ....78
4.14: Slinky™ GHX Hourly Fluid Temperature Predictions for East Lansing, MI, with and without Using the Fast Algorithm....79
4.15: Slinky™ GHX Hourly Fluid Temperature Predictions for Tempe, AZ, with and without Using the Fast Algorithm....80
4.16: Comparison between Temperature Response Factors of Horizontal and Vertical Slinky™ GHXs....81
4.17: Schematic of the Undisturbed Ground Temperature Calculation for Vertical Slinky™ GHXs....82
4.18: Horizontal and Vertical Slinky™ GHX Hourly Fluid Temperature Predictions for East Lansing, MI....84
4.19: Horizontal and Vertical Slinky™ GHX Hourly Fluid Temperature Predictions for Tempe, AZ....84

5.1: Schematic of the Ground Heat Transfer Model....86
5.2: Coupling of the Sub-models of the Slinky™ GHX Model....90
5.3: Plot of the Output Temperature Response Factors....92
5.4: Framework of the EnergyPlus Module for Slinky™ GHX Model....94
5.5: Three-dimensional View of the Modeled Building....97
5.6: Input Temperature Response Factors for Whole-Building Simulations....98
5.7: Annual Hourly Building Loads for the Simulated Building in Lansing, MI....99
5.8: Annual Hourly Building Loads for the Simulated Building in Phoenix, AZ....99
5.9: Three-year Hourly Fluid Temperature of Slinky™ GHX in Lansing, MI....100
5.10: Three-year Hourly Fluid Temperature of Slinky™ GHX in Phoenix, AZ....101

CHAPTER 1

INTRODUCTION

Horizontal ground heat exchangers (HGHXs) are most commonly laid in trenches at a depth of 0.9 to 1.8 m (3 to 6 feet) (Chiasson 1999). Alternatively, they are sometimes laid out during site excavation, and then buried; in this case, they may be deeper than typical trench depths. When compared to vertical ground loop heat exchangers, HGHXs usually have significantly lower installation costs, since trench excavation is considerably less expensive than drilling vertical boreholes. However, conventional straight tube horizontal GHXs require large amounts of land surface for installation, which limits the application of such GHX. As an alternative, Slinky™ GHXs, also known as slinky-coil GHXs (Fujii et al. 2012) or slinky-loop GHXs (Chong et al. 2013), use coiled tubing, with the individual coils spread out along the direction of the trench, as Figure 1.1&1.2 show. Slinky™ GHXs are characterized by the pitch p (the distance between loops) and the diameter of loops D. Compared to conventional straight tube HGHXs, Slinky™ GHXs have higher tube density per land area, allowing GHX to extract/inject more heat per land area. Hence, with the same cooling/heating loads, Slinky™ GHXs require less land area and excavation work than straight tube HGHXs. The compact Slinky™ GHX needs about one-third trench length compared to a two-pipe straight tube HGHX (Jones 1995).

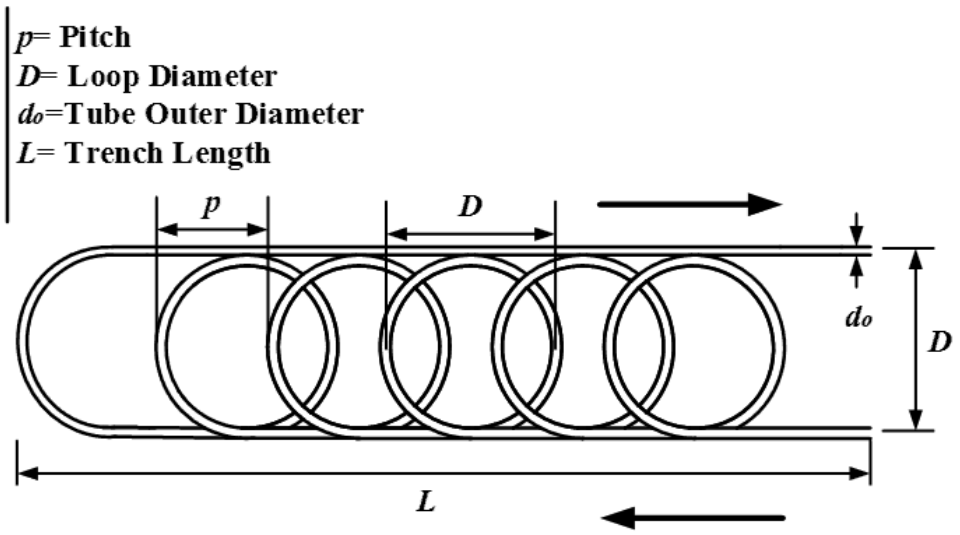

Figure 1.1: Schematic of a Typical Slinky™ Tube

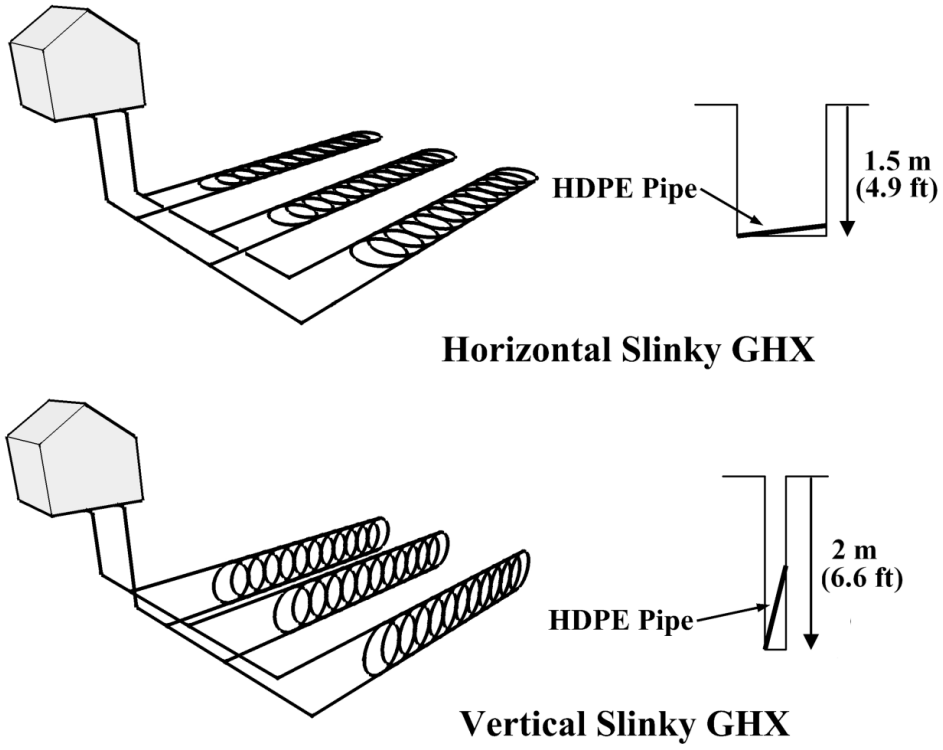

Figure 1.2: Schematics of Horizontal and Vertical Slinky™ Ground Heat Exchangers

Slinky™ GHXs can be placed either horizontally or vertically, as shown in Figure 1.2. If the excavation is made with a trenching machine, the Slinky™ is usually placed vertically or near-vertically in the narrow trench. However, backfilling the narrow trenches of a vertical Slinky™ GHX can be difficult and may resulting in air pockets around the tubing which will affect its thermal performance significantly if not backfilled correctly. A high-pressure water jet should be used (Jones 1995) in the backfilling process to prevent bridging of soil and air pockets. Conversely, when Slinky™ GHXs are placed in a large single excavation or in a wider trench dug with a backhoe, they are generally installed horizontally.

Though Slinky™ GHXs have existed for more than two decades, a suitable design tool is still absent. Due to their compact configuration, the thermal interaction between loops is considerable. In addition, because of its comparatively shallow buried depth, the above ground environment will affect the overall performance of a Slinky™ GHX significantly. The previous studies on the thermal performance of Slinky™ GHXs (Wu et al. 2010; Chong et al. 2013) are based on the numerical simulations of only one or two loops of a Slinky™ GHX using commercial CFD software with simplified boundary conditions. The effects of the thermal interaction between loops and the ground surface heat balance are not carefully considered in these studies.

The objective of this study is to develop a simulation model for Slinky™ GHXs. A ring source model is established to model the thermal response of Slinky™ GHX. According to the literature review in Chapter 2, the previous ring source models either focus only on the calculation of soil temperature response (Cui et al. 2011), or are intended to be used to determine the size of the GHX (Li et al. 2012). To develop a model suitable for whole-building energy simulation, several important issues are addressed in this study. The first is applying the ring source solutions in short variable time-step simulation environment. For annual simulations with short time steps (less than an hour), it is impractical to calculate the temperature variation of tubing wall at each time step by using the temperature response solution directly. Therefore, a *g-function* (temperature response

function) method similar to that used in vertical borehole models (Eskilson 1987; Yavuzturk and Spitler 1999) is introduced in this study. The analytical ring source solutions for temperature response function of both horizontal and vertical Slinky^{TM} GHXs are derived. Based on this, a computer program is written to generate a set of temperature response factors. The temperature response factors are used to calculate temperature variation of the tubing wall at each time step. The calculations of the ring source solution are isolated from the simulation process. Since the computation time is a key issue for energy simulation, the algorithm used to calculate the temperature response factors have been optimized with a significantly improvement in computation speed.

The second issue is the model's ability to couple to other components in a whole-system simulation that is part of a building simulation environment. The energy transfer between components is captured based on the change of fluid state. Therefore, for a component model that intends to be embedded in whole-building simulation environment, the model input is normally inlet fluid state; and the heat transfer rate is calculated as an output. However, the reviewed ring source models (Cui et al. 2011; Li et al. 2012) rely on the heat transfer rate of tubing being specified as an input. To solve this, the model presented in this paper is formulated to calculate exiting fluid temperature and heat transfer rate, with the knowledge of entering fluid temperature. The development of the model is presented in Chapter 3.

The third issue is the integration of the ground surface heat balance. Due to Slinky^{TM} GHXs' comparatively shallow buried depth, the thermal effect of the ground surface heat balance should be considered by the model. According to the principle of superposition (Claesson and Dunand 1983), the piping wall temperature of GHX is the sum of the undisturbed ground temperature at the buried depth and the piping wall temperature variation calculated from the temperature response solution. The undisturbed ground temperature reflects the thermal impact of the ground

surface heat balance. In this study, the undisturbed ground temperature is predicted by using a numerical three-dimensional ground heat transfer model.

Finally yet importantly, while a number of heat source models were proposed to predict the thermal performance of the GHXs with coiled tubing (Mukerji et al. 1997; Man et al. 2010; Cui et al. 2011; Man et al. 2011; Li et al. 2012), none of them have been validated against experimental field data that utilize coiled tubing as heat source and sink. The validation of this model is performed by using the published field test data of horizontal Slinky^{TM} GHXs (Fujii et al. 2012). Measured fluid temperature from three short-term (5 days) thermal response tests (TRTs) and a long-term (38 days) GSHP system test was compared with model predicted values. In addition, to verifying the validity of the fast algorithms that are used to calculate temperature response factors, two-year simulations at two locations are performed. The derived ring source solution is also verified by comparing the calculation results to the results of Li et al.'s (2012) solution. The validation and verifications of the model is presented in Chapter 4.

The model is implemented in a whole-building energy simulation program, EnergyPlus, where it is coupled with a numerical ground heat transfer model applied to predict the undisturbed ground temperature. The implementation of this model is covered in Chapter 5. Conclusions and recommendations are presented in Chapter 6.

CHAPTER 2

LITERATURE REVIEW

This section describes the previous work contributed or related to the development, validation and implementation of the Slinky™ GHX model. In the preliminary study, few mathematical models were found for Slinky™ GHXs. In the last several decades, various models for GHXs with different configurations were developed. These models can be divided into two main categories: analytical and numerical models. Due to Slinky™ GHXs' complex configuration, adopting either an analytical or numerical approach requires simplifications of its configuration to some degree. Three approaches were considered and compared in the preliminary study. First, the Slinky™ tubing can be simplified as a series of connected rings. A ring source model will be established for Slinky™ GHXs. According to the literature (Carslaw and Jaeger 1959; Marcotte and Pasquier 2009), by integrating the point source solution with regard to appropriate variables, the ring source solutions can be derived to describe the temperature response of the tube wall. Second, a Slinky™ GHX can be modeled as a thin plate heat exchanger. Fujii et al. (2012) presented a numerical simulation of Slinky™ GHXs by using a finite-element simulator. In this work, Slinky™ GHXs were modeled as a thin plate heat exchanger. However, the surface area of the thin plate is much larger than the Slinky™ tubes' surface area. An efficient method to resolve this problem does not exist. Therefore, this is not an ideal approach. Third, the Slinky™ tube can be replaced by a number of straight tubes with the same tube length and trench length. In the literature review, both numerical and analytical approaches are available for modeling straight

tube HGHXs. However, due to the compact size of Slinky^{TM} GHXs, a large number of straight tubes are anticipated for the replacement of a Slinky^{TM} GHX. Modeling these tubes' interaction numerically could be time consuming. Regarding the analytical approach, a similar methodology used in the ring source model (the first approach) is applied. While both the ring source model and the finite line source model are based on the same theories, the ring source model is more in accordance with the original configuration of a Slinky^{TM} GHX. Therefore, the first approach is chosen to model Slinky^{TM} GHXs. While the analytical approach was used to model the temperature response of Slinky^{TM} GHXs, the review of the numerical models (Lee 2008; Xing, 2010; Lee et al. 2013) contributes to the calculation of the undisturbed ground temperature. The validation of the Slinky^{TM} GHX model is verified based on the published experimental data in Fujii et al.'s paper (2012).

2.1 Analytical GHX Models

2.1.1 Theoretical Background

The principle of superposition serves as the basis for analytical models and is discussed in the work of Claesson and Dunand (1983). According to this principle, the complex heat transfer process associated with GHXs can be treated as the superposition of several independent elementary heat transfer processes. As Figure 2.1 shows, the temperature variation of the soil around two buried tubes is calculated as the superposition of the following terms: (a) the soil temperature variation due to the pipe 1 as a line source with isothermal boundary condition, (b) the soil temperature variation due to the pipe 2 as a line source with isothermal boundary condition, and (c) the soil temperature variation due to changing boundary temperature.

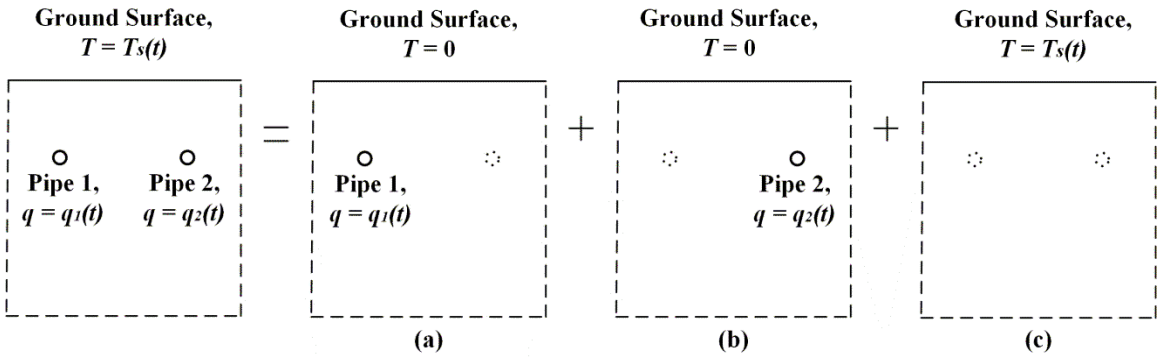

Figure 2.1: Schematic of the Superposition Principle

Besides the superposition of multiple heat sources in space, this principle can be used to deal with the variable heat rate in time. When the strength of a heat source is varying, the temperature response can be treated as the superposition of the responses to a series of constant step heat inputs. The superposition principle is only valid for the heat conduction problems with linear boundary conditions and governing equation.

According to the heat source theory, the summation of term (a) and (b) mentioned in the above case can be calculated using an analytical solution. This analytical solution is based on the continuous point source solution and Green's function theory. The differential equation of conduction of heat (Equation 2.1) is satisfied by the point source solution.

$$\frac{\partial^2 T}{\partial x^2} + \frac{\partial^2 T}{\partial y^2} + \frac{\partial^2 T}{\partial z^2} = \frac{1}{\alpha}\frac{\partial T}{\partial t} \tag{2.1}$$

where:

T is the temperature, in °C or °F,

t is time, in s,

α is the thermal diffusivity, in m^2/s or ft^2/s,

x, y, z are Cartesian coordinate, in m or ft

The continuous point source solution may be interpreted as the temperature variation in an infinite solid due to a finite quantity of heat q continuously generated from time t=0 onwards at a point. Based on Carslaw and Jaeger's (1959) work, the continuous point source solution can be written as:

$$T = \frac{q}{4\pi kd} erfc(\frac{d}{\sqrt{4\alpha t}}) \tag{2.2}$$

where:

T is the temperature variation, in °C or °F,

t is time, in s,

q is the quantity of heat, in W or Btu/h,

d is the distance from the point source, in m or ft,

k is the ground thermal conductivity, in W/m·K or Btu/h·ft·°F,

α is the ground thermal diffusivity, in m^2/s or ft^2/s,

erfc is the complementary error function

By integrating the continuous point source solution with the regard to appropriate variables, the solutions for continuous line, cylindrical surface and plane source are obtained (Carslaw and Jaeger 1959). These solutions can be used in modeling GHXs with the corresponding configurations.

The solutions mentioned above are for the heat conduction problems in an infinite medium. However, for the heat conduction problems related to GHXs, a more reasonable simplification of the ground domain is a semi-infinite medium. To obtain the solution of heat sources in the solid bounded by an isothermal surface, the method of images (Carslaw and Jaeger 1959) is applied.

As Figure 2.2(a) shows, fictitious heat sources are created symmetrical to the boundary with the same heat input rate, yet opposite in sign. Similarly, if the boundary surface is adiabatic instead of isothermal, the exact same heat sources are superimposed symmetrical to the boundary surface, as Figure 2.2(b) demonstrates.

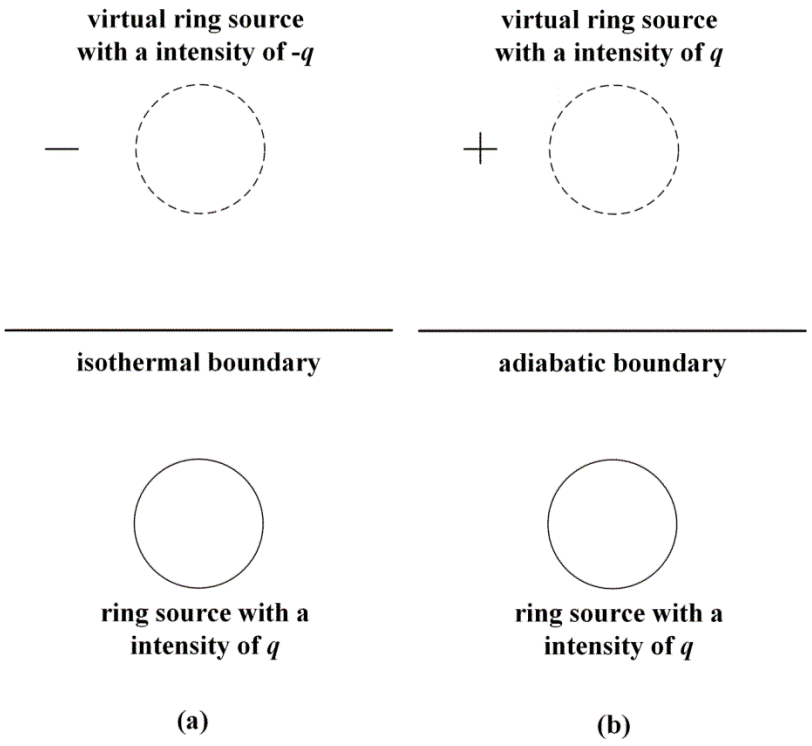

Figure 2.2: Schematic of the Method of Images

2.1.2 Line Source Models

Line source solution can be used to model the GHXs with vertical boreholes or straight buried tubes. The theory of applying infinite line source and finite line source solutions in modeling GHX is presented in the work of Ingersoll et al. (1954). In this work, the infinite line source solution is given as:

$$\Delta T = \frac{q}{2\pi k}\int_{\frac{r_d}{2\sqrt{\alpha t}}}^{\infty}\frac{e^{-\beta^2}}{\beta}d\beta = \frac{q}{2\pi k}I\left(\frac{r_d}{2\sqrt{\alpha t}}\right) \tag{2.3}$$

where:

$$I(x) = \int_x^{\infty} \frac{e^{-\beta^2}}{\beta} d\beta = -\frac{1}{2} Ei(-x^2)$$

ΔT is the temperature variation, in °C or °F,

k is the ground thermal conductivity, in W/m·K or Btu/h·ft·°F,

α is the ground thermal diffusivity, in m^2/s or ft^2/h,

q is the heat rate, in W or Btu/h,

r_d is the distance from the line source,

β is the integration variable

For $x < 0.2$, $I(x) = In\frac{1}{x} + \frac{x^2}{2} - \frac{x^4}{8} - 0.2886$. It's worth noticing that line source solutions can result in significant error when applied in the cases where $\alpha t^2/r < 20$. In addition, in Ingersoll et al.'s (1954) work, the line source theory is applied to model short pipes. Instead of using infinite line source model, a short pipe is modeled as a line source with a finite length. For the short pipe extends from z_1 to z_2, the finite line source solution is given as:

$$\Delta T = \frac{q}{4\pi k} \int_{z_1}^{z_2} \frac{dz}{\sqrt{z^2 + r^2}} \int_{\frac{\sqrt{z^2+r^2}}{2\sqrt{\alpha t}}}^{\infty} \frac{2}{\sqrt{\pi}} e^{-\beta^2} d\beta \tag{2.4}$$

where:

r is the radial coordinate,

z is the axial coordinate

Since $\int_{\frac{\sqrt{z^2+r^2}}{2\sqrt{\alpha t}}}^{\infty} (\frac{2}{\sqrt{\pi}} e^{-\beta^2}) d\beta = erfc(\sqrt{z^2 + r^2}/2\sqrt{\alpha t})$, Equation 2.4 can be rewritten as following:

$$\Delta T = \frac{q}{4\pi k}\int_{z_1}^{z_2} \frac{erfc(\sqrt{z^2+r^2}/2\sqrt{\alpha t})}{\sqrt{z^2+r^2}}\,dz \tag{2.5}$$

When applying infinite and finite line source solution in modeling GHXs, finite line source model has an advantage over infinite line source model by considering the axial effect. Studies have been done in last decade to perfect the theory. Finite line source models were developed for GHX with vertical boreholes (Zeng et al. 2002), inclined boreholes (Cui et al. 2006), and horizontal tubes (Fontaine et al. 2011). Marcotte and Pasquier (2009) gave a more general solution of the ground temperature response to vertical boreholes that permits the boreholes to start at any distance from the ground surface.

As Equation 2.5 indicates, the finite line source solution involves the calculation of a double integral. The finite line source model presented by Lamarche and Beauchamp (2007) has a modified expression for temperature response solution of vertical boreholes. The double integral appeared in the previous finite line source solution (Zeng et al. 2002) was eliminated, which makes the new solution numerically efficient. Another single integral finite line source solution is derived in Claesson and Javed's (2011) work. The finite line source solution is used to calculate the long-term temperature response of vertical boreholes in this work.

Line source models have two main limitations: first, the heat fluxes along tubes or boreholes of a GHX is assumed uniform (Malayappan and Spitler 2013); second, since the superposition principle is not valid if heat conduction equation is not linear (Claesson and Dunand 1983), the freezing and melting process of the soil is not considered. These two issues were discussed in Fontaine et al.'s (2011) work. According to this paper, exponential heat flux decay along the pipes of a GHX is assumed for the finite line source model. Based on the finite line source solution given in Marcotte and Pasquier (2009), an algorithm is then proposed to calculate the inlet and outlet fluid temperature of a buried tube by using the heat transfer rate of each segment of the tube. The correctness of the model is verified by two 3D finite element numerical

simulations. The thermal effect of freezing and melting process of the soil is also discussed in the paper. Numerical simulations with and without considering phase changes are performed. The results of these simulations are compared. The authors conclude that the simulations without considering phase change reproduce reasonable soil temperature during the heating period, yet overestimate the soil temperature during the summer time. A reasonable explanation for this conclusion may be that the phase change process of the soil (melting) only happened during the summer season for the place picked for this study (Kuujjuaq, Canada).

The non-dimensional temperature response function, also known as *g-functions*, is an approach proposed by Eskilson (1987) to calculate the temperature variation at borehole wall in response to step heat inputs. The temperature response of vertical boreholes to a single step heat input from minutes to decades is represented by a set of non-dimensional factors. By transferring the heat input function into piecewise constant step heat inputs, and superimposing with the corresponding temperature response function value at each step, the temperature variation at the borehole wall due to any arbitrary heat input function can be calculated. The temperature response function values are calculated by interpolating between the near temperature response factors. A typical set of temperature response factors are shown in Figure 2.3. The temperature response factors can be generated by using both numerical and analytical approaches (Eskilson 1987; Yavuzturk and Spitler 1999). A significant contribution of the *g-function* method is that, regardless of the configuration of a GHX and the time scale, a set of non-dimensional temperature response factors are sufficient to describe the thermal behavior of a GHX.

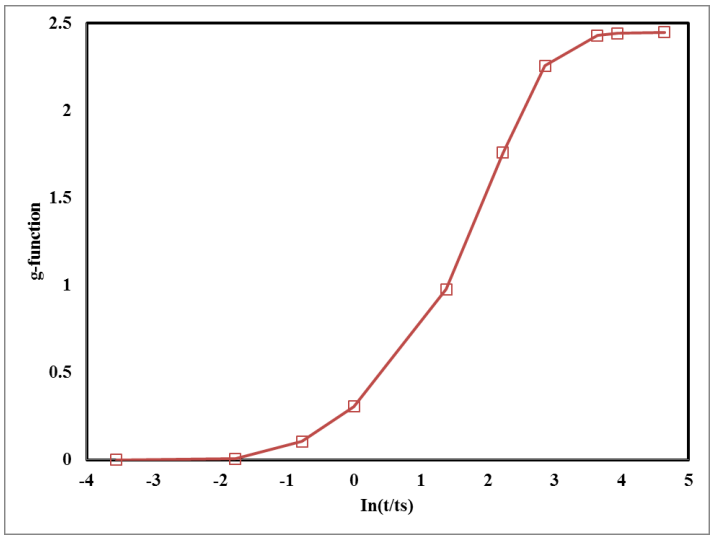

Figure 2.3: A Typical Set of Temperature Response Factors

2.1.3 Ring or Spiral Source Model

To reduce the initial cost and land area requirement of a GSHP system, specialized GHXs were developed, such as pile, sub-slab and Slinky^{TM} GHXs. The coiled tubing systems are adopted by these heat exchangers. When compared to traditional straight tubing or vertical boreholes, the configurations of these GHXs are more complex, which makes the development of mathematical models more challenging. However, the character of coiled tubing makes the ring or spiral source models an ideal approach.

Mukerji et al. (1997) developed a line source approximation (LSA) model for GHXs that use arbitrarily coiled tubes. In this model, the spiral or Slinky^{TM} coiled tubing is treated as a spiral or Slinky^{TM} heat source, with the heat source coiled in exactly the same pattern as the tube. To verify the validity of this method, the LSA method is applied to infinitely long straight tubes. The result is compared to published analytical solution (infinite line source solution). As the result of this study, the analytical solution for performance factor (PF) was derived. PF is the ratio of the heat transfer rate per unit tube length of coiled tubing to that of straight tubing. The authors

introduce the PF as a simple way to incorporate the design of Slinky™ GHX into existing HGHX design tools. However, the derived solutions are limited to the steady-state heat transfer case.

A ring source model for sub-slab GHX is presented in Braven and Nielson's (1998) paper. The ring source solution is derived from the instantaneous ring source solution given in Carslaw and Jaeger (1959):

$$T = \frac{q}{8(\pi\alpha t)^{3/2}} exp\left[-\frac{r^2 + R^2 + z^2}{4\alpha t}\right] I_0\left(\frac{rR}{2\alpha t}\right) \tag{2.6}$$

where:

I_0 is the modified Bessel function of the first kind.

r is the distance from the center of the ring, in m or ft,

R is the radius of the ring, in m or ft,

z is the vertical distance from the center of the ring, in m or ft

q is the heat input (J or Btu) by density (kg/m^3 or lbm/ft^3) and specific heat (J/kg·K or Btu/lbm·°F)

T is the temperature variation, in °C or °F,

k is the ground thermal conductivity, in W/m·K or Btu/h·ft·°F,

α is the ground thermal diffusivity, in m^2/s or ft^2/h,

t is time, in s

It's worth noticing that the heat rate of the ring source is $\rho c_p q$ instead of q. By integrating the instantaneous ring source solution given above over time, the continuous ring source solution is derived in the paper:

$$T = \int_0^t \left(\frac{q}{8(\pi\alpha(t-\tau))^{3/2}} exp\left(-\frac{{r_d}^2 + R^2 + z^2}{4\alpha(t-\tau)} \right) I_0\left(\frac{r_d R}{2\alpha(t-\tau)} \right) \right) d\tau \quad (2.7)$$

where:

τ is a variable of integration.

Since the sub-slab GHX is buried beneath the floor, the boundary surface is treated as isolated instead of isothermal. The seasonal soil temperature variation along depth is estimated using the Kusuda and Achenbach (1965) model. While the mean tube wall temperature is obtained based on the ring source solution and the superposition principle, the classical Log Mean Temperature Difference (LMTD) method is used in calculating the fluid temperature, as the following equation demonstrates:

$$T_{out} = T_{tw} + (T_{in} - T_{tw}) e^{-(\frac{UA}{\dot{m} c_p})} \quad (2.8)$$

where:

T_{out} is the outlet fluid temperature, in °C or °F,

T_{in} is the inlet fluid temperature, in °C or °F,

T_{tw} is the tube wall temperature, in °C or °F,

UA is the overall heat transfer coefficient,

$\dot{m}$ is the mass flow rate of the fluid, in kg/s or lb/s,

c_p is the specific heat of the fluid, in J/kg·K or Btu/lbm·°F

Both the inlet and outlet fluid temperature are unknowns and will be iterated until the calculated heat transfer rate matches with the input heat transfer rate. The input for this model is heat transfer rate, while the output variables are tube wall temperature, inlet and outlet fluid

temperature. The predicted tube wall temperature using monthly average ground load is validated against the field test data. The error is approximately within 2°C (4°F). The model is limited in simulating continuous operating conditions and lacks the ability to simulate short-term variation of fluid state.

Pile GHXs typically use spiral coils buried in the concrete piles of a building. Three models were developed for pile GHXs based on the cylindrical source (Man et al. 2010), ring source (Cui et al. 2011) and spiral source (Man et al. 2011) solutions. The spiral coils on piles were first modeled as cylindrical sources (Man et al. 2010). This model is unable to distinguish the effect of spiral pitches, which is important for the performance of pile GHX. Cui et al. (2011) then established a ring source model for pile GHX. Vertical spiral tubing of pile GHX is simplified as a series of ring sources. The infinite and finite ring source solutions of the soil temperature response are derived. The obtained solutions are similar to the solution given in Braven and Nielson's (1998) paper (Equation 2.7), yet in dimensionless form.

To obtain a better match with the configuration of the spiral coil used in pile GHXs, Man et al. (2011) proposed a spiral source model. The buried spiral coil is modeled as a spiral line source. The finite and infinite spiral source solution for pile GHXs are derived based on Green's function. Green's function, which can be treated as the instantaneous point source solution mentioned above, is given in the cylindrical coordinate system:

$$G(r,\varphi,z,t;r',\varphi',z',t') = \frac{1}{8[\pi\alpha(t-t')]^{3/2}} exp\left[-\frac{(r\cos\varphi - r'\cos\varphi)^2 + (r\sin\varphi - r'\sin\varphi')^2 + (z-z')^2}{4\alpha(t-t')}\right] \quad (2.9)$$

where:

r and r' are the radial coordinates, in m or ft,

z and z' are the axial coordinates, in m or ft,

φ and φ' are the angular coordinates, in rad,

t and t' are time, in s,

α is the ground thermal diffusivity, in m^2/s or ft^2/h

Equation 2.9 gives the temperature variation at point (r, φ, z) due to a point source emitting ρc_p quantity of heat at time t'. By integrating the above solution along an infinite spiral line, whose cylindrical coordinates are $r' = r_0, z' = b\varphi'/(2\pi)$, the infinite spiral solution for pile GHXs is derived as:

$$T = \frac{qb}{2\pi\rho c_p}\int_0^t dt' \int_{-\infty}^{\infty} \frac{q}{[\pi\alpha(t-t')]^{3/2}} \cdot exp\left[-\frac{r^2 + {r_0}' - 2r r_0\ \cos(\varphi-\varphi') + (z-\frac{b\varphi'}{2\pi})^2}{4\alpha(t-t')}\right] d\varphi' \tag{2.10}$$

where:

t' and φ' are variables of integration,

b is the spiral pitch, in m or ft,

r_0 is the spiral radius, in m or ft,

ρ is the soil density, in kg/m^3 or lb/ft^3,

c_p is the specific heat of the ground, in J/kg·K or Btu/lbm·°F

The finite spiral source solution is also derived, which integrates the Green's function along a finite spiral line with the respect to the finite spiral coil. Additionally, Man et al. (2011) gives the solutions of the temperature responses of tube wall and circulating fluid based on the finite spiral source solution, which is a significant complement for the previous work.

Li et al. (2012) presented a ring source model for horizontal Slinky™ GHX, called "spiral heat exchangers". According to the paper, Slinky™ tube is modeled as multiple ring sources in a semi-infinite homogeneous medium. In Li et al.'s (2012) work, the solutions for several different cases are derived and discussed in detail. First, the authors give the solution for the ground temperature variation at point (r, φ, z) in response to a single continuous ring source, with the ground assumed infinite medium:

$$\theta_{inf}(r,z,t) = \frac{{q_r}'}{4\pi k}\int_0^{2\pi}\frac{1}{r^*}erfc\left(\frac{r^*}{2\sqrt{\alpha t}}\right)d\sigma \tag{2.11}$$

where:

$$r^* = \sqrt{(r_0\cos\sigma - r\cos\varphi)^2 + (r_0\sin\sigma - r\sin\varphi)^2 + z^2}$$

θ is the temperature variation, in °C or °F,

r is the radial coordinate, in m or ft,

r_0 is the ring source radius, in m or ft,

z is the axial coordinate, in m or ft,

t is time, in s,

q_r' is the total heat flow rate of a ring source divided by 2π, in W or Btu/h,

k is the ground thermal conductivity, in W/m·K or Btu/h•ft•°F,

α is the ground thermal diffusivity, in m^2/s or ft^2/h,

σ, φ are the angle coordinate, in rad,

erfc is the complementary error function,

By using the characteristic length r_0 and the dimensionless variables: $R^* = r^*/r_0$, $R = r/r_0$, $Z = z/r_0$, $F_o = \alpha t/{r_0}^2$, and $\Theta_{inf} = \theta_{inf}\, kr_0/{q_r}'$, Equation 2.11 can be written in the dimensionless form:

$$\Theta_{inf}(r,z,t) = \frac{1}{4\pi}\int_0^{2\pi} \frac{1}{R^*} erfc\left(\frac{R^*}{2\sqrt{F_o}}\right) d\sigma \tag{2.12}$$

where:

$$R^* = \sqrt{(\cos\sigma - R\cos\varphi)^2 + (\sin\sigma - R\sin\varphi)^2 + Z^2}$$

In Equation 2.12, Θ_{inf} is not affected by the value of φ, according to the symmetry of a single ring source.

After giving the solution for ground temperature response to a single ring source, Li et al. (2012) discuss the case with multiple ring sources. While cylindrical coordinates are applied in the single and multiple ring source solutions, Cartesian coordinates are also used in the multiple ring source solution to account for the different positions of ring sources. The center of *i*th ring source is given as $(x_i + r_0\cos\sigma\,, r_0\sin\sigma\,, z_i')$. The authors consider the positions of ring's center to vary in the direction of *x* and *z*. However, as mentioned in Chapter 3, in real application, for horizontal Slinky™ GHXs, the positions of ring's centers are likely to vary in the direction of *x* and *y* only, determined by the pitch and the gap between rows of Slinky loops. The solution for the ground temperature variation in response to multiple ring sources is given by Li et al. (2012) based on Equation 2.12:

$$\theta_{inf,p} = \frac{kr_0}{{q_r}'}\sum_{i=0}^{n-1} \Theta_{inf}(X_i, Z_i', R, Z, F_o) \tag{2.13}$$

In Equation 2.13, the same the characteristic length $r_0$is applied. The use of both cylindrical and Cartesian coordinates unnecessarily complicates the application of this model.

While the above equations are for infinite medium, Li et al. (2012) derived the solutions for semi-infinite medium. The ground surface is assumed as either an isothermal surface for warm regions or an adiabatic surface for cold regions. When the boundary surface is considered as an isothermal surface, the single ring source solution in a semi-infinite medium is given as:

$$\theta_{sf}(r,z,t) = \frac{{q_r}'}{4\pi k}\int_0^{2\pi}\left[\frac{1}{r_+^*}erfc\left(\frac{r_+^*}{\sqrt{4\alpha t}}\right) - \frac{1}{r_-^*}erfc\left(\frac{r_-^*}{\sqrt{4\alpha t}}\right)\right]d\sigma \tag{2.14}$$

where:

$$r_+^* = \sqrt{(r_0\cos\sigma\ - r\cos\varphi)^2 + (r_0\sin\sigma - r\sin\varphi)^2 + (-z' - z)^2}$$

$$r_-^* = \sqrt{(r_0\cos\sigma - r\cos\varphi)^2 + (r_0\sin\sigma - r\sin\varphi)^2 + (z' - z)^2}$$

When the boundary surface is treated as an adiabatic surface, Equation 2.14 is revised to:

$$\theta_{sf}(r,z,t) = \frac{{q_r}'}{4\pi k}\int_0^{2\pi}\left[\frac{1}{r_+^*}erfc\left(\frac{r_+^*}{\sqrt{4\alpha t}}\right) + \frac{1}{r_-^*}erfc\left(\frac{r_-^*}{\sqrt{4\alpha t}}\right)\right]d\sigma \tag{2.15}$$

By applying the same rule as Equation 2.11 and 2.12, Equation 2.14 and 2.15 are given in the dimensionless format:

$$\Theta_{sf}(R,Z,F_o) = \frac{1}{4\pi}\int_0^{2\pi}\left[\frac{1}{R_+^*}erfc\left(\frac{R_+^*}{\sqrt{4F_o}}\right) \mp \frac{1}{R_-^*}erfc\left(\frac{R_-^*}{\sqrt{4F_o}}\right)\right]d\sigma \tag{2.16}$$

where:

$$R_+^* = \sqrt{(\cos\sigma - R\cos\varphi)^2 + (\sin\sigma - R\sin\varphi)^2 + (Z + Z')^2}$$

$$R_-^* = \sqrt{(\cos\sigma - R\cos\varphi)^2 + (\sin\sigma - R\sin\varphi)^2 + (Z - Z')^2}$$

Based on this, the solution for multiple ring sources in a semi-infinite medium is given in the dimensionless format:

$$\theta_{inf,p} = \frac{kr_0}{q_r{}'} \sum_{i=0}^{n-1} \Theta_{sf}(X_i, Z_i', R, Z, F_o) \tag{2.17}$$

The mean tube wall temperature is the key for GHX size determination and fluid temperature calculation. Li et al. (2012) gives the solution for a ring tube's mean wall temperature variation by considering it to be the summation of two parts: (a) the tube wall temperature response to this ring tube as a ring source, and (b) the tube wall temperature response to other ring tubes (ring sources), as Figure 2.4 shows. In Li et al.'s (2012) model, different solutions were given for part (a) and (b), respectively.

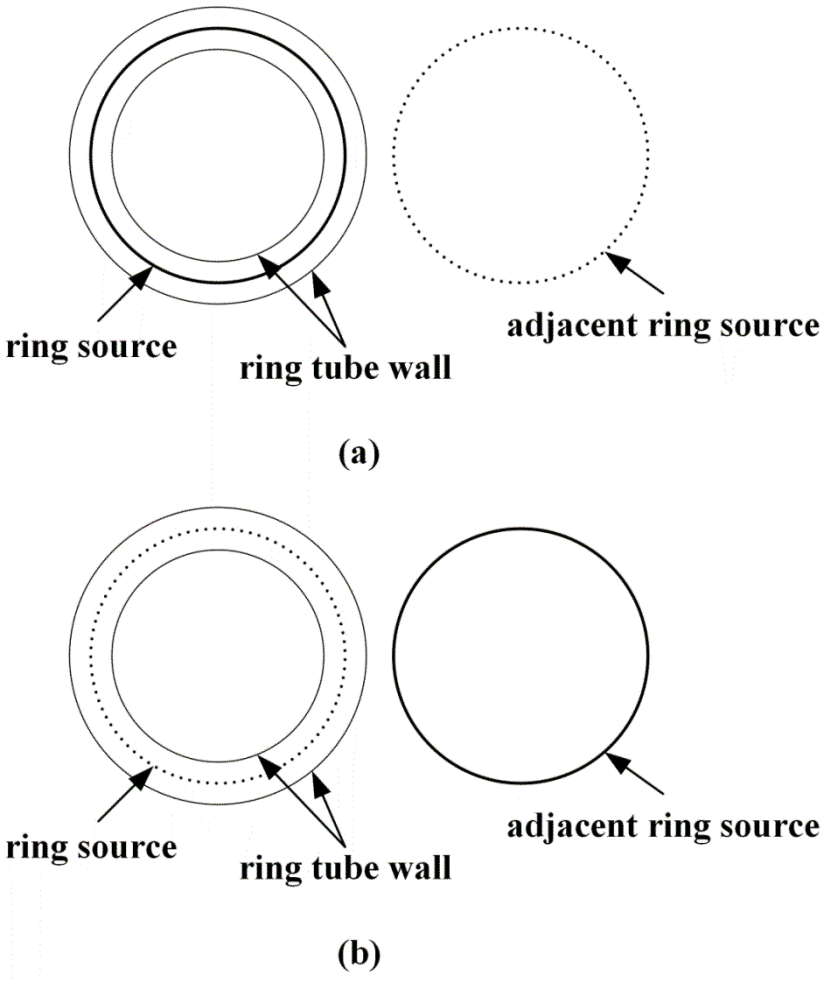

Figure 2.4: (a) Ring Tube Wall Temperature Response to This Ring Tube (b) Ring Tube Wall Temperature Response to Adjacent Ring Source

Regarding part (a), since the ring tube and ring source share the same center, the temperature variation of any cross-section of the tube is the same, as Figure 2.5 shows. The coordinates of the cross-section can be written as $[(r_0 + r_t \cos\gamma), 0, (r_t \sin\gamma - z')]$. Therefore, by integrating the single ring source solution along one cross-section, the solution to part (a) can be derived:

$$\Theta_{sf-sa}(R, F_o) = \frac{1}{2\pi}\int_0^{2\pi} \Theta_{sf}(R, Z, F_o)\, d\gamma \tag{2.18}$$

where:

$$R = \frac{r}{r_0} = \frac{r_0 + r_t \cos\gamma}{r_0}, (0 \le \gamma \le 2\pi)$$

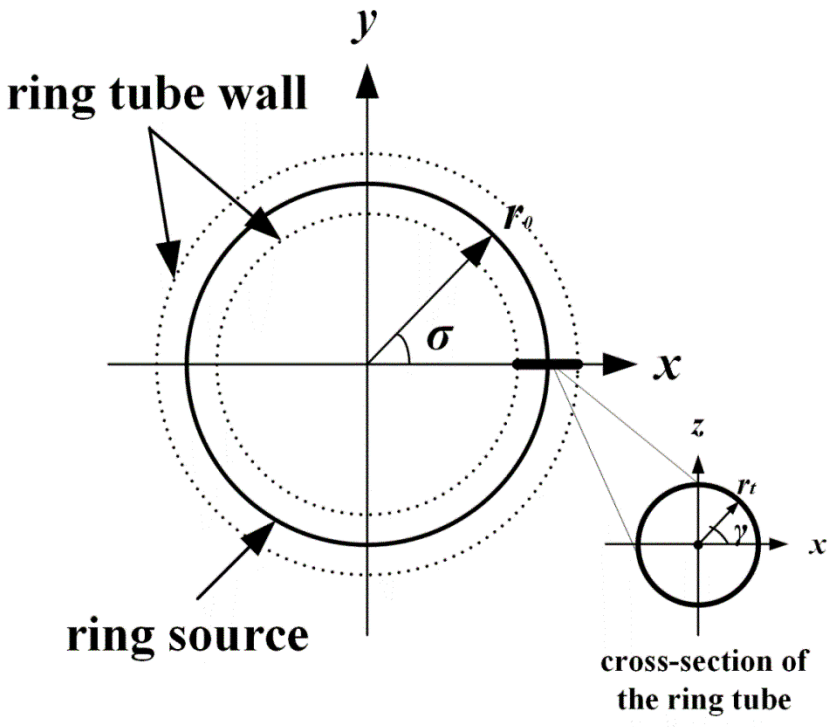

Figure 2.5: A Cross-section Represents the Whole Ring Tube in Calculating Mean Tube Wall Temperature Response of This Ring

For part (b), the diameter of the tube is neglected since the interval of the adjacent rings is considered much larger than the diameter of the tube. Therefore, the mean temperature variation

of the tube wall surface caused by the adjacent ring source is represented by the mean temperature variation of the centerline, as Figure 2.6 demonstrates. The solution for part (b) is then derived as:

$$\Theta_{sf-RSj,i}(R, F_o) = \frac{1}{2\pi}\int_0^{2\pi} \Theta_{sf}(R, Z, F_o)\, d\omega \tag{2.19}$$

where:

$$R = \frac{r}{r_0} = \frac{\sqrt{(x_j + r_0 \cos\omega)^2 + (y_j + r_0 \sin\omega)^2}}{r_0}, (0 \le \omega \le 2\pi)$$

Therefore, if a Slinky^{TM} GHX consists of *n* rings, then the mean tube wall temperature variation of ring *j* among these rings can be calculated based on the principle of superposition:

$$\Theta_{sf-RSj}(R, F_o) = \Theta_{sf-sa}(R, F_o) + \sum_{i=0, i\neq j}^{n-1} \Theta_{sf-RSj,i}(R_i, F_o) \tag{2.20}$$

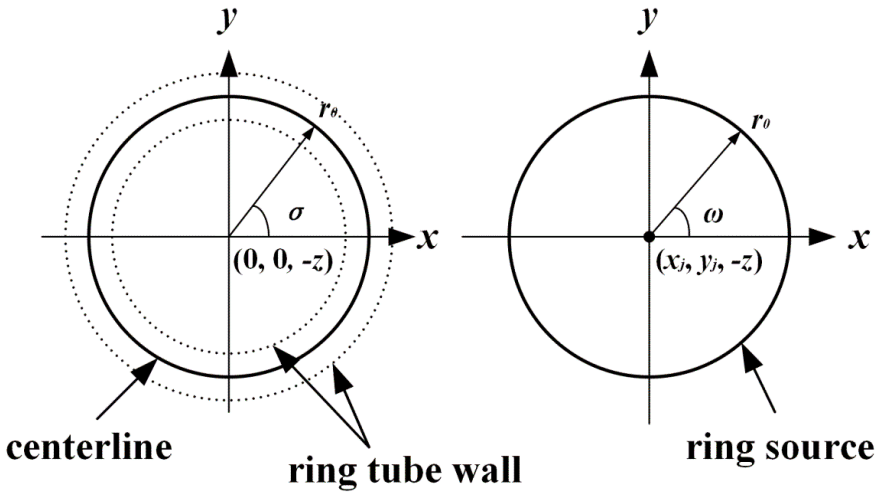

Figure 2.6: A Centerline Represents the Ring Tube in Calculating the Temperature Influence of Adjacent Ring Source

An experiment was conducted to verify the multiple-ring-source theory (Li et al. 2012). A well-insulated steel box was used in the experiment to created adiabatic boundary conditions. The temperature variation caused by a Slinky™ heater placed in the box is used to examine the validity of the multiple-ring-source theory. The soil temperature calculated using the multiple-ring-source model is compared with the measured data of temperature sensors buried around the Slinky™ heater. A fast algorithm was introduced to shorten the computation time. When the distance between two rings is far enough compared with the ring's radius, the temperature variation of ring 1 due to ring 2 can be considered as the variation at a point, whose distance to ring 2's center is the average value of all points on ring 1.

2.2 Numerical GHX Models

2.2.1 Numerical Models for GHXs with Straight Tubes

While line source theory has been widely adopted in modeling GHXs with straight tubes or boreholes, the simplifications of the original heat and mass transfer problem result in the neglect of several important issues, such as: moisture transport in the ground, ground freezing and the ground surface effect. Compared with the analytical line source approach, the numerical approaches usually give a better approximation of the ground heat and mass transfer process. Therefore, numerical models for GHXs usually contribute to a more comprehensive analysis of GSHP systems. Several numerical models for HGHXs with straight tubes will be discussed in this section.

Mei (1986) proposed three numerical models for: (a) single buried coil with ground freezing, (b) single buried coil with seasonal ground temperature variation, and (c) two vertical parallel buried coils with thermal interference. All these models were validated against the field experimental data.

The first model presented in Mei's (1986) work is a two-dimensional model with a radially symmetrical temperature profile. While the axial heat transfer of the soil domain is ignored, the axial fluid temperature variation is captured by calculating the fluid temperature of each cross-section. The effect of soil freezing around a buried pipe in considered in this model. The whole domain of heat transfer is divided into fluid region, pipe wall region, frozen soil region and nonfrozen soil region, as Figure 2.7 shows.

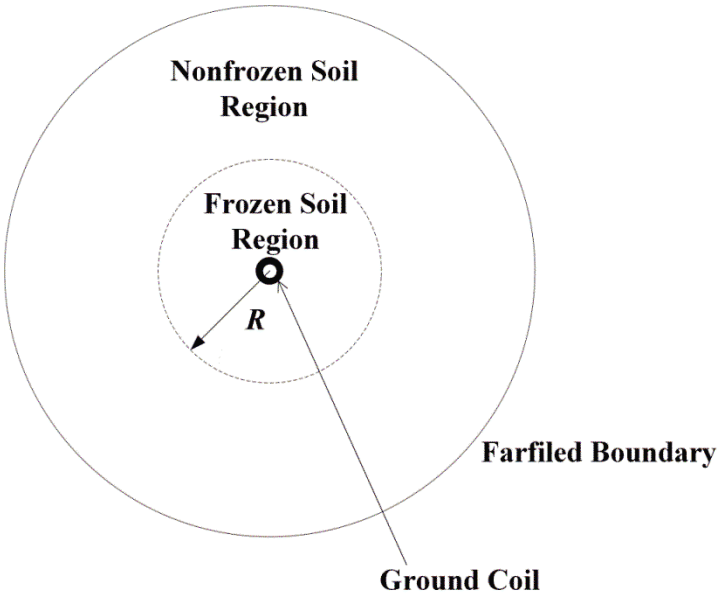

Figure 2.7: Schematic of Mei's (1986) First Model Considering Soil Freezing

The frozen soil region has different thermal conductivity and capacity with the nonfrozen soil region. The boundary between frozen and nonfrozen regions has an identical temperature (0°C (32°F) or the actual ground moisture frozen temperature). The location of this boundary is varying and determined according to this ground moisture frozen temperature. The governing equation of the boundary between frozen and nonfrozen regions is given, which takes account of the latent heat brought by the soil freezing process.

$$k_{fs}\frac{\partial T_{fs}}{\partial r}|_R - k_s\frac{\partial T_s}{\partial r}|_R = \rho_s ML\frac{dR}{dt} \tag{2.21}$$

where:

T_{fs} is the temperature of the soil-frozen region, in °C or °F,

T_s is the temperature of the nonfrozen region, in °C or °F,

k_{fs} is the thermal conductivity of the soil-frozen region, in W/m·K or Btu/h·ft·°F,

k_s is the thermal conductivity of the nonfrozen region, in m^2/s or ft^2/h,

t is time, in s,

r is the radial coordinate, in m or ft,

M is the moisture content, in (kg H_2O)/ (kg dry soil) or (lb H_2O)/ (lb dry soil),

L is the latent heat, in J/kg H_2O or Btu/lb H_2O,

R is the radius of the boundary between frozen and nonfrozen regions in cylindrical coordinate, in m or ft

In this model, the coil is considered buried far enough from the ground surface so that the near-surface effect can be ignored. The far-field boundary temperature uses the undisturbed ground temperature at the tube buried depth. Therefore, the whole temperature profile is kept radially symmetrical. This is an important simplification, which makes it feasible to determine the frozen region due to its symmetry. The Kusuda and Achenbach (1965) model is adopted in calculating the undisturbed ground temperature. The initial temperature of the fluid, the tube and the ground is also calculated by using the Kusuda and Achenbach (1965) model. The cyclic operating behavior of the heat pump system is considered in the model. When the system is off, the fluid temperature is assumed equal to the coil wall temperature.

The explicit finite-difference method is used to solve the model. A fixed spacing is used in the axial direction to generate the fluid and pipe wall nodes. Then in the cross-section showed in Figure 2.7, only a one-dimensional grid (radial) is needed due to the symmetry. The spacing of nodes in the nonfrozen soil region can set as unequal, increased along the radial direction. Two types of time steps are applied in the model. While the short time step is used in simulating the temperature profile of the fluid, pipe wall and frozen soil region, the long time step is used in the nonfrozen region.

Field validation of Mei's (1986) first model was performed, followed by parametric studies. Both the field validation and the parametric studies indicate that the ice forming around the buried pipe has relatively minor effect on its thermal performance. Only if the entering fluid temperature is much lower than the soil freezing point, will the effect possibly become significant. However, since most GSHP systems require that the flowing fluid is kept above -4°C (25°F), this situation is unlikely to happen.

Compared with the first model, the second model presented by Mei (1986) focuses on the near-surface effect. Instead of assuming deep buried depth, the tube is placed near the ground surface. The radius of the far-field boundary is the buried depth of the tube, as Figure 2.8 shows.

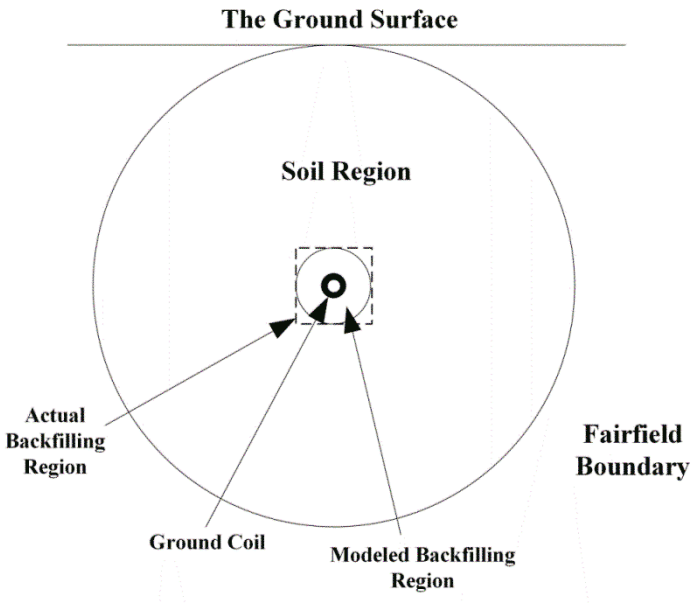

Figure 2.8: Schematic of Mei's (1986) Second Model Considering Seasonal Ground Temperature Variation

The effect of backfilling material around the buried pipe has been considered in the model. The energy balance equations of the second model are similar to the first model, except that the freezing process is ignored. At the far-field boundary, instead of using one uniform undisturbed ground temperature, the far-field boundary temperature is calculated according to the depth of the node by using the Kusuda and Achenbach (1965) model. Therefore, while the soil temperature is only the function of the radius and the distance along the coil in the first model, the soil temperature is also varying in the angular direction in the second model (fully two-dimensional).

The third model of Mei (1986) is a mathematical model for two buried coils. The thermal interference between the two coils is investigated in this model. As Figure 2.9 shows, two coils are buried in the same trench, one placed on the top of other.

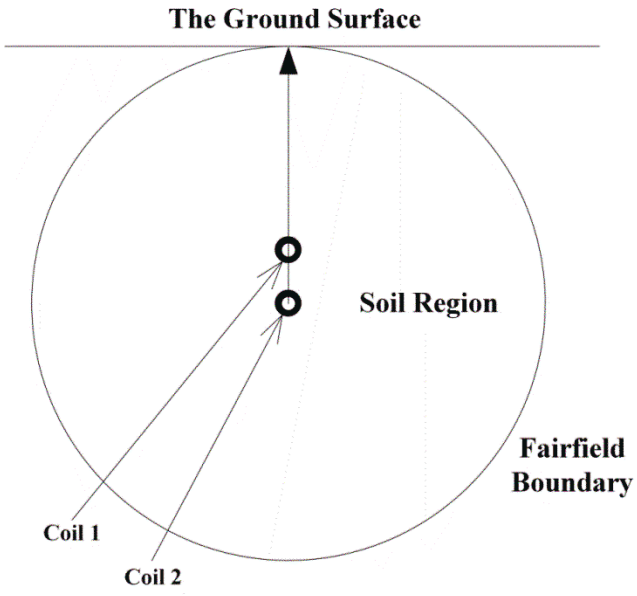

Figure 2.9: Schematic of Mei's (1986) Third Model Considering Thermal Interference

The governing equations of the model are similar to the equations of the second model. The radial coordinate system is still applied in this model with lower coil as its center. The radius of the far-field boundary is the depth of the lower pipe. The validation of this model indicates a clear effect of thermal interference between two coils.

Overall, the three numerical models presented in Mei's (1986) work are complements to previous line source models. In the comparison with the line source models (Mertz 1983; Kalman 1980), the numerical models are proved to have better prediction of the fluid temperature. However, Mei's (1986) models lack generality. Only single tube and vertical parallel double tube systems are considered in the models. The two main improvements to analytical models, the modeling of the soil freezing effect and the near-surface effect, cannot be included in one model. In addition, to account for the near-surface effect, Mei (1986) relies on the Kusuda and Achenbach (1965) model to calculate ground surface temperature variation and the undisturbed ground temperature. However, the usage of the Kusuda and Achenbach (1965) model is based on the published parameters for only limited sites. In the validation, Mei (1986) also indicates that the undisturbed

ground temperature predicted by the Kusuda and Achenbach (1965) model is too low when compared to the measured data.

Based on Mei's (1986) models, Piechowski (1999) developed another numerical model. Similar to Mei's (1986) models, the heat and mass transfer of the soil and tube wall is discussed in two-dimensional cross-sections. The axial heat and mass transfer of the soil and pipe wall is neglected. By calculating the temperature of the fluid node in a series of these cross-sections along the buried pipe, the fluid temperature profile can be obtained. Compared with Mei's (1986) models, Piechowski's (1999) model has two main improvements.

First, the mass transfer phenomenon is included in the model. The mass transfer here may refer to moisture migration. During the summer operation, the soil temperature around the buried pipe may increase significantly due to the heat rejection, which results in the moisture migration. As the result of moisture migration, the soil around buried tube is dried out. This can affect the performance of the GHX severely. Therefore, the proper modeling of moisture migration is of importance for the cooling operation of GSHP systems. While this model is developed to simulate the cooling operation, the freezing effect is ignored in the model.

Second, the two-coordinate approach is applied in solving the governing equations, as Figure 2.10 shows. Cylindrical coordinates are used in the vicinity of the tube surface (0.15 m (0.5 ft)) with an intensive grid. Since the steepest temperature gradient happens at the interface between soil and tube, the application of cylindrical and intensive grid can guarantee the accuracy of the model. Cartesian coordinates is applied in the remaining soil region with a coarse grid. Because of small temperature gradients in this region, the larger size cells can reduce computation time without the loss of accuracy. In addition, Cartesian coordinates have an advantage over cylindrical coordinate in modeling the interference between tubes. The boundary conditions in Piechowski's (1999) model are different with the boundary conditions in Mei's (1986) model.

The ground surface is treated as the convective type boundary. The other three boundaries are deemed as Dirichlet type boundaries. The temperatures of these three boundaries are assigned with the undisturbed ground temperature, which can be calculated by the Kusuda and Achenbach (1965) model.

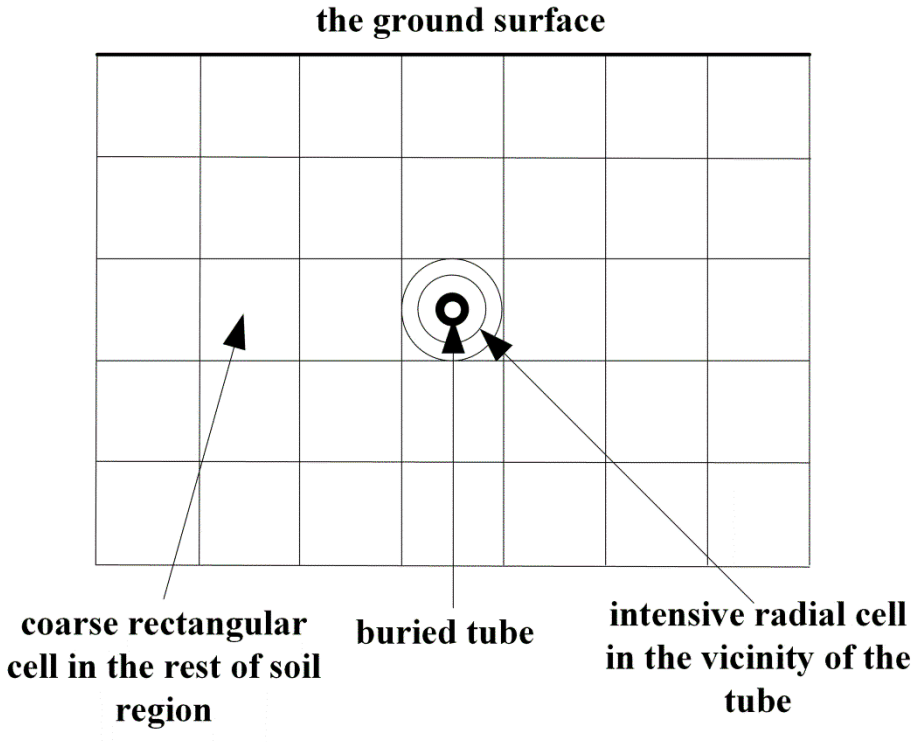

Figure 2.10: Schematic of the Discretization of the Soil Region in Two Coordinates

Xing (2010) proposed an explicit two-dimensional finite volume model for foundation heat exchangers (FHXs). FHXs are a new type GHXs that takes advantage of the existing excavations around the basement of a building during its construction period, which could reduce the excavation cost of trenches. A non-uniform rectangular grid is used in this model. The cells near the ground surface and the tubes are smaller. The tubes are represented as square areas that have the same size as the smallest cell. Instead of assuming single cell holding one tube, one fictitious rectangular tube is shared by four cells. In the previous numerical models, the ground surface is treated as either the convective type boundary (Piechowski 1999) or the far field boundary whose

temperature vary over time (Mei 1987). In this model, a detailed ground surface heat balance is applied, including the convection (Antonopoulos 2006), the incident short wave radiation (Walter et al. 2005), the net long wave radiation (Walter et al. 2005), and the evapotranspiration (Walter et al. 2005). Similar to the previous models (Mei 1987; Piechowski 1999), the Kusuda and Achenbach (1965) model is used to calculate the initial and lower boundary conditions.

Based on the Piechowski's (1999) model, Lee et al. (2013) presented a numerical model that can be applied in modeling both HGHXs and FHXs. The optimized grid scheme in Lee et al.'s (2013) model combine the merits of the grid schemes of the previous models (Piechowski 1999; Xing 2010). The vicinity of the pipe use radial cells while the non-uniform rectangular cells are applied in the rest of the soil region. The interference between GHXs and the basement wall or floor of a building is captured in this model by integrating the soil domain heat transfer with the zone heat balance. The model was implemented in the whole building simulation software EnergyPlus. The quasi-3D soil domain simulation is coupled with the fluid loop solver of EnergyPlus. The parametric study indicates that a coarse grid can guarantee the accuracy of the model. Compared to the number of cells in the previous two-dimensional model (Xing 2010), the number of cells in this three-dimensional model is much less. The soil moisture migration is ignored in this model. Both component-level and system level validation of this model were performed. In the component-level validation, the measured inlet fluid temperature at each time step is used as an input. The predicted outlet fluid temperature is compared to the measured data over the whole year, with a mean error of 0.3°C (0.54°F). In the system-level validation, the heat loads on the GHX calculated from measured data are used as the inputs instead of the inlet fluid temperatures. Because of this, any inaccuracy of the soil temperature response to the reject/extract heat will accumulate over time. In this case, the mean bias error in predicting the outlet fluid temperature is 1.3°C (2.3°F).

2.2.2 Numerical Models for GHXs with Coiled Tubes

Bi et al. (2002) proposed a numerical model for vertical double spiral coil (VDSC) GHXs. The model is cast for situations when there is only one VDSC or the interaction between VDSCs can be ignored. By taking advantage of the symmetry of VDSC, the complex three-dimensional heat conduction problem is transferred into a two-dimensional problem, as Figure 2.11 shows.

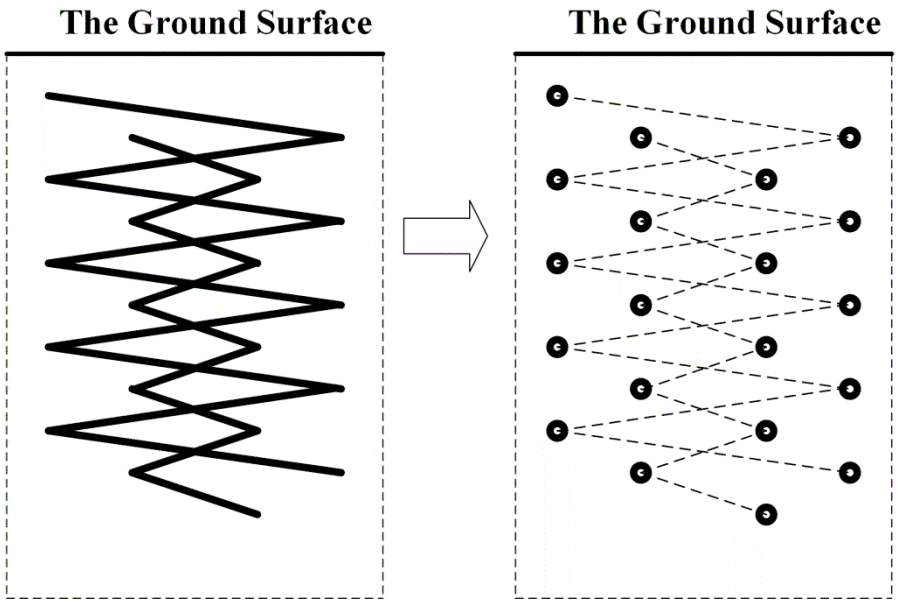

Figure 2.11: Schematic of the Simplification of the Three-dimensional VDSC Heat Conduction Problem

The top (ground surface), bottom, and right boundary are treated as Dirichelet type boundaries assigned with undisturbed ground temperature. The left boundary is treated as an adiabatic boundary since it is the symmetrical line. The cells that hold the coil are considered with an internal heat reservoir. The governing equation is given in cylindrical coordinate as:

$$\rho_s c_p \frac{\partial T}{\partial t} = \frac{\partial}{\partial z}\left(k\frac{\partial T}{\partial z}\right) + \frac{1}{r}\frac{\partial}{\partial r}\left(rk\frac{\partial T}{\partial r}\right) + S \tag{2.22}$$

where:

S is the generalized internal heat reservoir rate, in W/m^3 or Btu/h·ft^3,

ρ_s is the soil density, in kg/m^3 or lb/ft^3,

c_p is the specific heat of the ground, in J/kg·K or Btu/lbm·°F,

T is the ground temperature variation, in °C or °F,

r is the radial coordinate, in m or ft,

z is the axial coordinate, in m or ft,

k is the ground thermal conductivity, in W/m·K or Btu/h·ft·°F

Similar to line source models, the heat flux along the VDSC is assumed uniform. A detailed discussion of the heat transfer between coil tube and the fluid is absent in this work.

2.3 Numerical Simulations and Experimental Studies of Slinky™ GHXs

Wu et al. (2010) conducted both numerical and experimental research on Slinky™ GHXs. Three-dimensional numerical simulations of Slinky™ GHXs were performed using commercial CFD software. Due to the symmetry, only half of the Slinky™ loop is modeled. The simulated ground temperature distribution is validated against the measured data of a field experiment. The validated CFD model is then used to study the thermal performance of Slinky™ GHXs. The comparison with the straight tube HGHX indicates the Slinky™ GHX has better efficiency with the same trench space. In addition, parametric studies were performed to investigate the effect of different loop diameters and loop pitches on the performance of the Slinky™ GHXs.

While Wu et al.'s (2010) numerical study focuses on the short-term (140 hours) thermal performances of Slinky™ GHXs, Chong et al. (2013) presented a numerical study with the consideration of the long-term operations (60 days). Similar to Wu et al.'s (2010) work, a 3-D CFD model is built for the parametric analysis. The ground surface is set as a convective type

boundary with a wind speed of 3 m/s (9.84 ft/s) and ambient air temperature at 5°C (41°F). The temperature variation at the ground surface is therefore not considered. In this model, only one or two loops of a Slinky™ GHX are modeled by using the numerical simulator due to the computation burden. Therefore, the thermal interactions between loops are ignored or partially ignored. This CFD model is applied to simulate the Slinky™ GHXs with different parameters, namely, five different loop pitches, three different loop diameters, and three different soil thermal properties. As the results of the numerical simulations, the heat extraction rates per trench length at the equilibrium state (60^{th} day) for different cases are calculated. These heat extraction rates are used to determine the required sizes of the GHXs to meet the heating load of a 2-story house. After the sizes are determined, the corresponding amount of excavation work and pipe material can be determined and compared. The comparisons show that the different loop diameters and loop pitches can result in either more excavation work or a larger amount of pipe material. Soil thermal properties are of great importance for the thermal performance of a Slinky™ GHX. In addition, the cyclic operation of a GSHP system can largely increase the heat transfer rate when compared to the continuous operation.

As mentioned at the beginning of this chapter, Fujii et al. (2012) presented another study of Slinky™ GHXs. In this study, Slinky™ GHXs were simulated by using a finite-element simulator. In the numerical simulations, the Slinky™ GHX is modeled as a thin plate. The size of the thin plate is determined by keeping the flow volume and the trench size the same as the Slinky™ tube's values. However, in this case, the surface area of the thin plate heat exchanger is much larger than the Slinky™ GHX's surface area. To solve this, the thermal conductivity of the tube is reduced to account for the extra surface areas. A relationship between the modified thermal conductivity and the loop pitch was derived. The numerical simulation results were validated against the recorded data of three short-term thermal response tests (TRTs) and a long-term air-conditioning (A/C) test.

2.4 Applicability of Previous Work

In the review of previous work in developing mathematical models for GHXs, different approaches are presented and discussed, which can be divided into two main categories: analytical and numerical approaches. These approaches are compared; and their applicability to modeling Slinky^{TM} GHXs are discussed in this section.

Analytical models are based on the integration of the point source solution or Green's function. One significant merit with this type of models is that by integrating with the regard of different space variables, this type of models can be applied to modeling GHXs with various tubing configurations, such as vertical boreholes (Zeng et al. 2002), inclined boreholes (Cui et al. 22006), horizontal straight tubing (Fontaine et al. 2011), spiral tubing (Man et al. 2010; Cui et al. 2011; Man et al. 2011), and Slinky^{TM} tubing (Li et al. 2012) systems. Such flexibility of the analytical approach enables modeling complex tubing systems, such as the coiled tubing systems. In addition, by using the analytical approach, the thermal interferences between tubes or tubing systems can be modeled with a reasonable increase in computation time. In real applications, a compact tubing configuration may be adopted due to the restriction of available land area or the demands in reducing the excavation work. In this case, the thermal interference between tubes or tubing systems are significant for the thermal performance of the GHXs, especially for the long-term performance.

Based on the discussion above, the analytical approach is considered to be a feasible approach in modeling a Slinky^{TM} GHX and will be used to develop the model in this study. The analytical solution of ring source model will give the ground temperature at any point in the ground. By assuming the temperature of the tube wall is equal to the temperature of its contact soil, the solution of the tube wall temperature can be obtained. However, for a component model that will be embedded in a whole-building simulation environment, two issues need to be addressed after

obtaining the analytical solution. The first is applying the analytical solution in the short, variable time-step simulation environment. According to the superposition principle, the tube wall temperature response to the variable heat transfer load can be calculated by superimposing the temperature response to piecewise constant heat input at each time step. For annual simulations with short time steps (less than an hour), it is impractical to directly apply the analytical solution in calculating the tube wall temperature response at every time step. Eskilson's (1987) approach to this problem is the *g-function* method. A series of non-dimensional temperature response factors are used to describe the thermal behavior of a GHX. Based on the *g-function* value calculated by the interpolation between these factors, the tube wall temperature response at any desired time step can be calculated. The Eskilson (1987) approach is applied in this study.

The second issue is coupling to fluid loop simulation engine. In a whole-system simulation, the energy transfer between plant components is captured based on the change of fluid state. For a component model that is a part of the condenser loop, the model input is normally inlet fluid state; and the heat transfer rate is calculated as an output. However, for analytical GHX models, the calculations of the tube wall temperature are based on the heat inputs. The Yavuzturk and Spitler (1999) model provides a practicle method to solve this problem. By assuming the average fluid temperature as the average value of the entering and exiting temperature, the energy balance equations can be solved simultaneously. The heat transfer rate, tube wall temperature as well as exiting fluid temperature can be calculated, with the knowledge of the entering fluid temperature. Man et al.'s (2011) work applied a similar method to address these two issues for the pile GHX model. The temperature response function is named *p-function* in their work.

Due to Slinky^{TM} GHXs' comparatively shallow buried depth, the effect of the ground surface heat balance should be accounted for in the model. For the analytical approach, the effect of the ground surface temperature variation can be considered by superimposing the undisturbed ground temperature at each time step. However, with the consideration of a detailed heat balance at the

ground surface, the calculation of the undisturbed ground temperature relies on the numerical method, since the superposition principle is no longer valid for the non-linear boundary condition. According to the literature review, Lee et al. (2013) and Lee (2013) present a numerical model for straight tube HGHX with the application of the detailed ground surface heat balance. For this study, Lee et al. and Lee's (2013) model is modified to calculate the undisturbed ground temperature, without consideration of buried tubing or basement walls.

In conclusion, to cast a mathematical model for Slinky^{TM} GHXs, both analytical and numerical methods need to be applied. An analytical approach similar to Li et al.'s (2012) ring source model will be used derive the solution of the mean tube wall temperature. While Li et al.'s (2012) work focuses on sizing the system; the objective of this study is to present a Slinky^{TM} GHX model that is suitable for implementing as a component model in a whole-building energy simulation environment. Therefore, several features that will distinguish this work from Li et al.'s (2012) work are anticipated to be included in the model:

1. More generalized, straightforward solutions of the mean tube wall temperature are derived for Slinky^{TM} GHXs. The analytical solutions for both horizontal and vertical Slinky^{TM} GHXs are given. Li et al.'s (2012) choice of dual coordinate system requires unnecessary mapping between cylindrical and Cartesian coordinates, analytical solutions in this work are derived in a single coordinate system. According to Li et al.'s (2012) work, the calculations of the thermal interactions between rings neglect the tube diameter, which may affect the accuracy of the results when there are many overlaps between ring tubes. In our work, the effect of the tube diameter is considered.
2. The concept of temperature response function for Slinky^{TM} GHXs is introduced. A set of temperature response factors are calculated based on the derived analytical solutions. In Li et al.'s (2012) work, to deal with the variable heat transfer rate, the analytical solution is directly applied to calculate the tube wall temperature response at each time step. This

algorithm is not applicable for the whole-building energy simulation environment, which usually involve thousands of time steps in one simulation. In our model, temperature response factors are used to calculate the tube wall temperature response at each time step. The calculations of the complex analytical solutions of the temperature response function at each step are replaced with the interpolation between temperature response factors.

3. The model in this thesis is formulated to calculate exiting fluid temperature and heat transfer rate, with the knowledge of entering fluid temperature. In Li et al.'s (2012) model, the calculations of tube wall temperature and exiting fluid temperature are based on the knowledge of the heat transfer rate. However, as discussed above, for an energy simulation model, the heat transfer rate is usually an output instead of an input.
4. The detailed ground surface heat balance is included in our model based on Lee et al.'s (2013) numerical method. In Li et al.'s (2012) model, the ground surface is assumed to be either an isothermal surface for warm regions or an isothermal surface for cold regions. As mentioned above, for the purpose of energy simulation, the ground surface heat balance has a significant effect on the simulation results and must be included in the model.

CHAPTER 3

DEVELOPMENT OF A SLINKY™ GHX MODEL

3.1 Ring Source Model and Its Analytical Solutions

In the ring source model, the configuration of a typical Slinky™ tube is simplified as a series of connected rings, as Figure 3.1 shows.

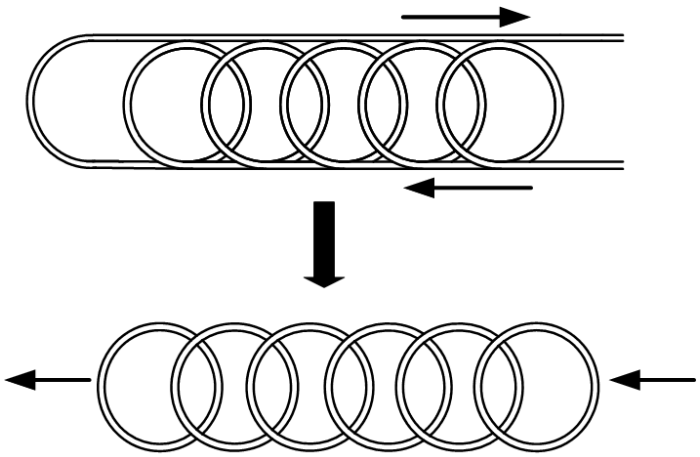

Figure 3.1: Simplification of a Slinky™ Tube

Several assumptions are made:

- The GHXs in a Slinky™ GHX field have uniform heat fluxs.
- The ground is treated as a semi-infinite homogenous medium.
- The thermal storage and thickness of the tube wall is neglected.

- The influence of the soil moisture transfer on the heat transfer is neglected.
- The soil freezing around the tubes is neglected.
- One Slinky^{TM} GHX field has only one pitch. In addition, for a given Slinky^{TM} GHX field, the model supports a single distance between the GHXs and only one GHX tube length.

3.1.1 Description of the Model

The principle of superposition serves as the basis for this ring source model. It is valid for the heat conduction process with linear boundary conditions and governing equation (Claesson and Dunand 1983). For the ring source model, the complicated heat transfer process of the buried coiled tubing is considered as the superposition of two independent elementary heat transfer processes, as Figure 3.2 shows.

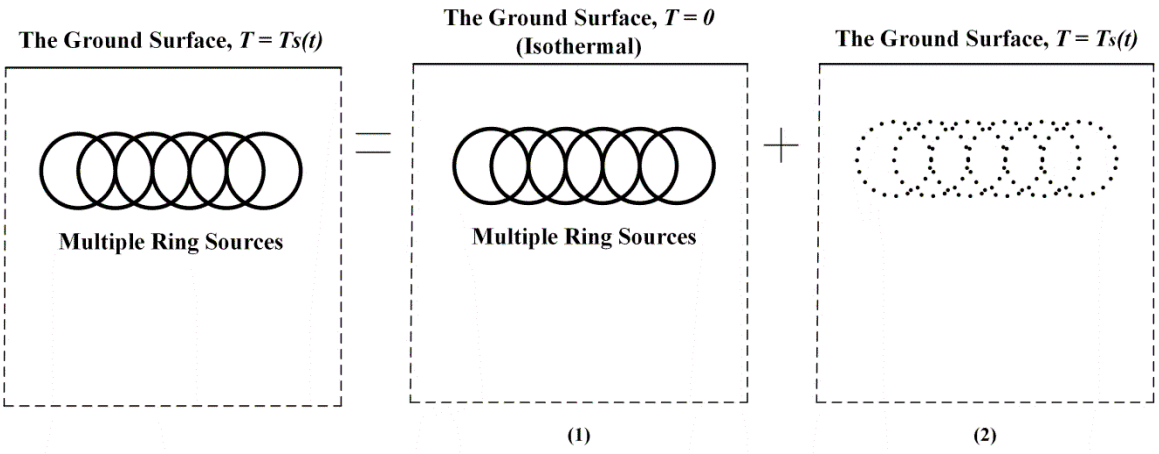

Figure 3.2: Schematic of the Slinky^{TM} GHX model

One is the heat transfer process of multiple ring sources in a semi-infinite medium with isothermal boundary. The other is the heat transfer process of a semi-infinite medium with changing boundary temperature. Therefore, to calculate the temperature variation of the ground, we need to consider the ground temperature variation due to multiple ring sources as well as the undisturbed ground temperature variation due to the changing ground surface temperature.

3.1.2 Solutions for Horizontal Slinky™ GHXs

The solution of the continuous point source gives the temperature variation at distance *d* after time *t*, due to a point source emitting continuously *q* units of heat per unit of time from *t*=0 onwards. The continous point source solution is given in Marcotte and Pasquier (2009) in the following form:

$$\Delta T(d,t) = \frac{q}{4\pi kd} erfc(\frac{d}{\sqrt{4\alpha t}}) \tag{3.1}$$

where:

T is the temperature variation, in °C or °F,

t is time, in s,

q is the quantity of heat, in W or Btu/h,

d is the distance from the point source, in m or ft,

k is the ground thermal conductivity, in W/m·K or Btu/h·ft·°F,

α is the ground thermal diffusivity, in m^2/s or ft^2/h,

erfc is the complementary error function

Marcotte and Pasquier (2009) gave the derivation of the finite line source solution from the point source solution. Applying the similar method, the ring source solutions for Slinky™ GHXs are derived. The solutions cover both horizontal and vertical Slinky™ GHXs, with one or multiple Slinky™ heat exchangers (E.g. interference between two nearby heat exchangers can be analyzed). In the subsequent discussion, an individual ring will be labeled as ring *i* or ring *j*.

As Figure 3.3 shows, point P_i is a fictitious representative point of a cross-section of ring tube i at angle φ. The distance between fictitious point P_i and point P_j is the average value of the distance between the outer point P_{io} and point P_j and the distance between the inner point P_{ii} and point P_j. Since the distance is the only changing variable, the average temperature perturbation of the cross-section is assumed as the temperature perturbation of the fictitious representative point P_i. Specially, when i is equal to j, the dashed line in Figure 3.3 shows the ring source of ring i itself. x_0 and y_0 are Cartesian coordinates of a ring's center. x_0 and y_0 are calculated based on the parameters of the Slinky™ GHX such as the pitch, the distance between Slinky™ tubes, and the ring diameter.

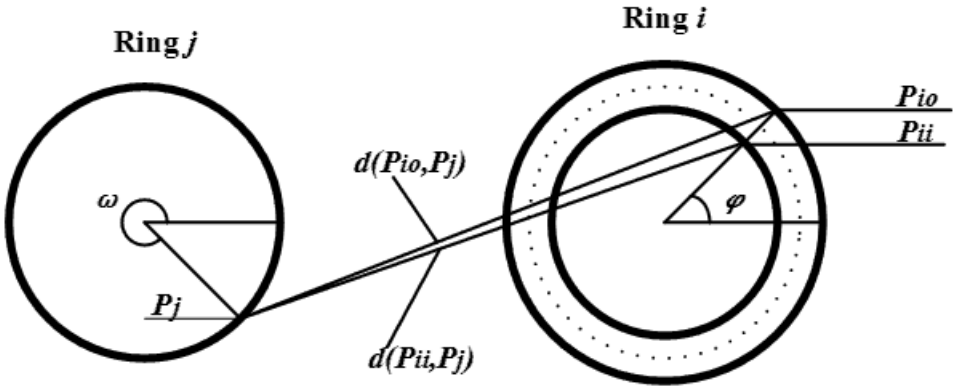

Figure 3.3: Distance between Fictitious Point P_i and Point P_j on Ring Source j

Assuming q_l is the heat input rate per trench length, then for a point source P_j on ring j, the intensity of heat input for the point source is $N_{tube} \cdot q_l \cdot L \cdot d\omega/(N_{ring} \cdot 2\pi)$. A large number of such point sources located along ring j constitute a ring source. The effect of this ring source can be viewed as the summation of the effect of these point sources. The temperature perturbation at point P_i caused by ring source j is then calculated by integrating the results of the point sources on ring j.

$$\Delta T(P_i, t) = \frac{q_l L N_{tube}}{8\pi^2 k N_{ring}} \int_0^{2\pi} \frac{erfc\left[d\left(P_j, P_i\right)/2\sqrt{\alpha t}\right]}{d(P_j, P_i)} d\omega \tag{3.2}$$

where:

$$d\left(P_j, P_i\right) = \frac{d\left(P_{ii}, P_j\right) + d\left(P_{io}, P_j\right)}{2}$$

$$d\left(P_{ii}, P_j\right)$$

$$= \sqrt{\left[x_{0i} + (R - r)\cos\varphi - x_{0j} - R\cos\omega\right]^2 + \left[y_{0i} + (R - r)\sin\varphi - y_{0j} - R\sin\omega\right]^2}$$

$$d\left(P_{io}, P_j\right) =$$

$$\sqrt{\left[x_{0i} + (R + r)\cos\varphi - x_{0j} - R\cos\omega\right]^2 + \left[y_{0i} + (R + r)\sin\varphi - y_{0j} - R\sin\omega\right]^2}$$

ΔT is the temperature variation, in °C or °F,

t is time, in s,

d is the distance between two points, in m or ft,

k is the ground thermal conductivity, in W/m·K or Btu/h·ft·°F,

α is the ground thermal diffusivity, in m^2/s or ft^2/h,

q_l is the heat rate per trench length, in W/m or Btu/h·ft,

L is the trench length, in m or ft,

N_{tube} is the number of Slinky™ tubes,

N_{ring} is the number of rings,

R is the radius of ring,

r is the radius of tube,

ω,φ is the angular parameter, in rad

x_{0i}, y_{0i} is the Cartesian coordinates of the center of ring i

x_{0j}, y_{0j} is the Cartesian coordinates of the center of ring j

As we discussed above, for Slinky^{TM} tubing buried underground, one elementary heat transfer process can be deemed as happening in a semi-infinite medium with isothermal boundary condition. The solution for this case is obtained by applying the method of images. A fictitious ring source j' is created for ring j, as Figure 3.4 shows.

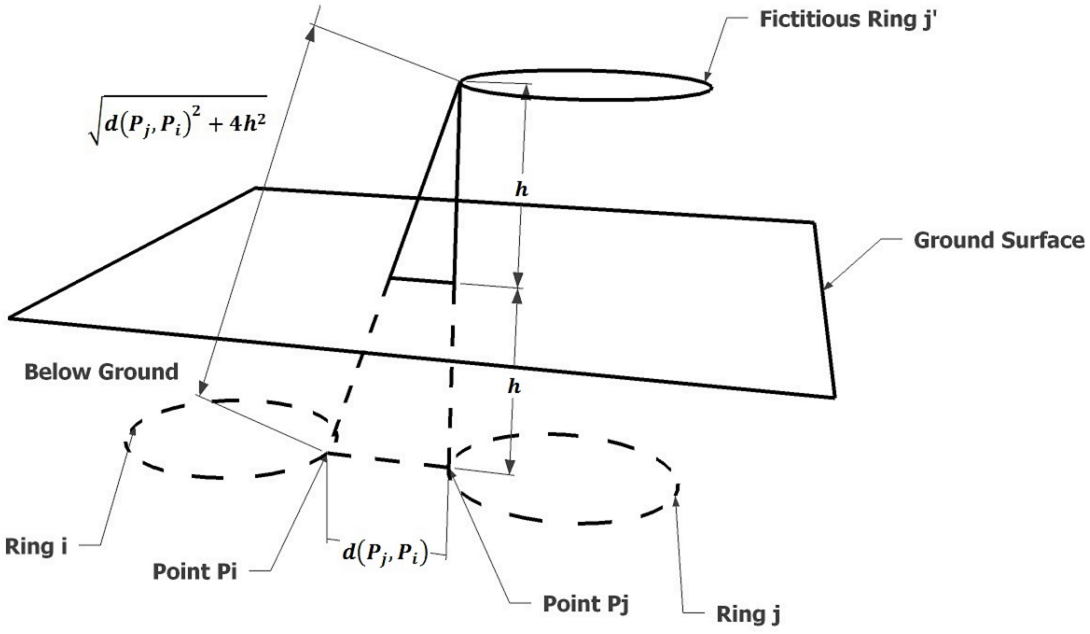

Figure 3.4: Three-dimensional View of Fictitious Ring Source of Ring j

For horizontal Slinky^{TM} GHXs, the fictitious ring source j' is located a distance $2h$ above the ring source j and has the same heat input rateand the opposite sign. Equation 3.2 is revised to include

the thermal effect of the fictitious ring source on the point. The distance between $P_{j'}$ and P_i can be expressed as $\sqrt{d(P_j,P_i)^2+4h^2}$. Then the revised solution is given as:

$$\Delta T(P_i,t)=\frac{q_l L N_{tube}}{8\pi^2 k N_{ring}}\int_0^{2\pi}\left[\frac{erfc\left(d(P_j,P_i)/2\sqrt{\alpha t}\right)}{d(P_j,P_i)}-\frac{erfc\left(\sqrt{d(P_j,P_i)^2+4h^2}/(2\sqrt{\alpha t})\right)}{\sqrt{d(P_j,P_i)^2+4h^2}}\right]d\omega \tag{3.3}$$

where:

h is the buried depth, in m or ft,

While Equation 3.3 gives the temperature perturbation of the fictitious point P_i (represent a cross-section of ring i), the average temperature perturbation of ring i caused by ring source j can be obtained by integration:

$$\Delta T_{j-i}(t)=\frac{q_l L N_{tube}}{16\pi^3 k N_{ring}}\int_0^{2\pi}\int_0^{2\pi}\left[\frac{erfc\left(d(P_j,P_i)/2\sqrt{\alpha t}\right)}{d(P_j,P_i)}-\frac{erfc\left(\sqrt{d(P_j,P_i)^2+4h^2}/(2\sqrt{\alpha t})\right)}{\sqrt{d(P_j,P_i)^2+4h^2}}\right]d\omega d\varphi \tag{3.4}$$

When i is equal to j, ΔT_{j-i} gives the temperature perturbation of the ring tube wall caused by the ring itself as a ring source. When i doesn't equal j, ΔT_{j-i} counts the thermal influence of ring source j on ring i. When summing up all the ΔT_{j-i} for any two rings, all the thermal interactions

between ring sources are considered. The mean tube wall temperature variation of a Slinky™ GHX can then be computed based on Equation 3.5:

$$\Delta\bar{T}(t) = \frac{1}{N_{ring}} \sum_{i=1}^{N_{ring}} \sum_{j=1}^{N_{ring}} \Delta T_{j-i}(t) \tag{3.5}$$

The *g-function* methodology is an approach proposed by Eskilson (1987) to calculate the vertical borehole wall temperature response. The temperature response of boreholes is converted to a set of non-dimensional temperature response factors, named *g-functions*. The *g-function* method is widely adopted in solving vertical borehole related problem. Follwing the definition of the *g-function*, the temperature response factors for Slinky™ GHXs is defined as:

$$g_s(t) = \frac{2\pi k}{q_l} \Delta\bar{T}(t) \tag{3.6}$$

where:

g_s is the temperature response function for Slinky™ GHXs,

k is the ground thermal conductivity, in W/m·K or Btu/h·ft·°F,

q_l is the heat rate per trench length, in W/m or Btu/h·ft

The reason that we use $2\pi k$ instead of k in Equation 3.6 is to keep consistent with the definition of the *g-function*, though the *g-function* is specific to the application to boreholes. The temperature response functions for a Slinky™ and a vertical GHX can be compared to estimate the differences between the thermal performances of a Slinky™ and a vertical GHX. In addition, since the *g-function* model for vertical GHXs has been implemented in the whole-building energy simulation program, EnergyPlus, as a component, the implementation of this Slinky™ model can incorporate with the existed component module for vertical GHXs, which use a set of temperature

response factors as an input. A temperature response factor is a temperature response function value that corresponds to a given time.

By combining Equations 3.4 to 3.6, the analytical solution of the temperature response function for horizontal Slinky™ GHXs is given as:

$$g_s(t) = \sum_{i=1}^{N_{ring}} \sum_{j=1}^{N_{ring}} \frac{LN_{tube}}{8\pi^2 {N_{ring}}^2} \int_0^{2\pi} \int_0^{2\pi} \left[\frac{erfc\left(d\left(P_j, P_i\right)/2\sqrt{\alpha t}\right)}{d\left(P_j, P_i\right)} - \frac{erfc\left(\sqrt{d\left(P_j, P_i\right)^2 + 4h^2}/(2\sqrt{\alpha t})\right)}{\sqrt{d\left(P_j, P_i\right)^2 + 4h^2}} \right] d\omega d\varphi \tag{3.7}$$

3.1.2 Solutions for Vertical Slinky™ GHXs

For vertical Slinky™ GHXs, the temperature variation at a point P_i caused by ring source j can still be calculated by using Equation 3.2, while the expressions for $d(P_{ii}, P_j)$ and $d(P_{io}, P_j)$ need to be revised, as Figure 3.3 and 3.5 demonstrate. Applying the same method as deriving the solutions for horizontal Slinky™ GHXs, the analytical solution of the temperature response function for vertical Slinky™ GHXs is obtained:

$$g_s(t) = \sum_{i=1}^{N_{ring}} \sum_{j=1}^{N_{ring}} \frac{LN_{tube}}{8\pi^2 {N_{ring}}^2} \int_0^{2\pi} \int_0^{2\pi} \left[\frac{erfc\left(d\left(P_j, P_i\right)/2\sqrt{\alpha t}\right)}{d\left(P_j, P_i\right)} - \frac{erfc\left(d\left(P_{j'}, P_i\right)/2\sqrt{\alpha t}\right)}{d\left(P_{j'}, P_i\right)} \right] d\omega d\varphi \tag{3.8}$$

where:

$$d\left(P_j, P_i\right) = \frac{d\left(P_{ii}, P_j\right) + d\left(P_{io}, P_j\right)}{2}$$

$$d(P_{j'}, P_i) = \frac{d(P_{ii}, P_{j'}) + d(P_{io}, P_{j'})}{2}$$

$$d(P_{ii}, P_j)$$

$$= \sqrt{\left[x_{0i} + (R-r)\cos\varphi - x_{0j} - R\cos\omega\right]^2 + \left[y_{0i} - y_{0j}\right]^2 + \left[z_{0i} + (R-r)\sin\varphi - z_{0j} - R\sin\omega\right]^2}$$

$$d(P_{io}, P_j) =$$

$$\sqrt{\left[x_{0i} + (R+r)\cos\varphi - x_{0j} - R\cos\omega\right]^2 + \left[y_{0i} - y_{0j}\right]^2 + \left[z_{0i} + (R+r)\sin\varphi - z_{0j} - R\sin\omega\right]^2}$$

$$d(P_{ii}, P_{j'})$$

$$= \sqrt{\left[x_{0i} + (R-r)\cos\varphi - x_{0j} - R\cos\omega\right]^2 + \left[y_{0i} - y_{0j}\right]^2 + \left[z_{0i} + (R-r)\sin\varphi - z_{0j} - 2h - R\sin\omega\right]^2}$$

$$d(P_{io}, P_{j'})$$

$$= \sqrt{\left[x_{0i} + (R+r)\cos\varphi - x_{0j} - R\cos\omega\right]^2 + \left[y_{0i} - y_{0j}\right]^2 + \left[z_{0i} + (R+r)\sin\varphi - z_{0j} - 2h - R\sin\omega\right]^2}$$

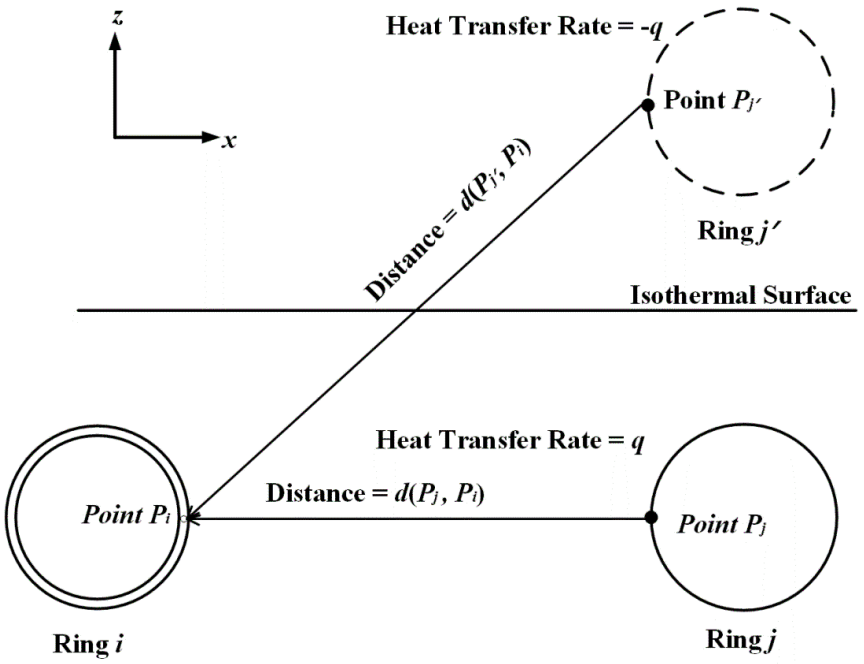

Figure 3.5: Two-dimensional View of the Calculation of the Thermal Interaction between Two Rings for Vertical Slinky™ GHXs

3.2 Calculation of Temperature Response Factors

A computer program is created to calculate temperature response factors for Slinky™ GHXs. The computer program can generate a set of temperature response factors for a given Slinky™ GHX. The generated factors cover the time range from one minute to ten years, which would satisfy most situations for whole-building energy simulations. While vertical borehole simulations are often done for longer periods, horizontal ground heat exchangers, being comparatively close to the surface do not have such long time constants. In simulations, the temperature response function value at any desired time step could be calculated by performing interpolation of the generated factors.

As Equation 3.7 and 3.8 indicate, the calculation of one temperature response factor requires $(N_{ring})^2$ calculations of the double integral. In real applications, the configuration of a Slinky™ GHX may consist of more than a hundred loops (rings). Therefore, computing one temperature

response factor for this Slinky^{TM} GHX requires more than ten thousand calculations of the double integral. Such calculation could be so time consuming that it hinders application of the model in simulation software. To shorten the calculation time of the temperature response factors, three improvements to the algorithm are made.

First, by taking the advantage of symmetry in the Slinky^{TM} GHX configuration, as Figure 3.6 demonstrates for a horizontal Slinky^{TM}, we need only calculate around a quarter of the interactions to get the mean wall temperature perturbation of the whole Slinky^{TM} GHX.

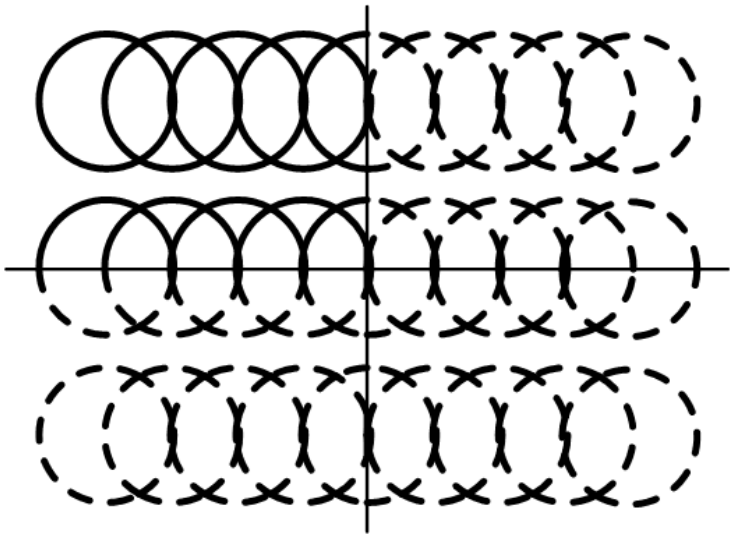

Figure 3.6: Schematic of the First Improvement to the Algorithm: Use of Symmetry

Second, according to Equation 3.4, the interaction effect between two rings decreases exponentially, as the distance increases. Therefore, if the distance between two rings is large enough, neglecting the interaction or calculating it with less accuracy will have little effect on the mean temperature perturbation of the ring tube wall.

A study was then conducted to investigate the affected region of a point source. The ground temperature perturbation after ten years in response to a point source with a constant 1 W heat rate was calculated and plotted against the distance from that point source, as Figure 3.7 shows.

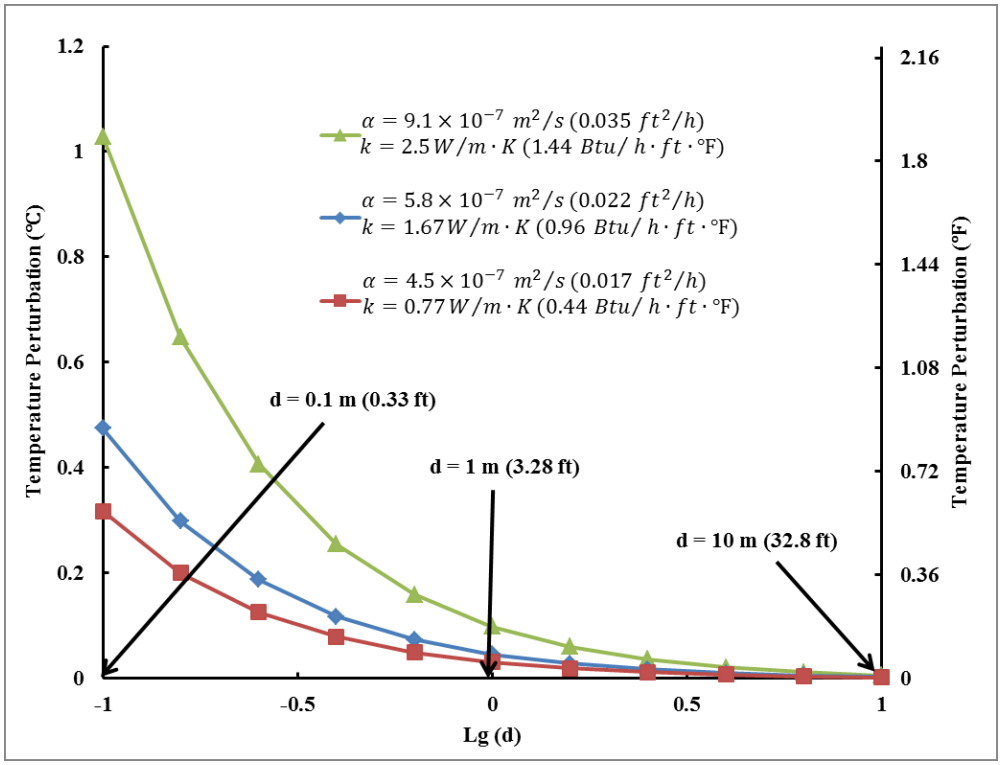

Figure 3.7: Temperature Perturbation versus Distance from the Point Source

Three sets of soil diffusivity and conductivity were applied in the calculations to account for different soil types. According to the plot, the temperature perturbation at 1 m (3.28 ft) is less than 10% of the temperature perturbation at 0.1 m (0.33 ft). The temperature perturbation at 10 m (32.8 ft) is less than 1% of the value at 0.1 m (0.33 ft). Therefore, by considering the distance to ring i, the surrounding rings are divided into three categories: near-field rings, middle-field rings and far-field rings. According to the above study, the near-field rings are defined as the rings whose centers are within 1 m + *D* (3.28 ft + *D*) distance of the center of ring *i*, as Figure 3.7 shows. *D* is the diameter of the ring. By setting the range at 1 m + *D* (3.28 ft + *D*), the distance between any point on ring *i* and any point on the near-field ring is larger than 1 m (3.28 ft). Following the same rule, the middle-field rings are defined as the rings whose centers are located between 1 m + *D* (3.28 ft + *D*) and 10 m + *D* (32.8 ft + *D*) distance of the center of ring *i*. Rings beyond 10 m + *D* (32.8 ft + *D*) distance are defined as far-field rings. In the calculation of tube

wall temperature perturbation of ring *i*, the near-field rings are calculated as ring sources; the interaction between the ring *i* and the middle-field rings are calculated as the interaction between two point sources at their centers with the same heat input strength; and the thermal effect of the far-field rings are ignored, as Figure 3.8 demonstrates:

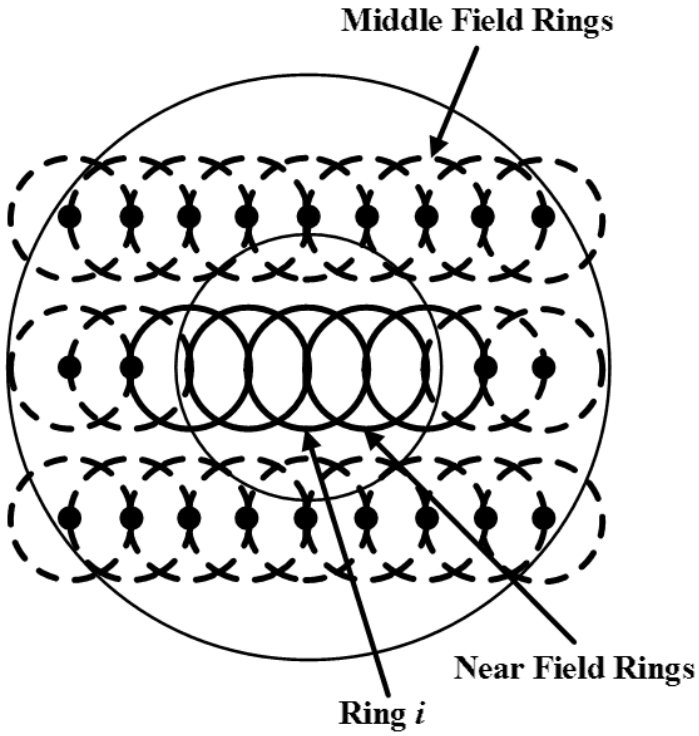

Figure 3.8: Schematic of the Second Improvement to the Algorithm: Dividing Surrounding Rings into Three Categories

Then the temperature influence of any middle-field ring on ring *i* is calculated by using Equation 3.9:

$$\Delta T_{j-i}(t) = \frac{q_l L N_{tube}}{4\pi k N_{ring}} \left[\frac{erfc\left(d(P_j, P_i)/2\sqrt{\alpha t}\right)}{d(P_j, P_i)} - \frac{erfc\left(\sqrt{d(P_j, P_i)^2 + 4h^2}/(2\sqrt{\alpha t})\right)}{\sqrt{d(P_j, P_i)^2 + 4h^2}} \right] \quad (3.9)$$

where:

$$d(P_j, P_i) = \sqrt{(x_{0i} - x_{0j})^2 + (y_{0i} - y_{0j})^2}$$

ΔT is the temperature variation, in °C or °F,

d is the distance between two points, in m or ft,

q_l is the heat rate per trench length, in W/m or Btu/h·ft,

L is the trench length, in m or ft,

N_{tube} is the number of Slinky™ tubes,

N_{ring} is the number of rings,

R is the radius of ring,

r is the radius of tube,

ω, φ is the angular parameter, in rad

x_{0i}, y_{0i} is the Cartesian coordinate of the center of ring i

x_{0j}, y_{0j} is the Cartesian coordinate of the center of ring j

As Equation 3.9 shows, the double integral is eliminated from the solution. $d(P_j, P_i)$ is the distance between the centers of two rings.

Third, while the last two improvements can reduce the computation time significantly, for the Slinky™ GHX that consists of a large number of rings, calculation of the temperature perturbation of each ring could still result in significant time consumption. Due to the second improvement, some rings may have exactly the same configuration of the surrounding rings. Therefore, these rings will have the same temperature perturbation. Instead of calculating the temperature perturbation of each of these rings, we can calculate only one of them. By doing this,

a large amount of computation burden can be taken, especially for those Slinky™ configurations that have a large number of rings.

To examine the improvement in computation time and the impact on the accuracy of the calculated results by applying these improvements, comparisons were made between the original program and the new program with the fast algorithm. Several calculations of the temperature response factors were performed by using the original and the new program. The calculation time and the calculated results were compared, as Figure 3.9 shows. Slinky™ GHXs that consist of 25, 50, and 100 rings were adopted in these calculations. The computation time of the temperature response factors by using the original program is 3, 11 and 46 minutes, respectively. The computation time increase equals the square of the increase in the number of rings. By using the new program with the fast algorithm, the computation time is reduced to: 28, 28 and 56 seconds, respectively. Besides the significant time reduction, the computation time does not increase necessarily as the number of rings increases by using the new program. Another computation was performed on a Slinky™ GHX that has 1000 rings by using the new program; the computation time is 3 minutes, which is within a good control regardless of the large number of rings. The computation results of the original and the new program, which are a set of temperature response factors, were compared. Among these comparisons, the largest difference is less than 0.8%. In conclusion, the program with the fast algorithm made the computation time within a reasonable range for the simulation purpose, meanwhile, with a good accuracy in the calculated results. By using the temperature response factors generated from the original and the new program, the calculated exiting fluid temperature of Slinky™ GHXs was compared in the case study section of this chapter.

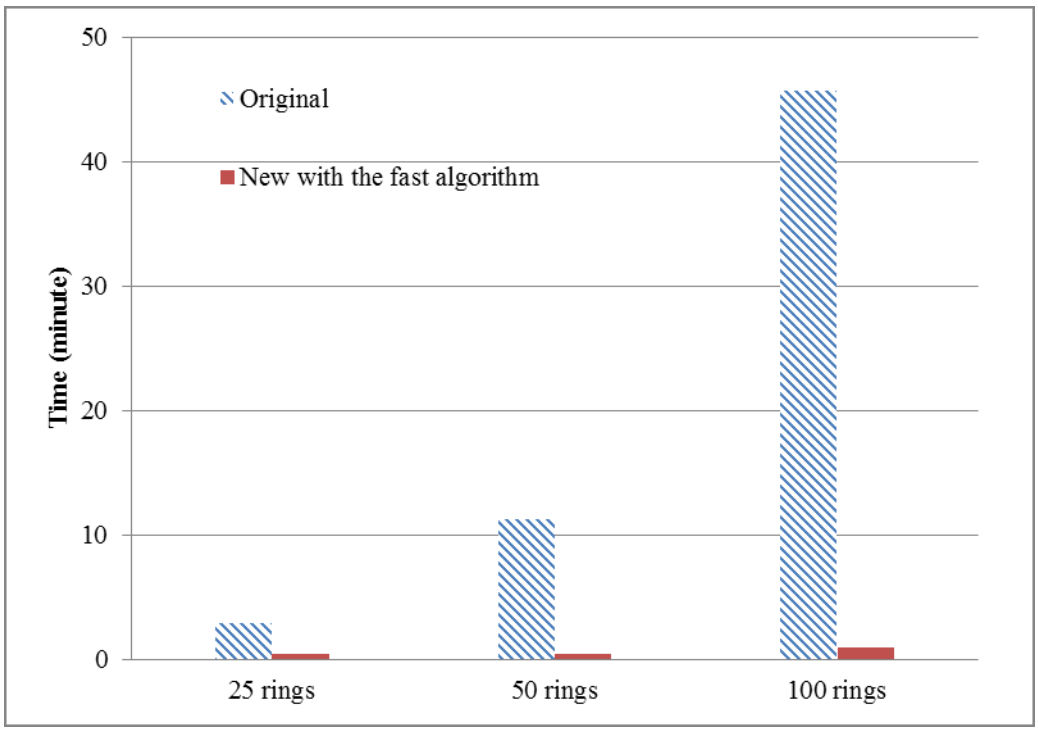

Figure 3.9: Comparisons of the Computation Speed of the Original Program and the New Program with the Fast Algorithm

3.3 Calculation of Fluid Temperature

3.3.1 Calculation of Mean Tube Wall Temperature

The temperature response factors are used in the calculation of the mean tube wall temperature at each time step. By knowing the heat input and the temperature response factors, we can obtain the mean temperature response of the tube wall at a given time. For simulations of GHXs, the heat transfer rates are functions of time, instead of constant values. In this study, the heat transfer rate function is decomposed into piecewise constant step heat inputs, as Figure 3.10 shows. The step heat inputs are then imposed at each time step with the corresponding temperature response factors, as Figure 3.11 shows. The superposition of the response of each step heat input gives the mean tube wall temperature response at the end of the last time step.

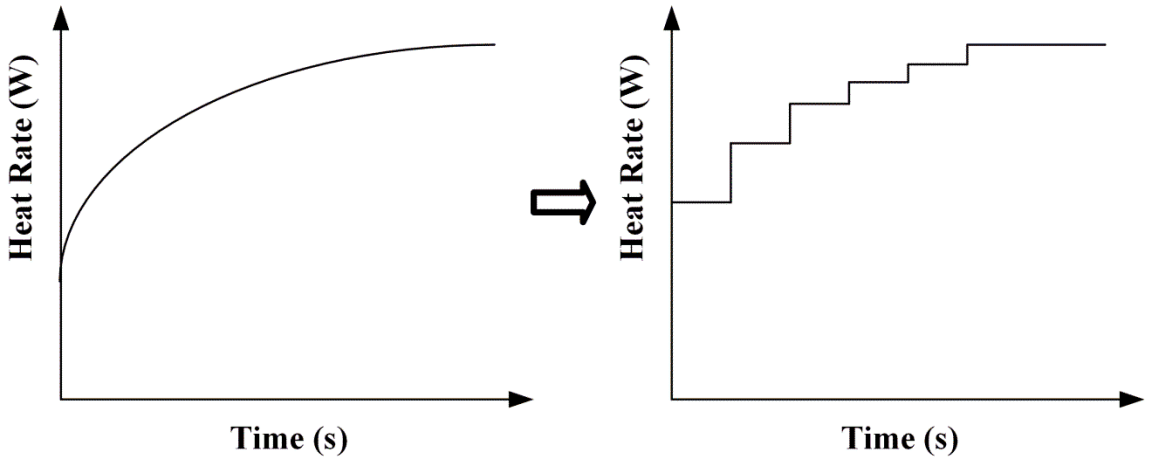

Figure 3.10: Decomposition of the Heat Inputs into Piecewise Constant Step Heat Inputs

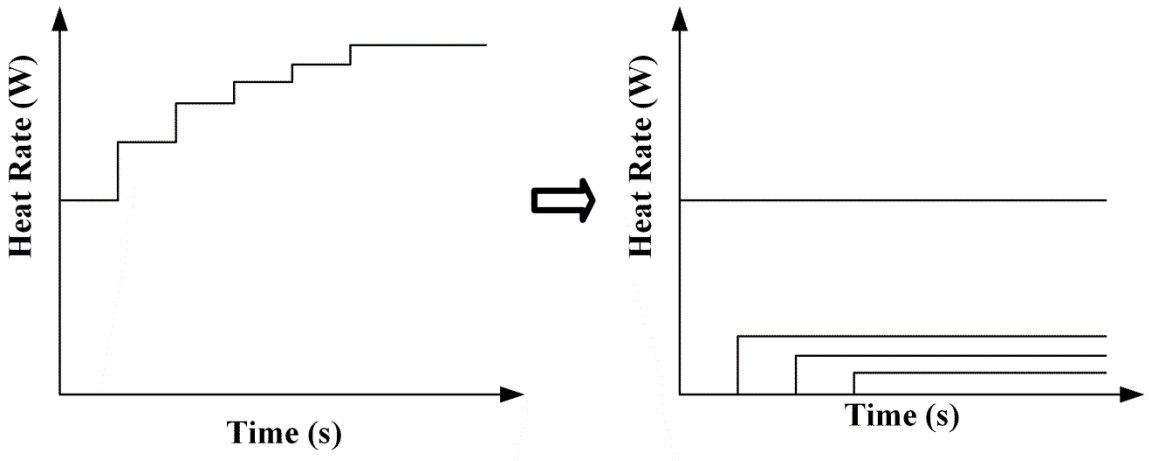

Figure 3.11: Superposition of Step Heat Inputs

For HGHXs, the ground surface heat balance will have a significant impact on the thermal performance of GHXs. This impact is accounted for by superimposing the undisturbed ground temperature, which is a function of time and buried depth. The calculation of the undisturbed ground temperature will be discussed in Chapter 5. The sum of the mean tube wall temperature response and the undisturbed ground temperature produces the mean tube wall temperature, as the following equation shows (Yavuzturk and Spitler, 1999):

$$T_{tw}(t_n) = T_{ground}(h, t_n) + \sum_{i=1}^{n} \frac{(q_{l_i} - q_{l_{i-1}})}{2\pi k} g_s(t_n - t_{i-1}) \quad (3.10)$$

where:

g_s is the temperature response function for Slinky™ GHX,

t_n and t_i are the time at the end of time step n or i, in s,

q_{li} is the heat input of time step i, in W/m or Btu/h·ft,

T_{ground} is the undisturbed ground temperature, in °C or °F,

T_{tw} is the mean tube wall temperature, in °C or °F,

h is the average buried depth of the GHX, in m or ft

3.3.2 Simple Tube Model

While the above equation allows the calculation of the mean tube wall temperature, the heat transfer rate has to be assumed at each time step. For the system energy simulation, the heat transfer rate is usually an output instead of an input. The entering fluid temperature is normally considered as an input for a GHX component. To utilize the temperature response function in calculating the exiting fluid temperature as well as the heat transfer rate, a simple tube model, as shown in Figure 3.12, is established with the following assumptions regarding the buried tubing:

- The heat transfer between tube wall and fluid is at quasi-steady state.
- The mean fluid temperature is the average value of the inlet fluid temperature and outlet fluid temperature.

According to these assumptions, we may have the following equations at time step n. Equation 3.11 is the expression of the second assumption we made above. Equation 3.12 gives the quasi-

steady state heat transfer rate in terms of the tube wall resistance R_{tw}, which can be calculated as the sum of the conduction resistance of the wall and the convection resistance between the wall and the fluid. Equation 3.13 gives the quasi-steady state heat transfer rate in terms of fluid transport.

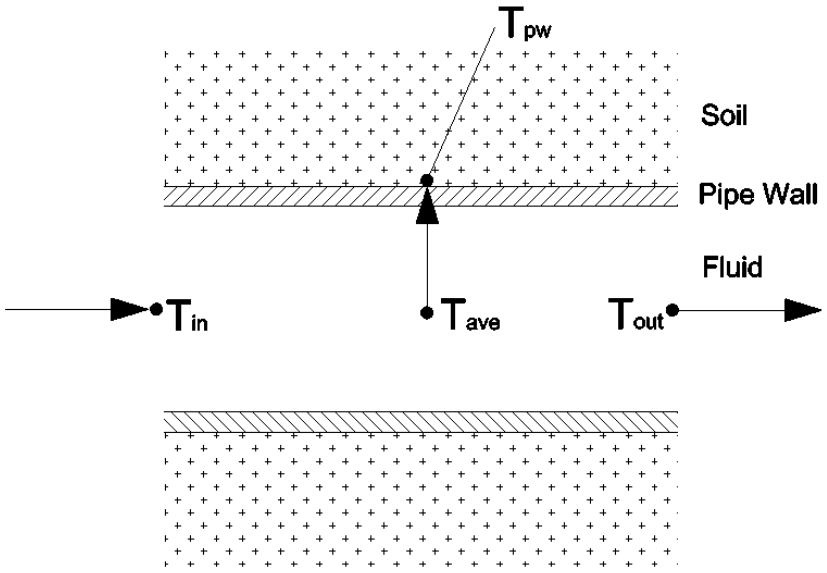

Figure 3.12: Schematic of Simple Tube Model

$$T_{avg}(t_n) = [T_{in}(t_n) + T_{out}(t_n)]/2 \tag{3.11}$$

$$T_{avg}(t_n) - T_{tw}(t_n) = q_{l_n} \frac{LN_{tube}}{2\pi R N_{Ring}} R_{tw} \tag{3.12}$$

$$q_{l_n} LN_{tube} = \dot{m} c_p [T_{in}(t_n) - T_{out}(t_n)] \tag{3.13}$$

where:

t_n is the time at the end of time step n, in s

T_{tw} is the mean tube wall temperature, in °C or °F,

T_{avg} is the mean fluid temperature, in °C or °F,

T_{in} is the inlet fluid temperature, in °C or °F,

T_{out} is the outlet fluid temperature, in °C or °F,

q_{ln} is the heat input of time step n, in W/m or Btu/h·ft

L is the trench length, in m or ft,

N_{tube} is the number of Slinky™ tubes,

N_{ring} is the number of rings,

R is the radius of ring, in m or ft,

R_{tw} is the the thermal resistant of the tube wall, in m·K/W or ft·°F·h/Btu

c_p is the specific heat of the ground, in J/kg·K or Btu/lbm·°F,

$\dot{m}$ is the mass flow rate of the fluid, in kg/s or lb/s

For the first time step (n=1), the heat transfer rate per trench length at the last time step (q_{l_0}) and the time at the beginning of this time step (t_0) are equal to zero. The interpolation of the obtained temperature response factors would generate the value of the temperature response function at time t_1 ($g(t_1)$). Then the above four equations have four unknowns: the heat transfer rate (q_{l_1}), the mean fluid temperature ($T_{avg}(t_1)$), the outlet fluid temperature ($T_{out}(t_1)$), and the mean tube wall temperature ($T_{tw}(t_1)$) at the first time step. By solving the four equations above simultaneously, we have the outlet fluid temperature ($T_{out}(t_1)$) and the heat transfer rate at the first time step (q_{l_1}) calculated. For the next time step, by using the heat transfer rate at the last step (q_{l_1}), the outlet fluid temperature ($T_{out}(t_2)$) and the heat transfer rate at the second time step (q_{l_2}) could be

calculated by solving the same set of equations. Follow this algorithm, the outlet fluid temperature and heat transfer rate at any desired time step can be calculated.

CHAPTER 4

VALIDATION, VERIFICATION AND APPLICATION

4.1 Verification of Ring Source Solution

Although the Slinky^{TM} GHX model presented in this thesis is developed independently of Li et al.'s (2012) work, the two models apply very similar methods in modeling Slinky^{TM} GHXs. Therefore, comparisons between the calculation results of the analytical solutions of the two models can serve to verify the ring source solutions derived in Chapter 3.

As discussed in Chapter 2, in calculating a ring tube's mean wall temperature response, Li et al. (2012) presents different analytical solutions for the following two cases: (a) the mean wall temperature response to the ring tube itself as a ring source, and (b) the mean tube wall temperature response to adjacent ring tubes (ring sources).

For case (a), our solution and Li et al.'s (2012) solution are applied in calculating a ring tube's mean wall temperature response to itself as a ring source. The soil thermal conductivity and diffusivity are chosen as 1.24 W/m·K and 5.33×10^{-7} m^2/s, following Chong et al. (2013). In addition, the heat input rate is assumed 22 W/m; and the buried depth is set at 1.5 m. Following Jones (1995), four diameters of the loop (ring) are chosen for this study: 0.9 m (36 in.), 0.8 m (32 in.), 0.7 m (28 in.), 0.6 m (24 in.), using ¾-inch diameter HDPE tube. As mentioned in Chapter 3, the analytical solution for the temperature response function is numerically implemented as a computer program. By making a slight change to the program, it can serve as the tool to compute

the mean tube wall temperature response by using the solution given in Chapter 3 (Equation 3.4 and 3.5). The commercial computer software Mathematica is used to calculate the results of Li et al.'s (2012) solution (Equation 2.17). The calculation results of the two solutions agreed to within ±0.0015°C for all four cases. The results for a loop diameter of 0.6 m (28 in.) are shown in Figure 4.1, with no discernible difference between the solutions. This comparison serves to verify both the derivation and the computation of the ring source solution for the mean tube wall temperature response presented in this thesis.

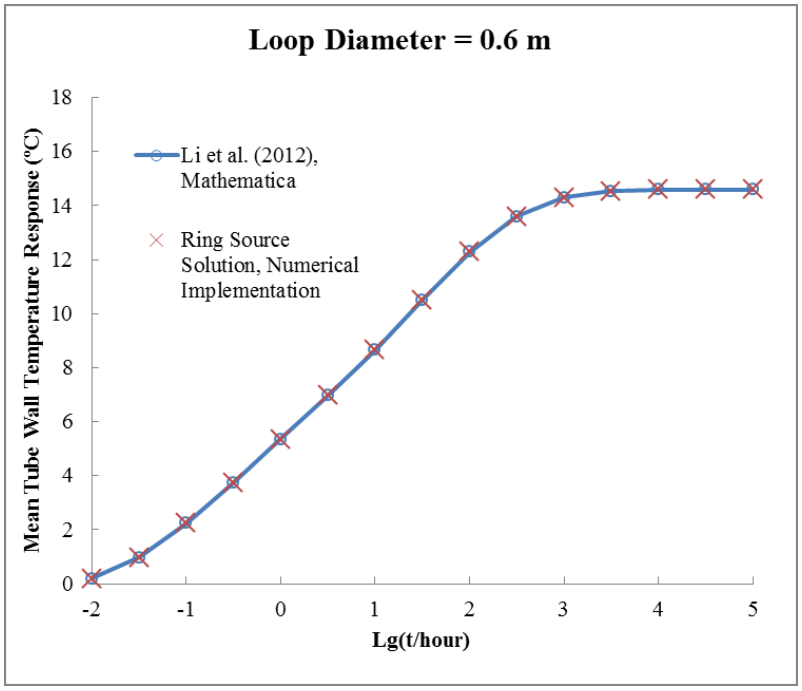

Figure 4.1: Comparisons of the Calculated Mean Tube Wall Temperature Response by Using Our Solution and Li et al.'s (2012) Solution, at D=0.6 m (24 in.)

For case (b), our solution and Li et al.'s (2012) solution are applied to calculate the temperature influence of an adjacent ring source on the tube wall. For the model developed in this thesis, the same solution used in case (a) (Equation 3.4 and 3.5) can be used in solving this problem. For Li et al.'s (2012) model, the solution to this case is given as Equation 2.18 instead of Equation 2.17, which is again calculated by using the software, Mathematica. The parameters in this study are

kept the same as in the case (a) except that the loop diameter is set at 0.9 m, while the pitch is varied. The pitch is set to the following values: 0.25 m (10 in.), 0.46 m (18 in.), 0.91 m (36 in.), 1.42 m (56 in.), following Jones (1995). The comparisons between the calculation results are shown in Figure 4.2. As expected, the agreement appears to be quite good. On closer inspection, however, the results show that for a pitch of 0.25 m (10 in.), Li et al.'s (2012) model predict 0.1°C higher than our model, as shown in Figure 4.3. When the pitch is 0.46 m (18 in.) and 0.91 (36 in.), Li et al.'s (2012) model tends to predict 0.06°C and 0.02°C higher than the model in this thesis, respectively. When the pitch is 1.42 m (56 in.), the differences between the results are less than ±0.0001°C. The reason for this is that Li et al.'s (2012) model ignores the diameter of the tube when calculating the thermal interactions between rings. Therefore, as the overlapped area between two rings increases (pitch= 0.91 m, 0.46 m and 0.25 m), the error associated with Li et al.'s (2012) solution increases, compared to our solution

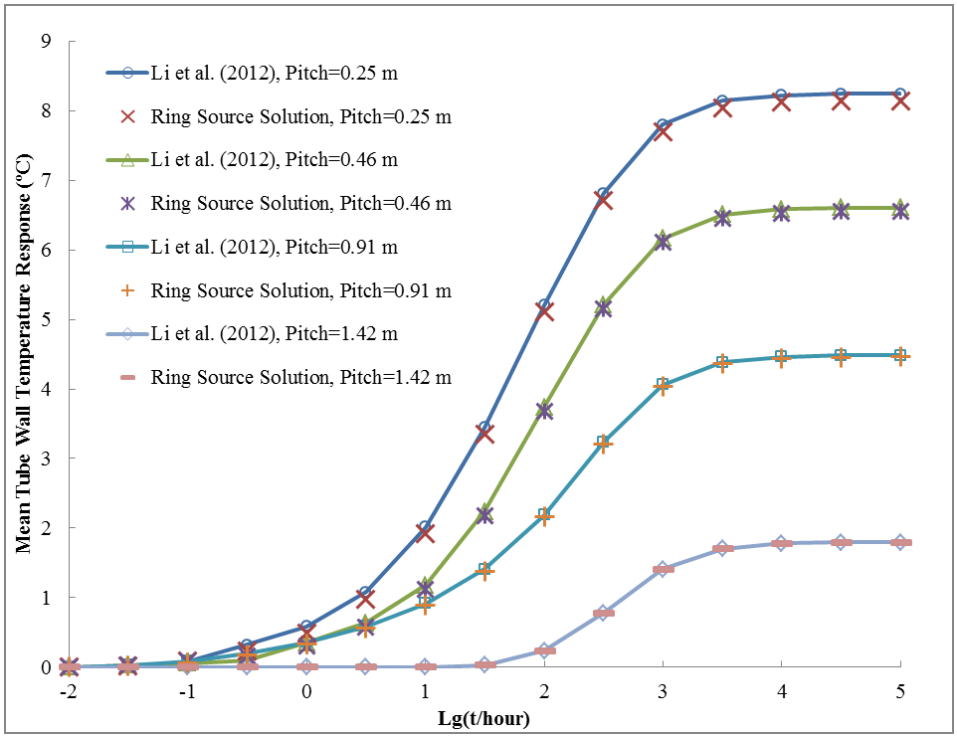

Figure 4.2: Comparisons of the Calculated Mean Tube Wall Temperature Response by Using Our Solution and Li et al.'s (2012) Solution with Different Pitches

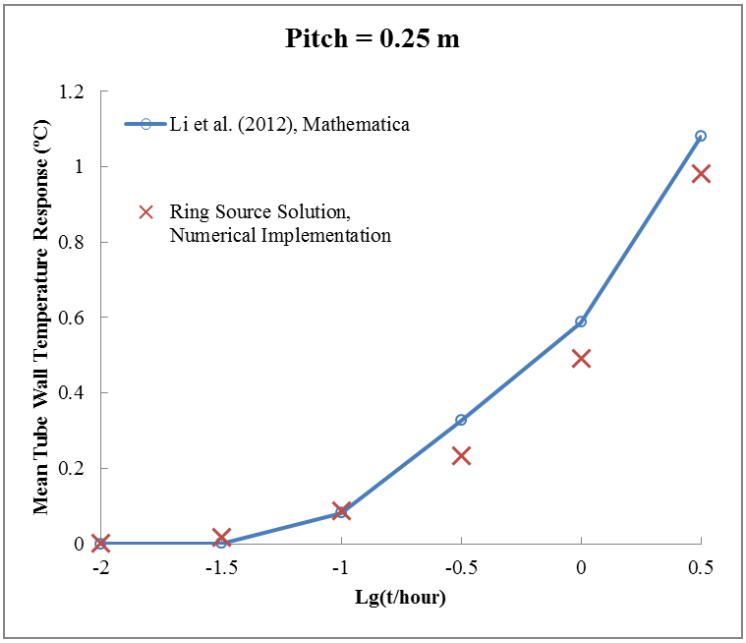

Figure 4.3: Comparisons of the Calculated Mean Tube Wall Temperature Response by Using Our Solution and Li et al.'s (2012) Solution, at p=0.25 m (10 in.)

In summary, although different solutions for mean tube wall temperature are derived in this thesis and by Li et al. (2012), the calculated results of these two solutions are almost the same. The noticeable differences are due to the neglect of tube diameter in Li et al.'s model (2012) when calculating the thermal interaction between two rings. Therefore, the solutions derived in Chapter 3 agree with Li et al.'s (2012) solutions.

4.2 Validation against Experimental Data

The calculation results of the model described in Chapter 3 are validated against published experimental data (Fujii et al. 2012) in this section. The experimental parameters and recorded data are taken from Fujii et al. (2012). Fujii et al. (2012) does not present the experimental uncertainty associated with their results. According to the paper, three short-term thermal response tests (TRTs) and one long-term air-conditioning (A/C) test were conducted in the year 2008 and 2009. Horizontal Slinky™ GHXs were used as heat sources and sinks in these tests.

The Slinky™ GHXs in these tests have different tubing lengths and pitch values while they share the same buried depth and trench length. The Slinky™ loops were placed in 1.5 m (4.9 ft) deep U-shaped trenches, as Figure 4.4 shows. To model the horizontal Slinky™ GHX described in Fujii et al. (2012), the U-shaped Slinky™ tubing is simplified as two parallel Slinky™ heat exchangers with the same total tube length, as Figure 4.4 shows. The two parallel GHXs are connected in series.

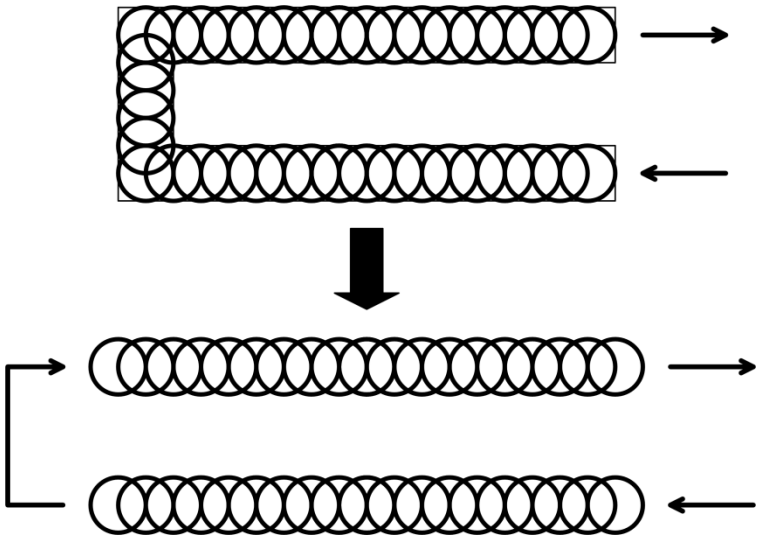

Figure 4.4: Simplification of the Slinky™ GHXs Used in the Field Tests

The thermal conductivity of the soil sample taken from 1.5 m (4.9 ft) depth in the test site was measured and given in the paper. The fluid flow rate in each test was controlled and recorded using valves with flow meters. Thermocouples were installed to measure various temperature values, which include the inlet and outlet fluid temperature of the Slinky™ GHXs, the far field ground temperature at 1.5 m (4.9 ft) depth (the buried depth of the GHXs), etc.

4.2.1 Short-term Thermal Response Tests

Three TRTs were conducted from the year 2008 to 2009. In each TRT, the GHX was connected to an electrical heater and a pump, as Figure 4.5 demonstrates; the system ran continuously for 5

days. Measured inlet (entering) and outlet (exiting) fluid temperature of the GHX in each TRT were plotted in Fujii et al.'s (2012) paper. The measured farfield ground temperature at 1.5 m (4.9 ft) depth during each TRT was used as the undisturbed ground temperature in this study.

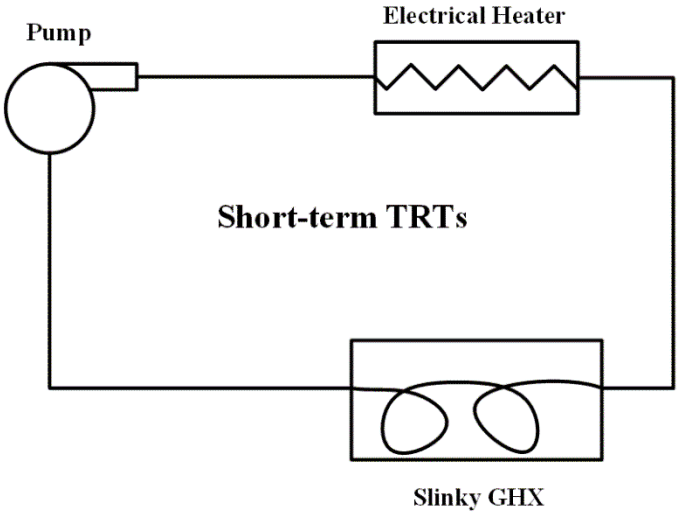

Figure 4.5: Schematic of the Experimental Facilities in TRTs

The parameters for the GHXs used in three TRTs are given in Table 4.1 and Table 4.2. Using the parameters in Table 4.1 and Table 4.2, the temperature response factors for the Slinky^{TM} GHX are generated, shown in Figure 4.6. The horizontal Slinky^{TM} GHXs used in TRT 1 and long-term A/C test have the same configuration. The Slinky^{TM} GHXs used in TRT1, TRT2 and TRT3 were named GHX1, GHX2 and GHX3, respectively. From Figure 4.6, we may tell that the temperature response factors of these GHXs have similar values in the first few hours. After that, the curve of the temperature response factors of GHX1 starts to deviate from the other two. This indicates the onset of the interaction between loops for GHX1, loop interaction is affected by the pitch of loops. The pitch of GHX1 is 0.4 m (1.31 ft), which is smallest among the three. The deviation between the curves of GHX2 and GHX3 begins at around the 30th hour of the operation time. This time is when the interaction between loops happens for GHX2, whose pitch is 0.6 m (1.97 ft). All three curves tend to constant values after about 5 years.

Table 4.1: Constant Parameters in the Tests

Parameter	Value	Parameter	Value
Diameter of loops	0.8 m (2.62 ft)	Soil thermal conductivity	1.09 W/m·K (0.63 Btu/h·ft·°F)
Inner diameter of tube	24 mm (0.94 in.)	Tube thermal conductivity	0.35W/m·K (0.20 Btu/h·ft·°F)
Buried depth	1.5 m (4.92 ft)	Gap between Slinky^{TM} tubes	2 m (6.56 ft)
Trench length	72 m (236.22 ft)	Thickness of tube	5 mm (0.2 in.)

Table 4.2: Variable Parameters in the Tests

Test	Pitch	Tube Length	Avg. Mass Flow Rate	Avg. Heat Load
TRT1	0.4 m (1.31 ft)	500m (1640 ft)	0.17 kg/s (22.88 lb/min)	61.1 W/m (63.5 Btu/h·ft)
TRT2	0.6 m (1.97 ft)	380m (1247 ft)	0.19 kg/s (24.89 lb/min)	63.0 W/m (65.5 Btu/h·ft)
TRT3	0.8 m (2.62 ft)	308m (1010 ft)	0.20 kg/s (26.72 lb/min)	63.3 W/m (65.8 Btu/h·ft)
A/C	0.4 m (1.31 ft)	500m (1640 ft)	0.23 kg/s (30.82 lb/min)	25.5 W/m (26.5 Btu/h·ft)

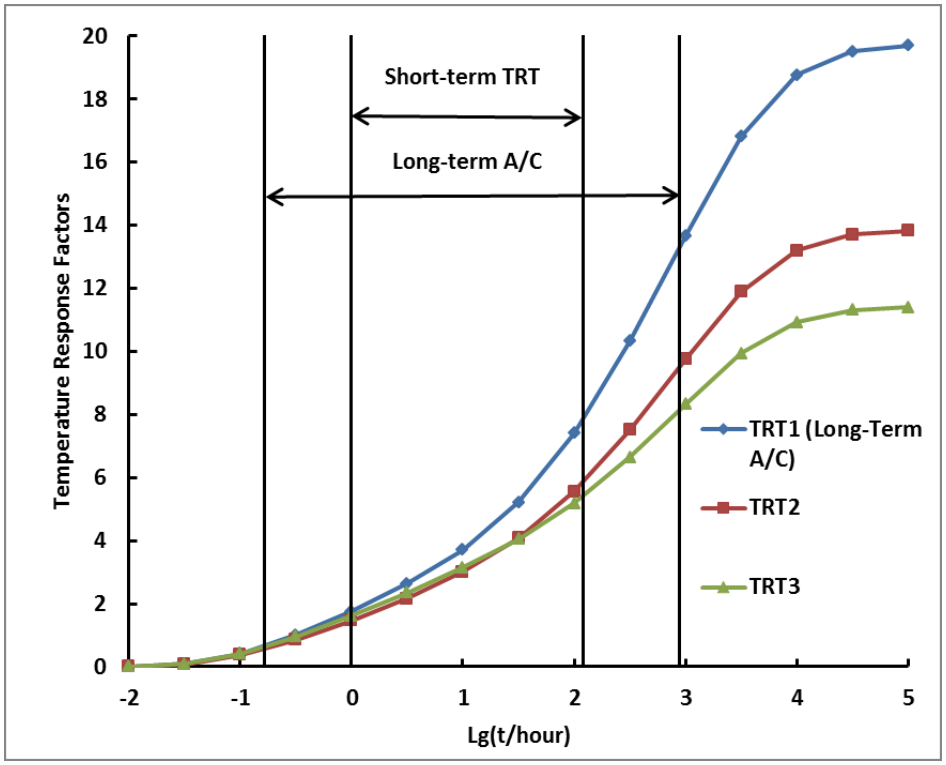

Figure 4.6: Calculated Sets of Temperature Response Factors

The generated three sets of temperature response factors were used in the Slinky GHX™ model to calculate the outlet fluid temperature of the GHXs. The hourly measured inlet and outlet fluid temperatures in TRTs were calculated by interpolating the data points that were digitized from the figures in Fujii et al. (2012). The hourly measured inlet temperature was used as an input. Another input in the simulations is the undisturbed ground temperature, using the measured far-field ground temperature given in Fujii et al.'s (2012) paper: 25.6°C (78.1°F), 24.4°C (75.9°F) and 24.0°C (75.2°F), for TRT1, TRT2, and TRT3, respectively. The hourly outlet temperature in TRTs was calculated and plotted in Figure 4.7, 4.8, 4.9. The calculated hourly outlet fluid temperatures show a good agreement with the measured values. The root mean square error (RMSE) of the calculated outlet temperature in TRT1, TRT2 and TRT3 is 0.27°C (0.49°F), 0.16°C (0.29°F), and 0.15°C (0.27°F), respectively. The maximum error is -0.45°C (-0.81°F), -

0.52°C (-0.94°F), and 0.37°C (0.67°F), which appear at the 28th, 1st and 3rd hour of the operation time, respectively.

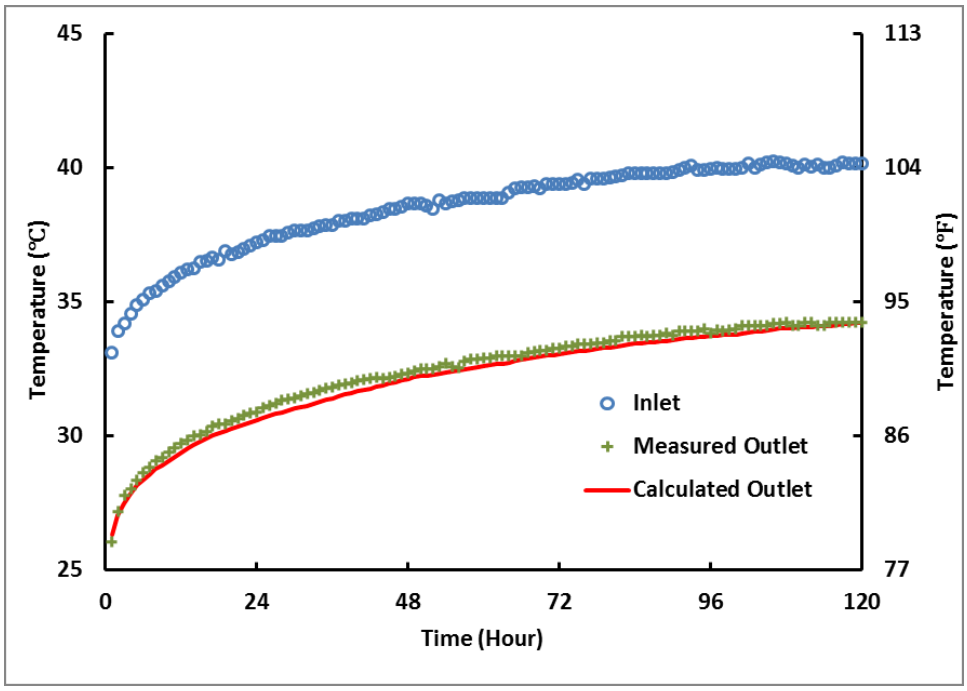

Figure 4.7: Comparison of Hourly Outlet Fluid Temperature of the Slinky^{TM} GHX in TRT1

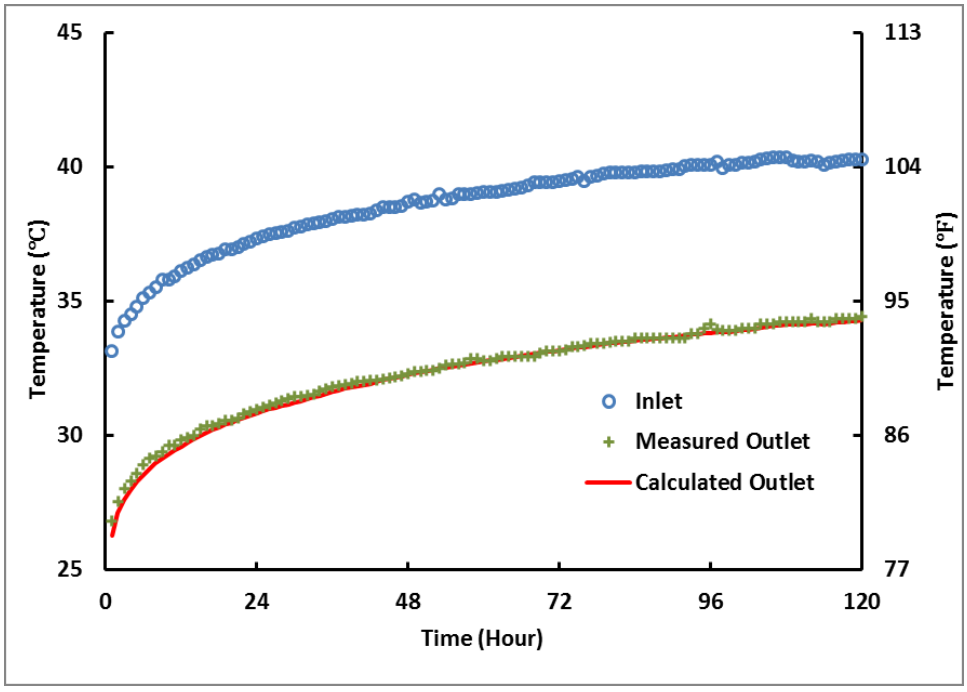

Figure 4.8: Comparison of Hourly Outlet Fluid Temperature of the Slinky™ GHX in TRT2

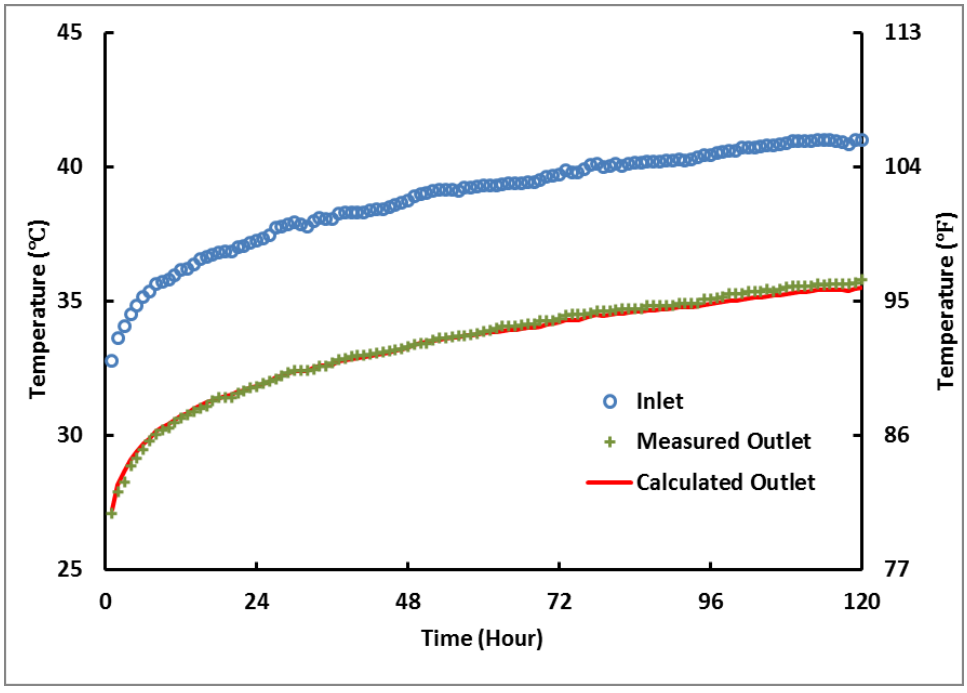

Figure 4.9: Comparison of Hourly Outlet Fluid Temperature of the Slinky™ GHX in TRT3

4.2.2 Long-term System Test

The long-term system (A/C) test was performed for 38 days from Jan. 19. 2009 to Feb. 27, 2009. In the long-term A/C test, the GHX was connected to a water-source heat pump and a pump, as Figure 4.10 shows. The water-source heat pump and the pump were placed in a house that has another air-source heat pump to maintain the room temperature. The system ran 20 hours a day.

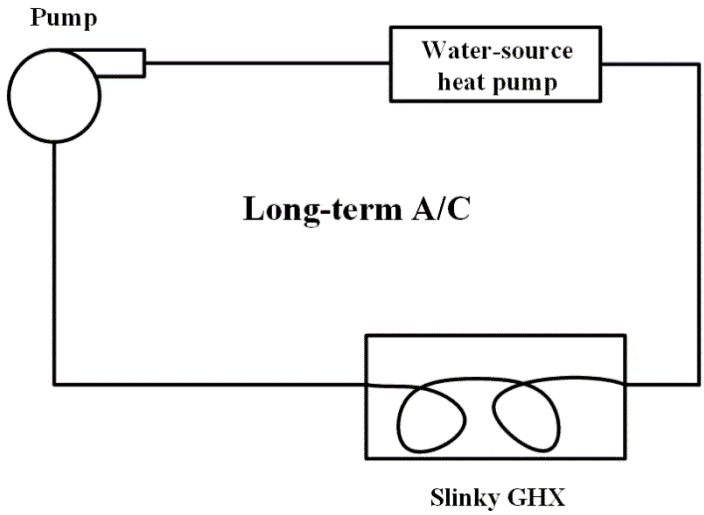

Figure 4.10: Schematic of the Experimental Facilities in the System Test (A/C Test)

The parameters for the GHXs used in the long-term system test are given in Table 4.1 and Table 4.2. Using the parameters in Table 4.1 and Table 4.2, the temperature response factors for the Slinky^{TM} GHX used in the system test were generated, as shown in in Figure 4.6. The generated temperature response factors were used as an input in calculating the outlet fluid temperature of the GHX.

In the long-term A/C test, the inlet and outlet fluid temperatures were recorded every ten minutes during the run period. Dr. Fujii, the author of the paper (Fujii et al., 2012), provided the original data. During the system off time, the modeling assumes that there is no heat transfer to the Slinky^{TM} GHXs. The measured inlet temperature at 10 minutes intervals was input to predict the

outlet temperature. The far-field ground temperature at 1.5 m (4.9 ft) depth during the system test period was plotted in Fujii et al.'s (2012) paper. Totally 58 data points were digitized from the plot. The undisturbed ground temperature at -1.5 m (-4.9 ft) was also calculated and input every ten minutes by interpolating between these 58 data points. The calculation results of outlet fluid temperature are shown in Figure 4.11. The RMSE between the calculated and measured values is 0.15°C (0.27°F), while the maximum error is -0.57°C (-1.03°F). The maximum error happens at the beginning of the running period at the 27th day. From the figure, we find out that the relatively large error always appear at the beginning of the running periods. This could be associated with the assumption that no heat transfer occurs during the off time. In addition, at the beginning of each on-cycle, the fluid temperature tends to approach the room temperature. This temperature may not be included in the recorded data, which could also affect the calculation result. Overall, the predicted outlet temperature matches well with the measured values in the 38-day A/C (system) test.

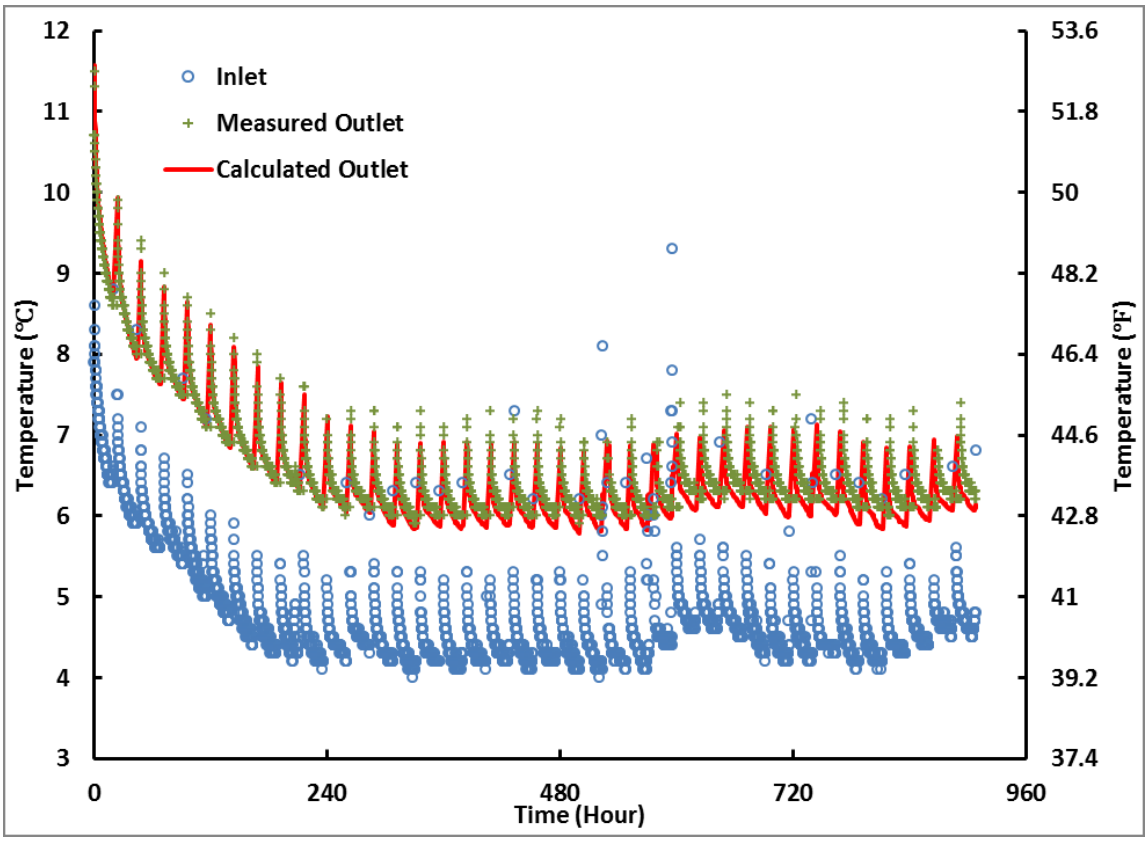

Figure 4.11: Comparison of Every Ten Minutes Outlet Fluid Temperature of the Slinky™ GHX in Long-term System (A/C) Test

In summary, the model predicted outlet temperature shows a good agreement with the measured data of three TRTs and one long-term A/C test. The errors are within ±0.6°C (±1.08°F). The range of the RMSEs is 0.15-0.3°C (0.27-0.54°F). While this model is designed for simulation purpose, the time scale may vary from minutes to years. The ranges of the temperature response factors applied in the short-term and long-term calculations are indicated in Figure 4.6. Though the time range (10 minutes to 38 days) may consider not wide enough, the temperature response factors largely finish its increase within this time range. Therefore, these comparisons may pose a significant examination to the feasibility of the Slinky™ GHX model.

4.3 Verification of Fast Algorithm

To examine the impact of the fast algorithm on the accuracy of the model, two-year simulations were made by using the temperature response factors calculated using the program with and without the fast algorithm. The Slinky™ GHX used in the long-term system test, which is described in section 4.2, is chosen for the simulations. In addition, the same soil properties and constant flow rate were assumed in the simulations. The Kusuda and Achenbach model (1965) was adopted to predict the undisturbed ground temperature used in the simulations. According to the model, the undisturbed ground temperature versus time of year and depth was given by the following equation:

$$T_{ground}(h,t) = T_{AE} - SA \cdot e^{-\sqrt{\frac{\pi}{\alpha \cdot TP}} \cdot h} \cdot \cos\left(\frac{2\pi}{TP} t - \sqrt{\frac{\pi}{\alpha \cdot TP}} \cdot h - PA\right) \tag{4.1}$$

where:

T_{ground} is the undisturbed ground temperature, in °C or °F,

t is time of the year, starting from January 1st, in hr,

h is the average buried depth of the GHX, in m or ft,

T_{AE} is the annual average earth temperature, in °C or °F,

SA is the surface temperature amplitude, in °C or °F,

TP is the period of ground temperature cycle (8766 hr), in hr,

PA is the phase angle of temperature at surface, in rad,

α is the ground thermal diffusivity, in m^2/s or ft^2/h,

Three parameters: annual average earth temperature, surface temperature amplitude, and phase angle of temperature at surface are needed in the above equation. They were given for selected sites in the United States in Kusuda and Achenbach's paper (1965). Among these sites, East Lansing, MI and Tempe, AZ were chosen as the locations for the simulations since they are considered representative for heating-dominated and cooling-dominated climates.

A 25 m^2 house with a 1 m^2 window was modeled as a single zone in EnergyPlus to generate the annual load profile at the two locations. The cooling and heating setpoints for the house are 26.1°C (79°F) and 19.4°C (67°F), respectively. Regarding the internal heat gain, the occupancy is assumed 20 m^2/person with a heat gain of 132 W/person. The lighting gain is set as 10.8 W/m^2. The calculated hourly cooling and heating loads for the two locations are given in Figure 4.12 and Figure 4.13, with cooling load shown as negative and heating load as positive.

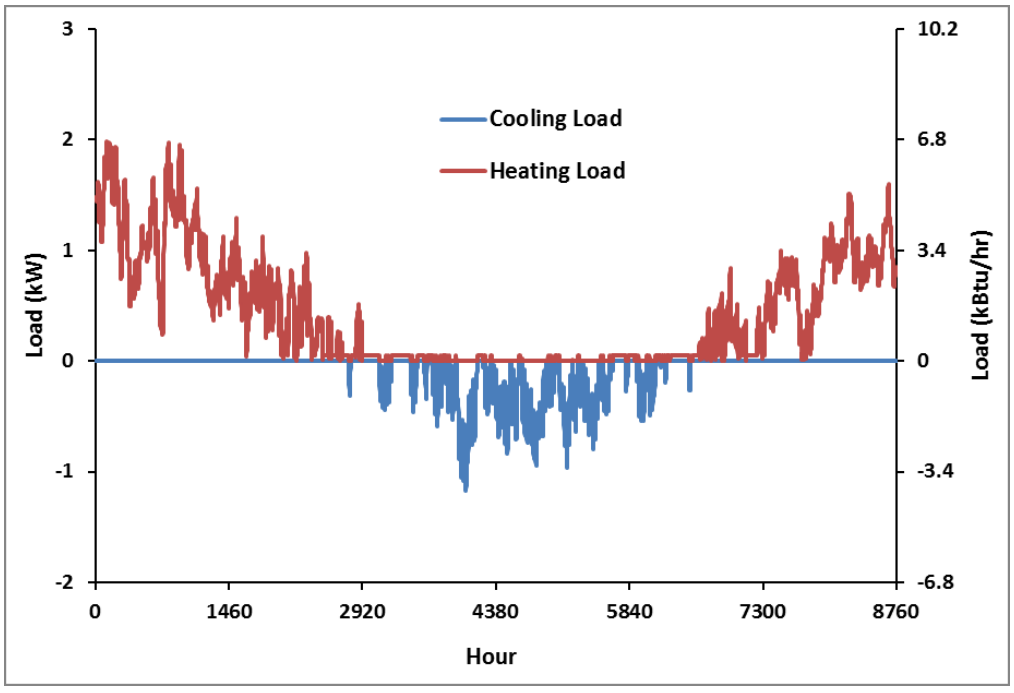

Figure 4.12: Annual Hourly Building Load Profile for the Example Building in East Lansing, MI

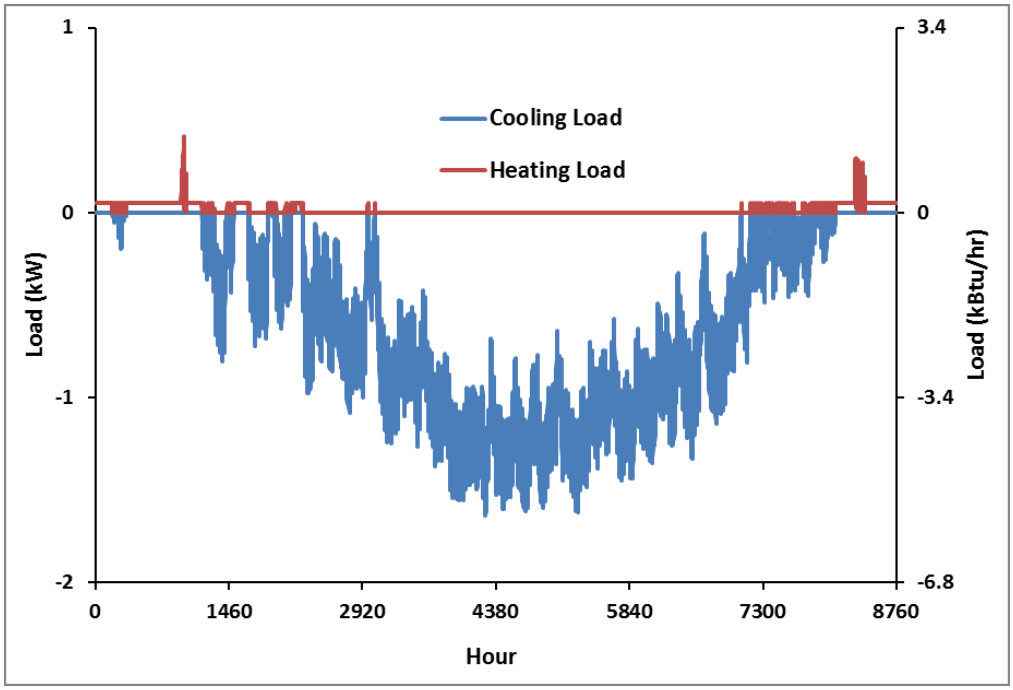

Figure 4.13: Annual Hourly Building Load Profile for the Example Building in Tempe, AZ

The hourly loads were directly assigned to the GHX to simulate the hourly entering and exiting fluid temperature. The heat transfer fluid in the GHX is assumed as water with 10% propylene glycol. The simulations were run for a two-year period to avoid the error brought by the assumed initial conditions. To examine the effect of applying the fast algorithms on the simulation results, the temperature response factors calculated by the original and the fast program were used to simulate the fluid temperature. The results of the second year are shown in Figure 4.14 and Figure 4.15 for the two locations. For East Lansing, MI, as Figure 4.14 shows, the maximum and minimum exiting (outlet) fluid temperature is 15.9°C (60.6°F) and 0.32°C (32.6°F), respectively. There is little difference between the calculated exiting fluid temperature with and without applying the fast algorithm; the two curves overlay each other as Figure 4.14 demonstrates. The RMSE is 0.14°C (0.25°F), with a maximum error of -0.3°C (-0.54°F). For Tempe, AZ, as Figure 4.15 shows, the maximum and minimum exiting fluid temperature becomes 31°C (87.8°F) and 16.9°C (62.4°F). Similar to the results of East Lansing, MI, the exiting fluid temperature curves

calculated based on the original and the fast program are very close to each other in Figure 4.15, with a RMSE of 0.15°C (0.27°F) and a maximum error of 0.24°C (0.43°F).

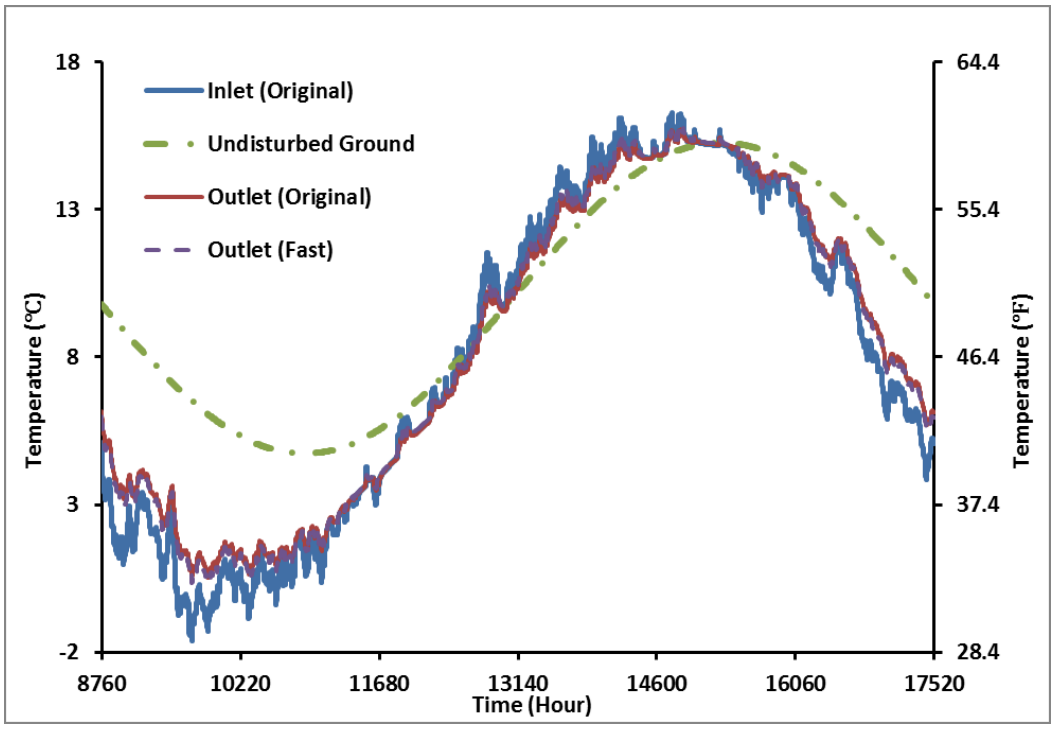

Figure 4.14: Slinky™ GHX Hourly Fluid Temperature Predictions for East Lansing, MI, with and without Using the Fast Algorithm

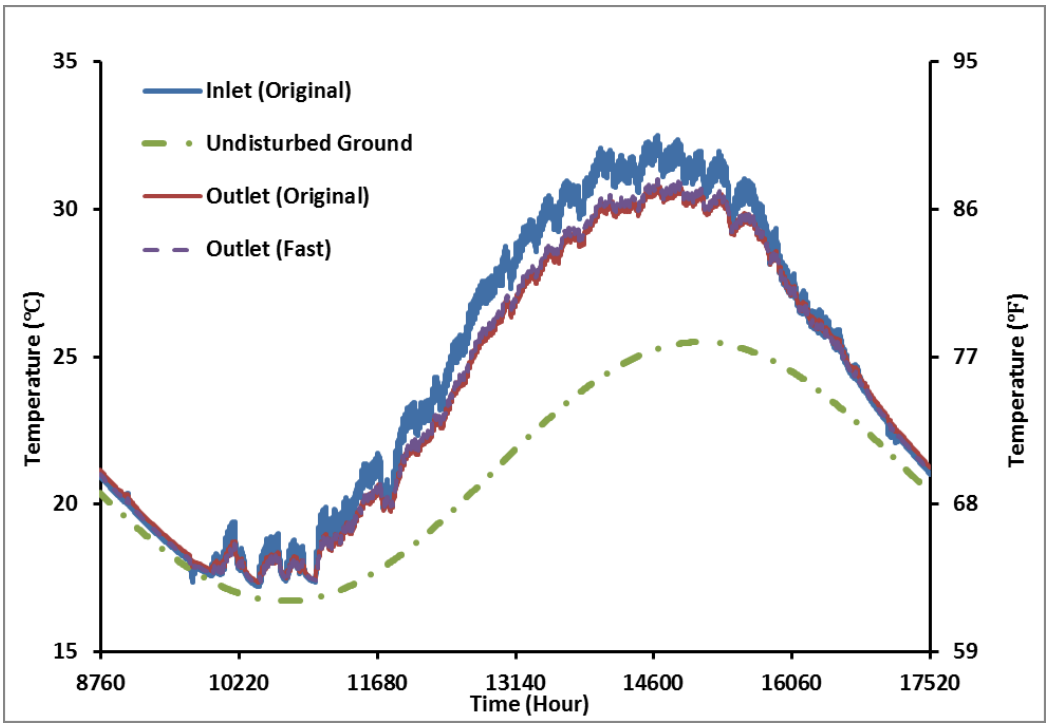

Figure 4.15: Slinky™ GHX Hourly Fluid Temperature Predictions for Tempe, AZ, with and without Using the Fast Algorithm

4.4 Application to Vertical Slinky™ GHXs

According to the literature review (Li et al. 2012; Fujii et al. 2012; Wu et al. 2010), there are fewer studies on vertical Slinky™ GHXs than on horizontal ones. By comparing with horizontal Slinky™ GHXs, we may have a better understanding of the thermal performance of vertical Slinky™ GHXs.

The vertical configuration can result in differences in temperature response factors as well as in the average undisturbed ground temperature. According to our comparisons, for the horizontal and vertical Slinky™ GHXs that use the same Slinky™ tubing and have the same average buried depth, the differences of temperature response factors are within ±1%, as Figure 4.16 shows. The configurations of the Slinky™ GHXs used in TRT1 and TRT3 were applied in the comparisons. The description of the configurations can be found at section 4.2 of this chapter.

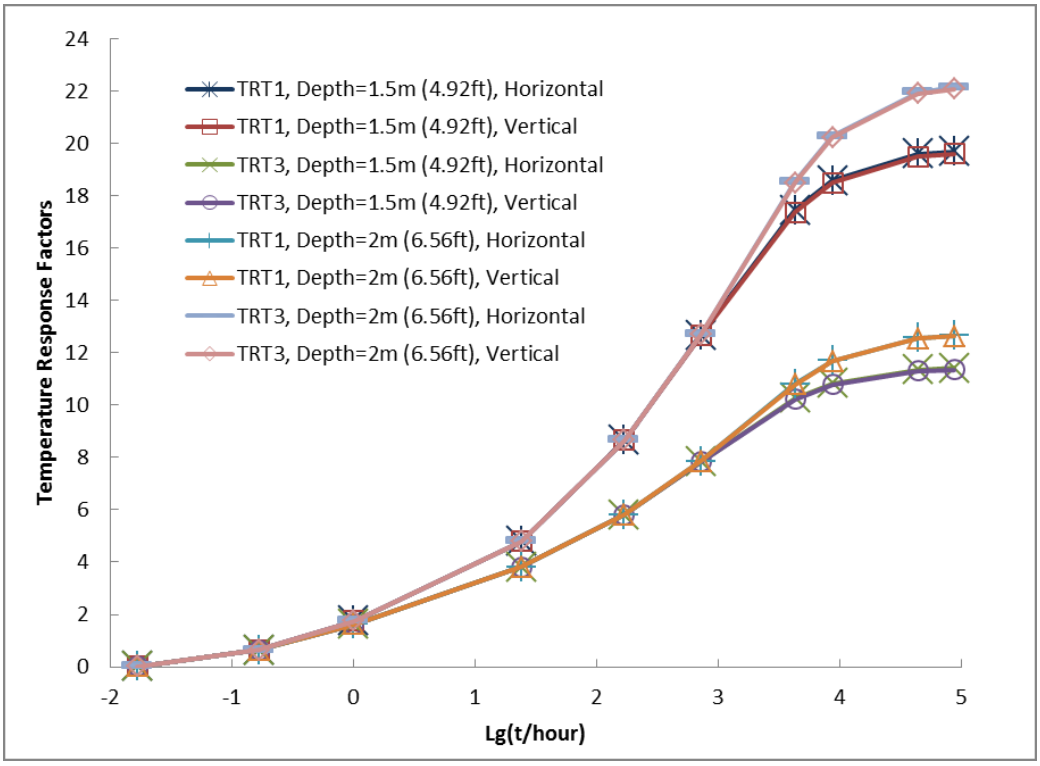

Figure 4.16: Comparison between Temperature Response Factors of Horizontal and Verical Slinky™ GHXs

Regarding the average undisturbed ground temperature, for a horizontal Slinky™ GHX, we can use the undisturbed ground temperature at its buried depth, which can be considered as a constant value. However, for vertical Slinky™, the depth of the buried tubing is varying. The average undisturbed ground temperature for a vertical Slinky™ GHX should be the average value of the undisturbed ground temperatures of every small tube segment; the accurate solution requires a single integration. A simple method is then proposed to calculate the undisturbed ground temperature for a vertical Slinky™ GHX, as Figure 4.17 shows. It is considered as the average value of the undisturbed ground temperature at a vertical Slinky™ loop's the upper most, middle and lower most position, which could be written as the following equation:

$$T_{ground}(t) = \frac{1}{3}\left[T_{ground,up}\left(h - \frac{D}{2}, t\right) + T_{ground,mid}(h,t) + T_{ground,lo}\left(h + \frac{D}{2}, t\right)\right] \quad (4.2)$$

where:

T_{ground} is the undisturbed ground temperature for vertical Slinky™ GHX, in °C or °F,

$T_{ground,up}$ is the undisturbed ground temperature at a vertical Slinky™ loop's the upper most position, in °C or °F,

$T_{ground,mid}$ is the undisturbed ground temperature at a vertical Slinky™ loop's the middle position (loop's center), in °C or °F,

$T_{ground,up}$ is the undisturbed ground temperature at a vertical Slinky™ loop's the lower most position, in °C or °F,

t is time, in hr,

h is the average buried depth of the GHX, in m or ft

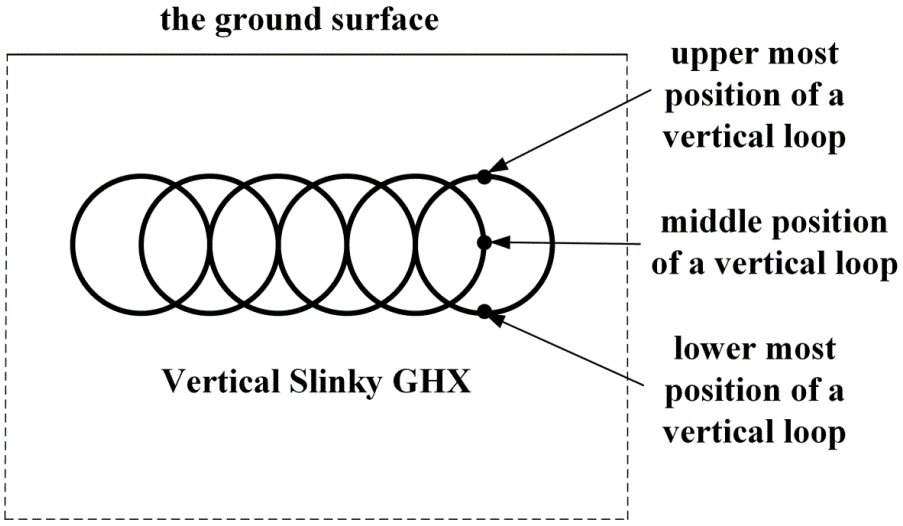

Figure 4.17: Schemtic of the Undisturbed Ground Temperature Calculation for Vertical Slinky™ GHXs

Two-year simulations on both horizontal and vertical Slinky™ GHXs were made at the two locations discussed in section 4.3: East Lansing, MI and Tempe, AZ. The same building loads, soil properties and horizontal Slinky™ GHX's configuration used in section 4.3 were applied in this study. The vertical Slinky™ GHX is assumed to have the same average buried depth as the horizontal one. The Kusuda and Achenbach model (1965) is adopted in calculating the undisturbed ground temperature at different depth. The simulated exiting fluid temperature and undisturbed ground temperature were plotted in Figure 4.18, 4.19 for the two locations, respectively. As the figures show, small differences were observed between the exiting fluid temperature of the horizontal and the vertical Slinky™ GHX, as the curves tend to overlay each other. The average difference between the horizontal and vertical GHX's exiting fluid temperature is ±0.14°C (±0.27°F) for East Lansing, MI and ±0.13°C (±0.23°F) for Tempe, AZ. According to the two-year simulations, vertical and horizontal Slinky™ GHXs with same Slinky™ tubing and average buried depth have very similar thermal performance.

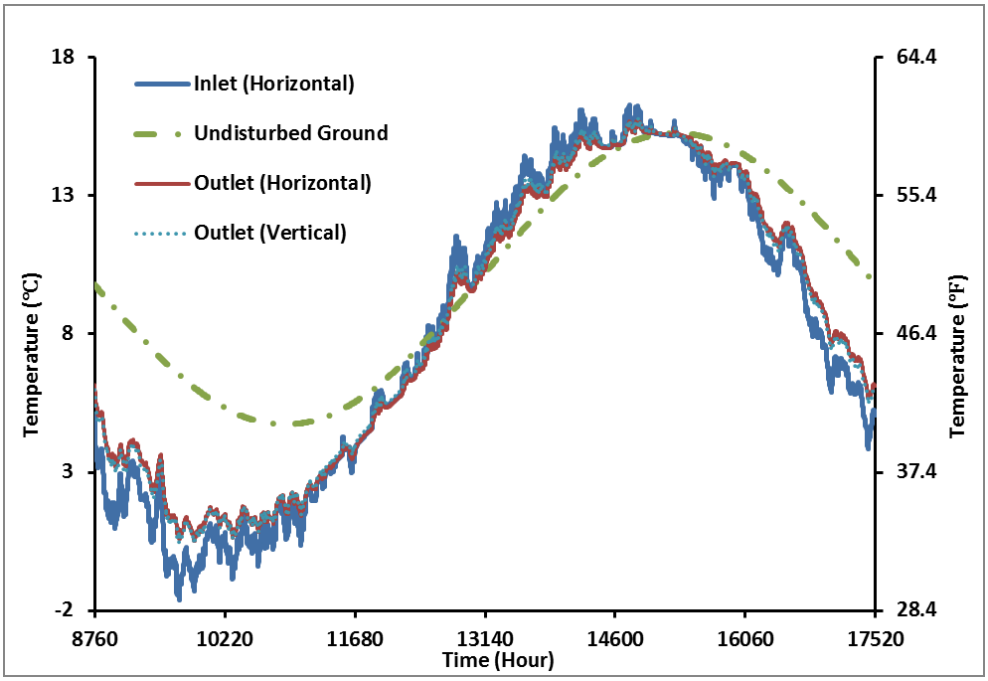

Figure 4.18: Horizontal and Vertical Slinky™ GHX Hourly Fluid Temperature Predictions for East Lansing, MI

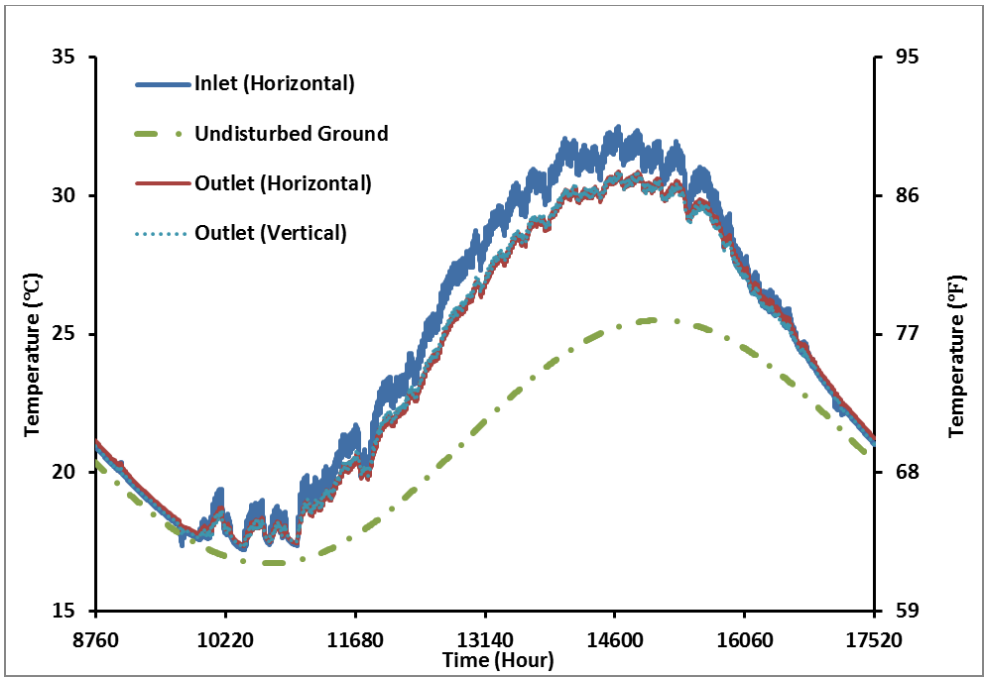

Figure 4.19: Horizontal and Vertical Slinky™ GHX Hourly Fluid Temperature Predictions for Tempe, AZ

CHAPTER 5

IMPLEMENTATAION IN ENERGYPLUS

5.1 Ground Heat Transfer Model

According to the principle of superposition, the complex heat conduction problem associated with Slinky™ GHXs can be deemed as the superposition of two independent less complicated heat conduction problems, as described in Chapter 3.

As described in Chapter 3, the second heat conduction problem is to obtain the undisturbed ground temperature. In this problem, the ground surface is assumed as a Dirichlet type boundary ($T = T_s(t)$). The boundary temperature (ground surface temperature) is a function of time and is determined by a detailed ground surface heat balance. To calculate the temperature of the ground surface and the ground domain at a given time, a three-dimensional numerical model is applied.

This numerical model is based on the previous GHX models proposed by Lee (2013) and Lee et al. (2013). While Lee's (2013) model involves considerations of buried tubes and basement walls in the ground domain, the numerical model presented in this work is a ground heat transfer model that calculates the undisturbed ground temperature with a detailed ground surface heat balance. A uniform, rectangular grid is applied in this model, as Figure 5.1 shows. The governing equation for the whole ground domain is given as:

$$\frac{\partial T}{\partial t} = \alpha \left(\frac{\partial^2 T}{\partial x^2} + \frac{\partial^2 T}{\partial y^2} + \frac{\partial^2 T}{\partial z^2} \right) \tag{5.1}$$

where:

T is the temperature, in °C or °F,

t is time, in s,

α is the ground thermal diffusivity, in m^2/s or ft^2/h,

x, y, z are Cartesian coordinate, in m or ft

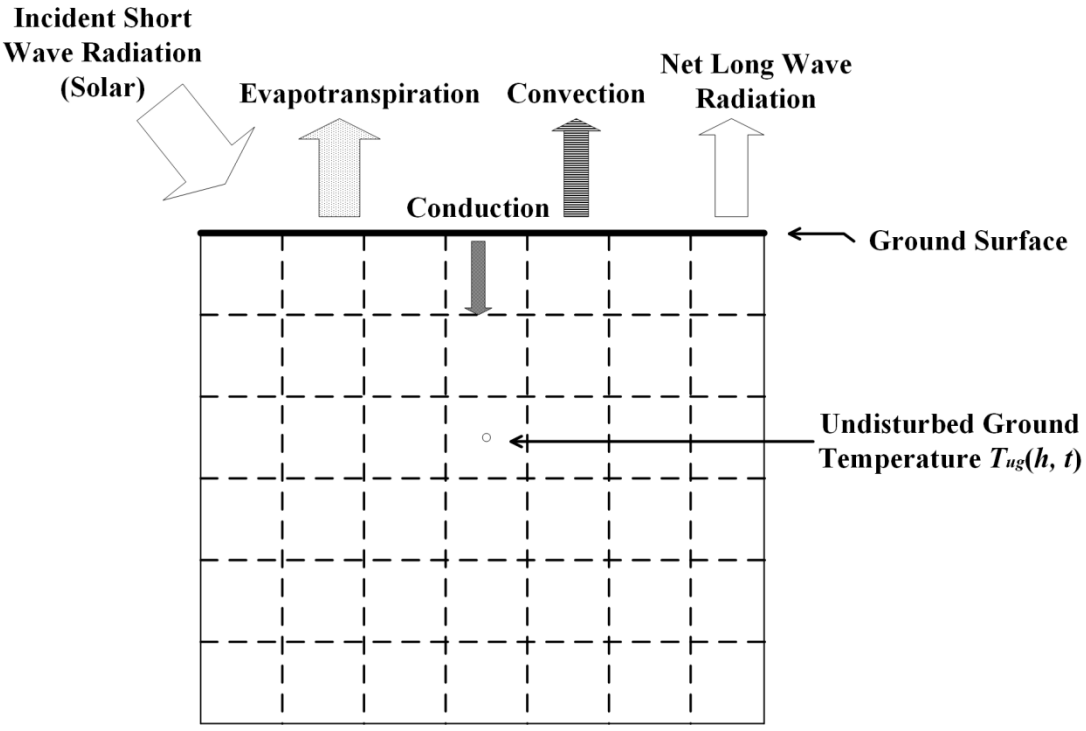

Figure 5.1: Schematic of the Ground Heat Transfer Model

While semi-infinite medium is assumed in the second problem, boundaries in all directions have to be set for this numerical model. Except for the ground surface, the temperatures of other boundaries are calculated using the Kusuda and Achenbach model (1965). As Figure 5.1 shows, the undisturbed ground temperature is considered as a function of depth h and time t.

A detailed ground surface heat balance is applied in this model. The convection heat transfer, the incident short wave radiation, the net long wave radiation and the evapotranspiration are considered balanced by the heat transferred to the interior of the ground domain:

$$q_{cond} = q_{conv} + q_{rad\_s} + q_{rad\_L} + q_{evap} \tag{5.2}$$

where:

q_{cond} is the heat transfer to the ground domain due to the ground surface heat balance, in W/m^2 or Btu/ft^2·h,

q_{conv} is the convection heat transfer to the ground surface, in W/m^2 or Btu/ft^2·h,

q_{rad_s} is the incident short wave radiation, in W/m^2 or Btu/ft^2·h,

q_{rad_L} is the net long wave radiation, in W/m^2 or Btu/ft^2·h,

q_{evap} is the heat loss through evapotranspiration, in W/m^2 or Btu/ft^2·h

The calculations of the convection, radiation and evapotranspiration are subject to the ground surface type. In this model, the surface is assumed covered by the grass. The detail of the calculations of the convective heat transfer, and the net long wave radiation can be found at Xing (2010). Antonopoulos's (2006) approach is applied by Xing (2010) in estimating the convection heat transfer at the ground surface:

$$q_{conv} = h_c(T_a - T_s) \tag{5.3}$$

$$h_c = \frac{\rho_a c_{pa}}{208} u_{wind} \tag{5.4}$$

where:

q_{conv} is the convection heat transfer to the ground surface, in W/m^2,

h_c is the convention coefficient, in W/m^2·K,

ρ_a is the air density, in kg/m^3,

c_{pa} is the air specific heat, in J/kg·K,

u_{wind} is the wind velocity, in m/s,

T_s is the ground surface temperature, in °C,

T_a is the air temperature, in °C

The equation recommended by Walter et al. (2005) is used in calculating the net long wave radiation:

$$R_L = \sigma {T_a}^4 (0.34 - 0.14\sqrt{e_a})(1.35\frac{R_s}{R_{scs}} - 0.35) \tag{5.5}$$

where:

R_L is the net long wave radiation, in MJ/m^2·d

σ is the Stefan-Boltzmann constant,

T_a is mean hourly temperature of the air, in K,

e_a is actual air vapor pressure, in kPa

R_s is the measured incident short wave radiation, in MJ/ m^2·d

R_{scs} is the calculated clear sky short wave radiation, in MJ/m^2·d

The calculation of evapotranspiration is using the approach proposed by Allen et al. (1998), according to Lee et al. (2013):

$$h_{fg}E = \frac{\delta(G_r - G_s) + \frac{\rho_a c_{pa} e'}{R_{aero}}}{\delta + \gamma(1 + \frac{R_s}{R_{aero}})} \tag{5.6}$$

where:

h_{fg} is the latent heat of vaporization,

E is the rate of evapotranspiration,

δ is the slope of saturation vapor pressure temperature relationship

γ is the psychometric constant

G_r is the net radiation to the ground surface

G_s is the soil heat flux from the surface

ρ_a is the air density, in kg/m^3 or lb/ft^3,

c_{pa} is the air specific heat, in J/kg·K or Btu/lb·°F,

e' is the vapor pressure deficit of the air

The incident short wave radiation can be obtained from a TMY3 weather file. According to Xing et al. (2012), the absorptivity is chosen as 0.77 based on Walter et al.'s (2005) recommendation.

The soil freezing and melting process is also considered in the numerical model. The effective heat capacity method (Lamberg et al. 2004) is used in modeling the soil freezing and melting process. By giving the soil in freezing /melting process a much higher heat capacity than its heat capacities at frozen or nonfrozen state, the amount of latent heat released or absorbed can be simulated.

In conclusion, the mean tube wall temperature of a Slinky^{TM} GHX can be calculated as the superposition of two terms: the mean temperature response of the tube wall and the undisturbed ground temperature at the GHX's buried depth. In this section, a three-dimensional numerical model is presented to calculate the undisturbed ground temperature. The detailed ground surface heat gain and loss is modeled. In addition, the soil freezing and melting process is considered in this model. It is worth noting that this model does not model the soil freezing/melting around

buried tubes, since this process is largely determined by the heat extracted from the buried tubes instead of the thermal effect of the ground surface.

5.2 Implementation in EnergyPlus

The modeling of a Slinky™ GHX is based on the coupling of three parts: the calculation of the temperature response factors, the calculation of the undisturbed ground temperature, and the calculations of exiting fluid temperature and heat transfer rate, as Figure 5.2 shows.

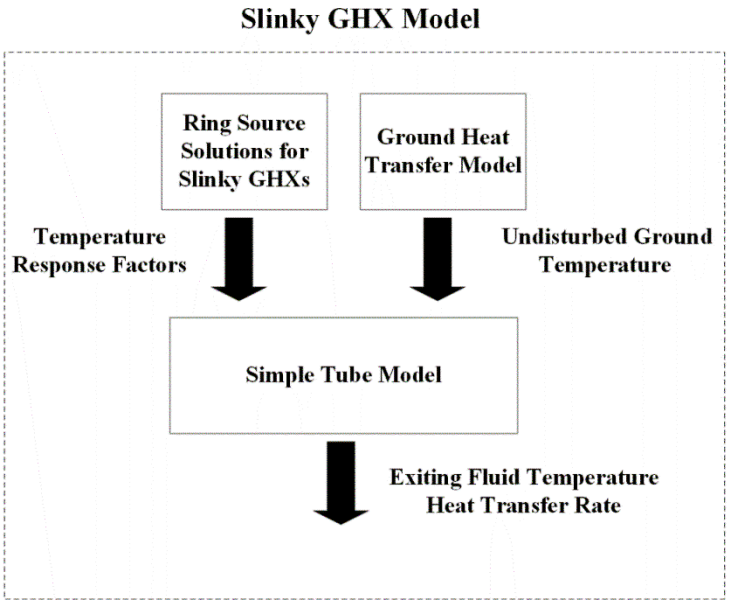

Figure 5.2: Coupling of the Sub-models of the Slinky™ GHX Model

As described in Chapter 3, the ring source solutions are proposed to calculate the temperature response factors of a Slinky™ GHX. Based on the derived solutions, a computer program with fast calculation algorithm is created to generate a set of temperature response factors for a defined Slinky™ GHX field. The input parameters of this program are given in Table 5.1. A typical set of output temperature factors are plotted in Figure 5.3.

Table 5.1: Input Parameters for Temperature Response Factors Calculation Program

Parameters	
R	Radius of Rings (Loops) (m)
α	Thermal Diffusivity (m^2/s)
h	Tube's Buried Depth (m)
r	Tube's Outer Radius (m)
N_{tube}	Number of Slinky™ Tubes
N_{rings}	Number of Rings (Loops)
L	Trench's Length (m)
p	Pitch between Loops (m)
D	Distance between Slinky™ tubes (Trenches) (m)

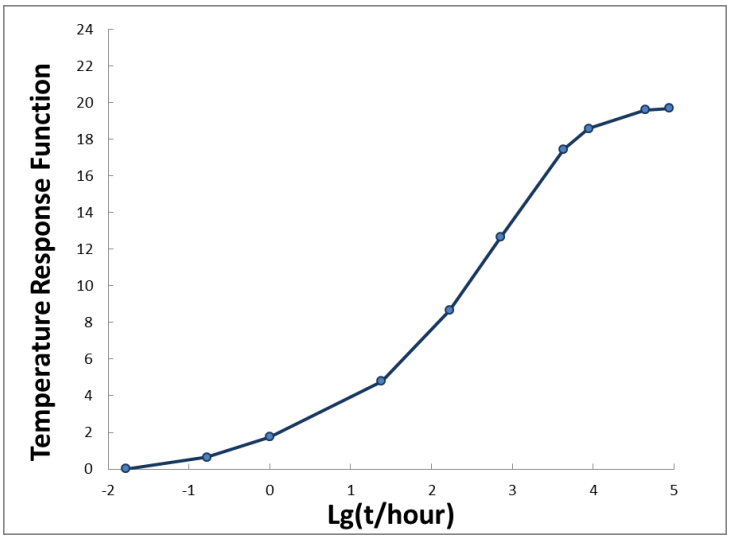

Figure 5.3: Plot of the Output Temperature Response Factors

The simple tube model use the temperature response factors as an input and is applied to calculate the exiting fluid temperature without assuming the heat transfer rate, as described in Chapter 3. Another input for the simple tube model is the undisturbed ground temperature at the buried depth of the GHX. As discussed in the last section, the three-dimensional ground heat transfer model is used to calculate the undisturbed ground temperature.

The Slinky™ GHX model is implemented in EnergyPlus as a plant component that serves the condenser supply side. Instead of writing a complete new EnergyPlus module for this Slinky™ GHX model, the implementation is based on the revision and coupling of two existed plant component modules: "PlantGroundHeatExchangers" and "PlantPipingSystemManager". The first module is created based on the vertical ground loop heat exchanger model (Yavuzturk and Spitler 1999; Murugappan 2002), while the second module corresponds to the numerical horizontal ground heat exchanger model proposed by Lee (2013) and Lee et al. (2013).

The simple tube model applies a similar approach as the Yavuzturk and Spitler's (1999) model in calculating the exiting fluid temperature, which uses a set of temperature response factors as an input and assumes a constant flow rate along the boreholes. The mean tube wall temperature is

calculated based on Eqaution 3.10 given in Chapter 3 and the interpolation of the input temperature response factors. The mean fluid temperature is assumed as the average value of the inlet and outlet fluid temperature in both models. Therefore, the "PlantGroundHeatExchangers" module is revised to serve as the implementation of our simple tube model. A number of changes are made to the original module, such as the calculation of the grout resistance is eliminated; the calculated undisturbed ground temperature is imposed at every time step instead of assuming as a constant value.

As described in the last section, the ground heat transfer model uses the same numerical approach in simulating the ground domain (without buried tubes or basement walls in it) and applies the same boundary conditions as the Lee's (2013) model. Therefore, the EnergyPlus module "PlantPipingSystemManager", which is the implementation of Lee's (2013) model in EnergyPlus, is revised to serve as the implementation of our ground heat transfer model. The undisturbed ground temperature at a desired depth is the only output of the revised module.

The two revised modules are integrated, which serve as the EnergyPlus component module for the Slinky^{TM} GHX model. The framework of this module is shown in Figure 5.4. The input objects for this EnergyPlus plant component model are listed in Table 5.2.

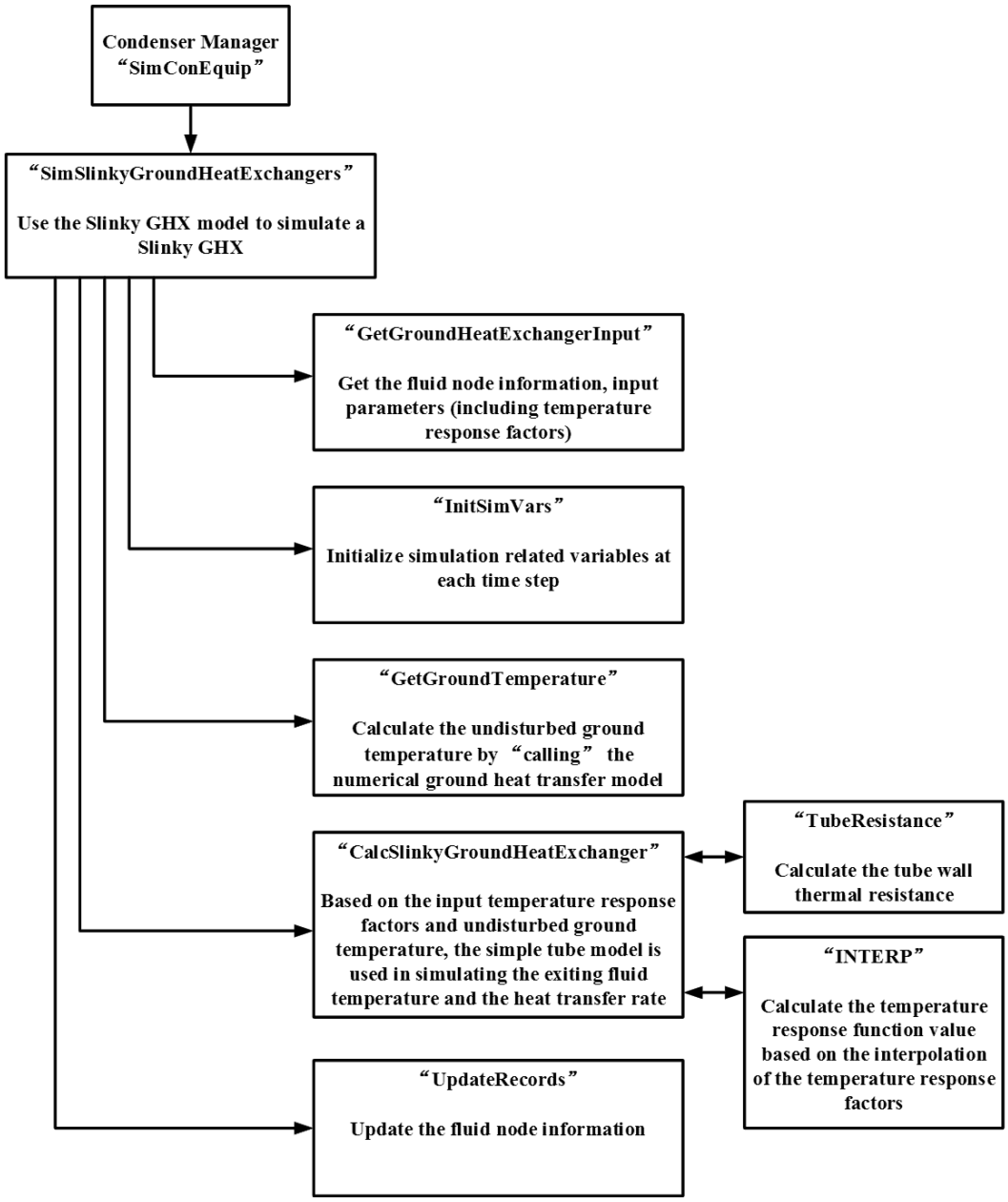

Figure 5.4: Framework of the EnergyPlus Module for Slinky™ GHX Model

Table 5.2: Input Parameters for the EnergyPlus Module

Parameters	Units	Parameters	Units
Maximum Flow Rate	m^3/s	X-Direction Domain Length	m
Total Tube Length	m	Y-Direction Domain Length	m
Tube Radius	m	Z-Direction Domain Length	m
Ground Thermal Conductivity	W/m-K	X-Direction Mesh Density	
Ground Thermal Heat Capacity	J/m^3-K	Y-Direction Mesh Density	
Design Flow Rate	m^3/s	Z-Direction Mesh Density	
Tube Thermal Conductivity	W/m-K	Kusuda and Achenbach Average Surface Temperature	°C
Tube Outer Diameter	m	Kusuda and Achenbach Amplitude of Surface Temperature	°C
Tube Thickness	m	Kusuda and Achenbach Phase Shift of Minimum Surface Temperature	days
Maximun Length of Simulation	years	Soil Moisture Content Volume Fraction	percent
Temperature Response Factors (A Set)		Soil Moisture Content Volume Fraction at Saturation	percent
Evaportranspiration Ground Cover Parameter		Convergence Criterion for the Cartesian Ground Domain Iteration	°C
		Maximum Iterations in the Cartesian Ground Domain Iteration	

The implementation of the Slinky™ GHX model in EnergyPlus is based on the revision and integration of two existed component modules, with only necessary changes to the original code to enable performing simulations under the EnergyPlus environment. Further work is required to

create a new, independent component module for Slinky™ GHX, based on the method presented in this chapter.

5.3 Preliminary Evaluation

Based on the updated EnergyPlus with the Slinky™ GHX component, multi-year whole-building simulations are performed to evaluate our implementation. In the simulations, with the consideration of real world applications of Slinky™ GHXs, a GSHP system consists of Slinky™ GHXs and a water-to-air heat pump is used to serve a residential house. The simulations are run for two locations: Lansing, MI and Phoenix, AZ, which are considered representative for heating-dominated and cooling-dominated climate, respectively. In addition, the two locations' imbalanced annual building loads will result in a significant increase or decrease of the ground temperature in the long term. Therefore, our model's ability in modeling a Slinky™ GHX's long-term performance can be examined through these multi-year simulations.

5.3.1 Input Description

The building used in the simulations is a 3 m high residential house with a total floor area of 150 m^2. The total glazing area is 23.3 m^2, as Figure 5.5 shows. The building is modeled as one zone. Following Cullin et al. 2012, the total lighting and equipment heat gain is set at 8.2 W/m^2; the infiltration rate is assumed as 0.5 ach; the cooling and heating setpoints are 24.5°C and 21.7°C; respectively.

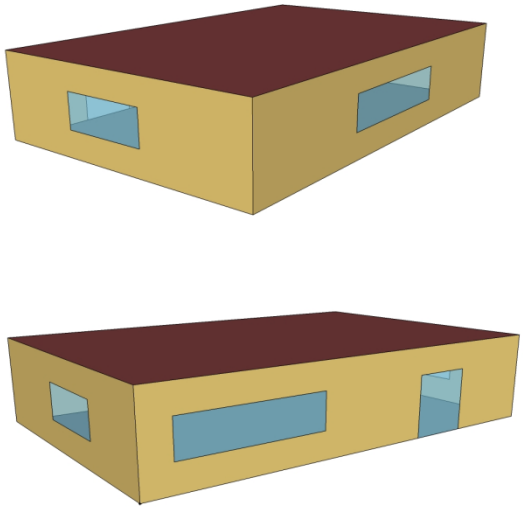

Figure 5.5: Three-dimensional View of the Modeled Building

A water-to-air heat pump is used to condition the building. The water-to-air heat pump has a rated total cooling capacity of 8600 W and a rated total heating capacity of 8850 W. An equation-fit model is used to simulate the heat pump. The heat pump is configured with a blow through fan. The condenser loop has a constant speed pump, operating continuously with a rated flow rate of 0.505 kg/s. Slinky^{TM} GHXs are used in the condenser supply side, with a total tube length of 1250 m. The calculated temperature response factors for the Slinky^{TM} GHX field are plotted in Figure5.6.

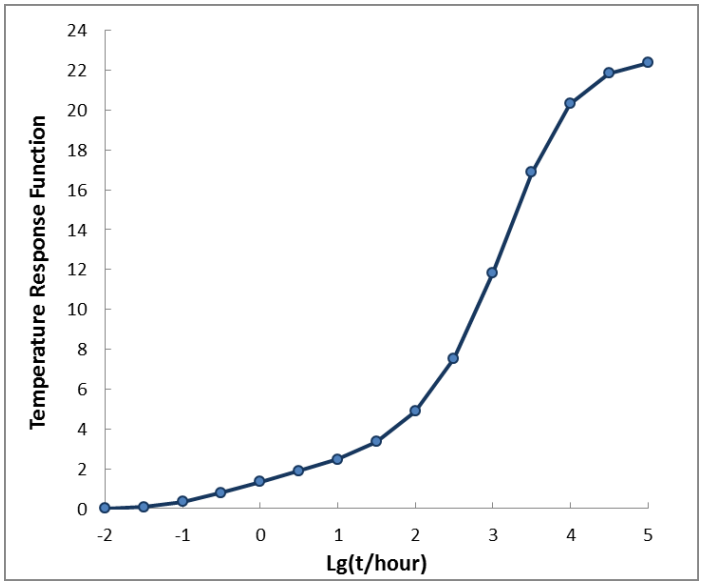

Figure 5.6: Input Temperature Response Factors for Whole-Building Simulations

5.3.2 Simulation Results

The simulated building load profiles for the two locations: Lansing, MI and Phoenix, AZ are shown in Figure 5.7 and Figure 5.8, respectively. As we expect, the heating loads are dominated for Lansing, MI. Even in the summer time, there are significant amount of heating loads during the night time. For Phoenix, the building loads are cooling dominated. The cooling loads are noticeable even during the winter season. The maximum heating load for Lansing, MI is less than 8850 W, while the maximum sensible cooling loads for Phoenix, AZ is less than 6000 W. Therefore, our selected water-to-air heat pump is anticipated to meet the cooling/heating loads without additional cooling/heating source.

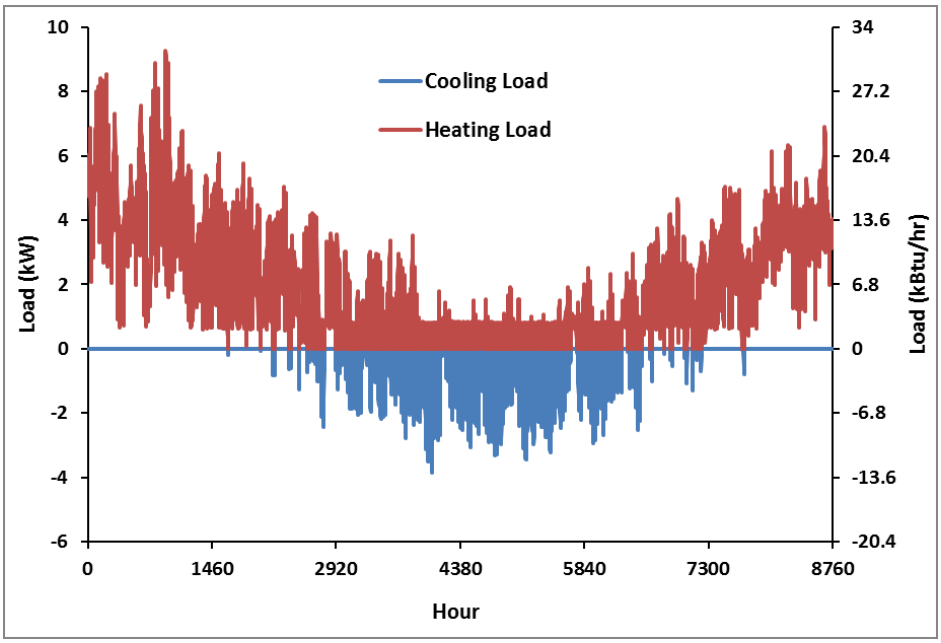

Figure 5.7: Annual Hourly Building Loads for the Simulated Building in Lansing, MI

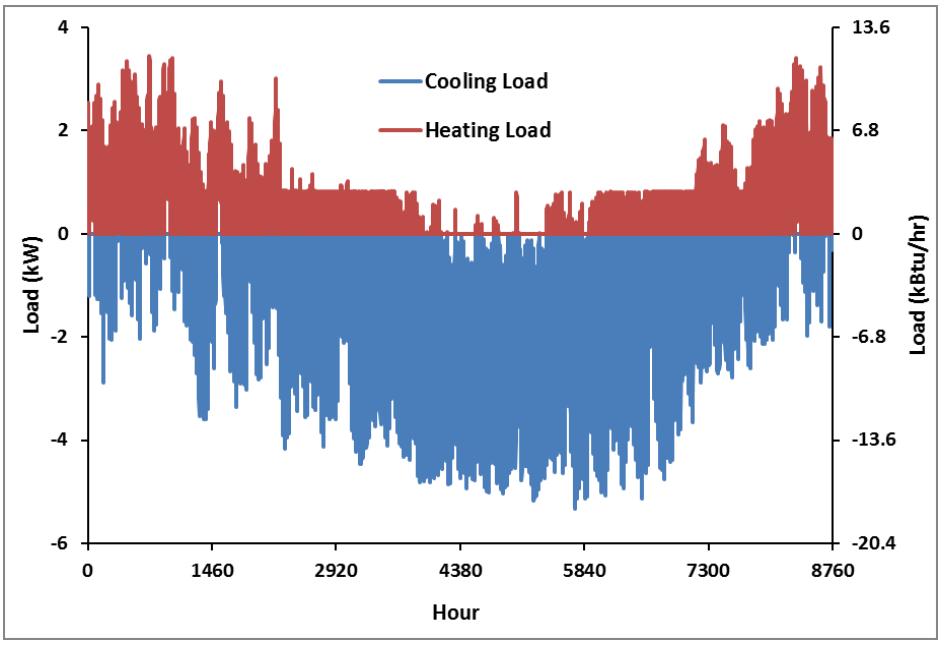

Figure 5.8: Annual Hourly Building Loads for the Simulated Building in Phoenix, AZ

The simulated hourly inlet and outlet fluid temperature of the Slinky™ GHX field for three years are shown in Figure 5.9 and 5.10. From the figures, we can tell that the Slinky™ GHX fields

almost reach steady state in the second year, which agrees with the temperature response function plotted in Figure 5.6. Due to the imbalanced loads of the two locations, we observe an obvious decrease or increase of the ground temperature in the second year of the simulations. For Lansing, MI, when compared to the first year, the ground temperature is lower in the second year due to the heating dominated climate. For Phoenix, AZ, the ground temperature in the second year is significant higher than the first year because of the large cooling demand. Overall, the simulated results for these two locations agree with our expectations.

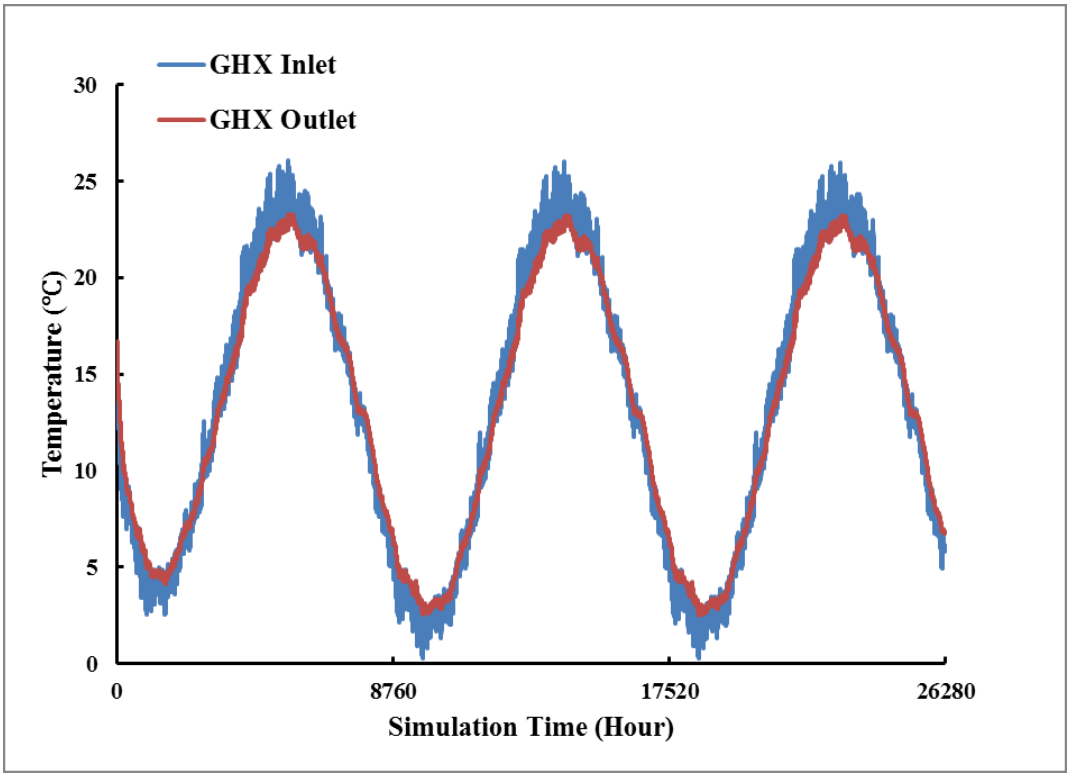

Figure 5.9: Three-year Hourly Fluid Temperature of Slinky^{TM} GHX in Lansing, MI

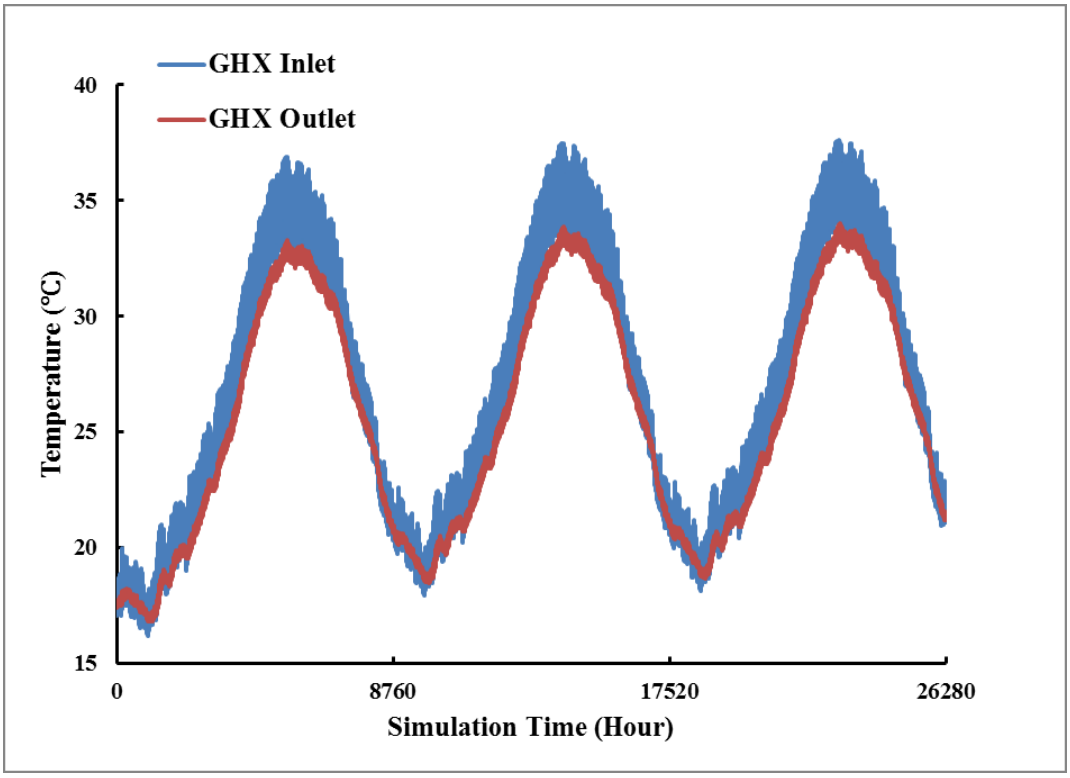

Figure 5.10: Three-year Hourly Fluid Temperature of Slinky™ GHX in Phoenix, AZ

CHAPTER 6

CONCLUSIONS AND RECOMMENDATIONS

6.1 Conclusions

This thesis presents the development, validation and implementation of a Slinky™ GHX Model. An accurate model for simulation purpose is developed for Slinky™ GHXs, with the consideration of the intensive thermal interactions between loops and the near-surface effect. While the analytical solutions have an advantage in accounting for the thermal interactions between loops, only numerical model can include a detailed ground surface heat balance. In this work, analytical and numerical approaches are combined in solving the complex heat conduction problem to achieve a good balance of efficiency and accuracy.

The ring source solutions for the temperature response of both horizontal and vertical Slinky™ GHXs is derived based on the point source solution given in Marcotte and Pasquier (2009), and agreed with Li et al.'s (2012) solutions with negligible differences (within ±0.0015°C) in the sample calculations. The algorithm used to calculate the response factors have several features that significantly increase the computation speed. The calculation of a set of temperature factors for a Slinky™ GHX with 100 loops is within one minute. For use in system simulations where the GHX may be connected to other components, the model is formulated to calculate both heat transfer and exiting fluid temperature, given entering fluid temperature. The thermal effect of the ground surface heat balance on GHXs is accounted for by superimposing the undisturbed ground

temperature. A three-dimensional numerical model is adopted in calculating the undisturbed ground temperature with the consideration a detailed ground surface balance.

The model is validated against the published experimental data demonstrated in Fujii et al. (2012). The simulated hourly and sub-hourly exiting fluid temperatures were compared with the measured data from three short-term TRTs and a long-term system. In the comparisons between the model predicted hourly exiting temperature and the measured hourly values from three 5-day TRTs, the maximum error is -0.52°C (-0.94°F), while the RMSEs are 0.27°C (0.49°F), 0.16°C (0.29°F), 0.15°C (0.27°F), respectively. In the comparison with the measured data from the 38-day system test, with a ten-minute time step, the RMSE is 0.15°C (0.27°F); and the maximum error is -0.57°C (-1.03°F). The model is implemented in the whole-building energy simulation software EnergyPlus as a plant component based on two existed EnergyPlus modules.

6.2 Recommendations

First, the proposed model is based on two assumptions: (1) the heat transfer rates of the tubes in a Slinky^{TM} GHX field are uniform; (2) the mean fluid temperature is the average value of the entering and exiting fluid temperature. The second assumption relies on the first assumption. These two assumptions will result in inaccuracy in calculating the temperature response function (Malayappan and Spitler 2013) as well as the exiting fluid temperature (Marcotte and Pasquier 2008; Beier 2011). It turns out that the heat flux is neither uniform for boreholes in a field (Malayappan and Spitler 2013) nor uniform along a single borehole (Marcotte and Pasquier 2008; Beier 2011). The ignorance of the first fact, called ‘edge effect’ in Malayappan and Spitler’s (2013) work, will cause a significant error when the borehole number is large and when time is long. The second assumption will result in a significant error when time is short or the flow rate is low. Therefore, a better approach to model a Slinky^{TM} GHX field without assuming a uniform flow rate along the tubes is highly desired in the future.

Second, the soil freezing around the tube and the moisture transfer are ignored in this model, while they are important for thermal performance of a GHX. In heating mode, especially under extreme conditions, the soil around the tube may freeze, which can change the heat transfer process significantly. In contrast, in cooling mode, the high ground temperature near the tube due to heat injection may cause the moisture migration. As the result of moisture migration, the soil around buried tube could dry out. This will affect the performance of a GHX severely. Therefore, the phenomenon of soil freezing and moisture migration around the buried tube is anticipated to be modeled in the future.

Third, while this study provides a feasible approach for implementing the Slinky^{TM} GHX model in the whole-building simulation software, EnergyPlus, more programming, debugging and validation work is required to cast a new and integrated EnergyPlus module for Slinky^{TM} GHX modeling in the future.

Fourth, the model can serve as a tool for some further studies. One possible study will be simulating the minimum recommended land areas for installing Slinky^{TM} GHXs to satisfy the heating/cooling loads of a typical residential house at different locations, by using the implemented Slinky^{TM} model in EnergyPlus. A table of the simulated minimum land areas at different locations can be made. The simulation results are recommended to be further verified using the existing experimental data or design data. While the simulated results consider the local weather data and the thermal interactions, the table will provide an important reference for designers. Another possible study will be applying the similar approach in modeling straight tube HGHXs. By comparing the simulation results of the model with the existing numerical model's (Lee 2013) results. The correctness or limitations of the approach presented in this thesis can be further studi

REFERENCES

Allen, R. G., L. S. Pereira, D. Raes, and M. Simth. 1998. Crop evapotranspiration- Guidelines for computing crop water requirements. *FAO Irrigation and Drainage Paper No 56.*

Antonopoulos, V. Z. 2006. Water movement and heat transfer simulations in a soil under ryegrass. *Journal of Biosystems Engineering* 95(1): 127-138.

Beier, R. A. 2011. Vertical temperature profile in ground heat exchanger during in-situ test. *Renewable Energy* 36: 1578-1587.

Bi, Y., L. Chen, and C. Wu. 2002. Ground heat exchanger temperature distribution analysis and experimental verification. *Applied Thermal Engineering* 22: 183-189

Braven, D., and E. Nielson. 1998. Performance prediction of a sub-slab heat exchanger for geothermal heat pumps. Journal of Solar Energy Engineering, *Transactions of the ASME* 120: 282-288.

Carslaw, H., Jaeger, J. 1959. *Conduction of Heat in Solids*, 2nd ed. Oxford, UK: Oxford University Press.

Chiasson, A.D. 1999. Advances in modeling of ground-source heat pump systems. Master Thesis, Department of Aerospace and Mechanical Engineering, Oklahoma State University, USA.

Chong, C.S.A., G. Gan, A. Verhoef, R. G. Garcia, P. L. Vidale. 2013. Simulation of thermal performance of horizontal slinky-loop heat exchangers for ground source heat pumps. *Applied Energy* 104:603-610.

Claesson, J., and A. Dunand. 1983. Heat extraction from the ground by horizontal pipes—a mathematical analysis. Department of Mathematical Physics, Lund University, Lund, Sweden.

Claesson, J., S. Javed. 2011. An analytical method to calculate borehole fluid temperatures for time-scales from minutes to decades. *ASHRAE Transactions* 117(2):279–288.

Cui, P., X. Li, Y. Man, and Z. Fang. 2011. Heat transfer analysis of pile geothermal heat exchangers with spiral coils. *Applied Energy* 88:4113–4119.

Cui, P., H. Yang, and Z. Fang. 2006. Heat transfer analysis of ground heat exchangers with inclined boreholes. *Applied Thermal Engineering* 26:1169–117

Cullin, J.R., L. Xing, E. Lee, J.D. Spitler, and D.E. Fisher. 2012. Feasibility of\ foundation heat exchangers for residential ground source heat pump systems in the United States. *ASHRAE Transactions*. 118(1):1039-1048.

Eskilson, P. 1987. Thermal Analysis of Heat Extraction Boreholes. Doctoral Thesis, Department of Mathematical Physics, Lund University, Lund, Sweden.

Fontaine, P.-O., D. Marcotte, P. Pasquier, and D. Thibodeau. 2011. Modeling of horizontal geoexchange systems for building heating and permafrost stabilization. *Geothermics* 40:211–220.

Fujii, H., K. Nishi, Y. Komaniwa, and N. Chou. 2012. Numerical modeling of slinky-coil horizontal ground heat exchangers. *Geothermics* 41:55–62.

Ingersoll, L.R., O.J. Zobel, and A.C. Ingersoll. 1954. *Heat Conduction with Engineering Geological and Other Applications*. Madison, WI: The University of Wisconsin Press.

Jones, F. 1995. Closed Loop Geothermal Systems – Slinky™ Installation Guide. Rural Electric Research Project 86-1, National Rural Electric Cooperative Association, Electric Power Research Institute, and International Ground Source Heat Pump Association.

Kusuda, T., and P. R. Achenbach. 1965. Earth temperature and thermal diffusivity at selected stations in the United States. Technical Report, National Bureau of Standards, Washington, D.C..

Lamarche, L., B. Beauchamp. 2007. A new contribution to the finite line-source model for geothermal boreholes. *Energy and Buildings*, 39:188–198.

Lee, E. S. 2008. Development, verification, and implementation of a horizontal buried pipe ground heat transfer model in EnergyPlus. Master Thesis, Department of Aerospace and Mechanical Engineering, Oklahoma State University, Stillwater, USA.

Lee, E. S. 2013. An improved hydronic loop system solution algorithm with a zone-coupled horizontal ground heat exchanger model for whole building energy simulation. Ph.D. Thesis. Department of Aerospace and Mechanical Engineering, Oklahoma State University, Stillwater, USA.

Lee, E. S., D.E. Fisher and J.D. Spitler. 2013. Efficient horizontal ground heat exchanger simulation with zone heat balance integration. *HVAC&R Research* 19(3): 307-323.

Li, H., K. Nagano, Y. Lai. 2012. A new model and solutions for a spiral heat exchanger and its experimental validation. *International Journal of Heat and Mass Transfer* 55:4404-4414.

Malayappan, V. and J.D. Spitler. 2013. Limitations of using uniform heat flux assumptions in sizing vertical borehole heat exchanger fields. *Proceedings of Clima 2013*. June 16-19. Prague

Man, Y., H. Yang, N. Diao, P. Cui, L. Lu, and Z. Fang. 2011. Development of spiral heat source model for novel pile ground heat exchangers. *HVAC&R Research* 17(6):1075-1088.

Man, Y., H. Yang, N. Diao, J. Liu, and Z. Fang. 2010. A new model and analytical solutions for borehole and pile ground heat exchangers. *International Journal of Heat and Mass Transfer* 53:2593–601.

Marcotte, D., P. Pasquier. 2008. On the estimation of thermal resistance in borehole thermal conductivity test. *Renewable Energy* 33: 2407–2415.

Marcotte, D., P. Pasquier. 2009. The effect of borehole inclination on fluid and ground temperature for GLHE systems. *Geothermics* 38(4):392–398.

Mei, V. C. 1986. Horizontal ground-coil heat exchanger theoretical and experimental analysis. Technical report. Oak Ridge National Laboratory.

Metz, P. D. 1983. A simple computer program to model three-dimensional underground heat flow with realistic boundary conditions. *Journal of Solar Energy Engineering* 105(1): 42-49.

Mukerji, S., K.A. Tagavi, and W.E. Murphy. 1997. Steady-state heat transfer analysis of arbitrary coiled buried pipes. *Journal of Thermophysics and Heat Transfer* 11(2): 182-188

Murugappan, A. 2002. Implementing ground source heat pump and ground loop heat exchanger models in the EnergyPlus simulation environment. Master Thesis, Department of Aerospace and Mechanical Engineering, Oklahoma State University, USA.

Piechowski, M. 1999. Heat and mass transfer model of a ground heat exchanger: theoretical development. *International Journal of Energy Research* 23(7): 571-588.

Walter, I. A., R. G. Allen, R. Elliott, D. Itenfisu, P.Brown, M. E. Jensen, B. Mecham, T. A. Howell, R. Snyder, S.Eching, T.Spofford, M.Hattendorf, D.Martin, R.H.Cuenca, and J. L. Wright. 2005. The ASCE standardized reference evapotranspiration equation. Standardization of Reference Evapotranspiration Task Committee Final Report. American Society Civil Engineers, Environmental and Water Resources Institute. Reston, Virginia.

Wu, Y., G. Gan, A. Verhoef, P.L. Vidale, R.G. Gonzalez. Experimental measurement and numerical simulation of horizontal-coupled slinky ground source heat exchangers. *Applied Thermal Engineering* 30: 2574–2583.

Xing, L. 2010. Analytical and numerical modeling of foundation heat exchangers. Master Thesis, Department of Aerospace and Mechanical Engineering, Oklahoma State University, USA.

Xing, L., J. R. Cullin, J. D. Spitler. 2012. Modeling of foundation heat exchangers—Comparison of numerical and analytical approaches. *Building Simulation* 5: 267-279

Yavuzturk, C., and J.D. Spitler. 1999. A short time step response factor model for vertical ground loop heat exchangers. *ASHRAE Transactions* 105(2): 475-485.

Zeng, H.Y., N.R. Diao, and Z.H. Fang. 2002. A finite line-source model for boreholes in geothermal heat exchangers. *Heat Transfer-Asian Research* 31(7): 558–567.

VITA

Zeyu Xiong

Candidate for the Degree of

Master of Science

Thesis: DEVELOPMENT AND VALIDATION OF A SLINKY^{TM} GROUND HEAT EXCHANGER MODEL

Major Field: Mechanical Engineering

Biographical: Born in Quanzhou, Fujian, People's Republic of China on September 25, 1989.

Education:

Completed the requirements for the Bachelor of Science in Mechanical Engineering at Southwest Jiaotong University, Chengdu, Sichuan in 2010.

Professional Memberships:

ASHRAE student member 2012-present